Spring 2023

Experimental and Numerical Analysis of a Commercial Phase Change Material Melting at Different Inclinations

Andrew Heiles
Embry-Riddle Aeronautical University, heilesa@my.erau.edu

EXPERIMENTAL AND NUMERICAL ANALYSIS OF A COMMERICAL PHASE CHANGE MATERIAL MELTING AT DIFFERENT INCLINATIONS

by

Andrew J. Heiles

A Thesis Submitted to the College of Engineering Department of Mechanical Engineering in Partial Fulfillment of the Requirements for the Degree of Master of Science in Mechanical Engineering

Embry-Riddle Aeronautical University
Daytona Beach, Florida
March 2023

EXPERIMENTAL AND NUMERICAL ANALYSIS OF A COMMERICAL PHASE CHANGE MATERIAL MELTING AT DIFFERENT INCLINATIONS

by

Andrew J. Heiles

This thesis was prepared under the direction of the candidate's Thesis Committee Chair, Dr. Sandra Boetcher, Professor, Daytona Beach Campus, and Thesis Committee Members Dr. Rafael Rodriguez, Professor, Daytona Beach Campus, and Dr. Mark Ricklick, Professor, Daytona Beach Campus, and has been approved by the Thesis Committee. It was submitted to the Department of Mechanical Engineering in partial fulfillment of the requirements for the degree of Master of Science in Mechanical Engineering

Thesis Review Committee:

_____

Sandra Boetcher, Ph.D.
Committee Chair

_____ _____

Rafael Rodriguez, Ph.D.
Committee Member

Mark Ricklick, Ph.D.
Committee Member

_____ _____

Jean-Michel Dhainaut, Ph.D.
Graduate Program Coordinator,
Mechanical Engineering

Patrick Currier, Ph.D.
Department Chair,
Mechanical Engineering

_____ _____

James Gregory, Ph.D.
Dean, College of Engineering

Christopher Grant, Ph.D.
Associate Vice President of Academics

_____

Date

Acknowledgements

First and foremost I would like to thank my parents for all of the support they have given to me throughout my academic career, and for their continuing encouragement for me to pursue higher levels of education and challenge myself academically.

I would like to also thank my advisor and the other members of my committee for their help and support in both the completion of this paper and throughout my undergraduate and graduate degrees. They have been responsible for introducing me to the study of heat transfer and research in thermal science applications, and have helped me foster a passion for this subject which I will carry on into my career.

Abstract

Researcher: Andrew J. Heiles

Title: Experimental and Numerical Analysis of a Commercial Phase Change Material Melting at Different Inclinations

Institution: Embry-Riddle Aeronautical University

Degree: Master of Science in Mechanical Engineering

Year: 2023

The study of various phase change materials (PCM), experimentally and numerically, have been completed over the past several years to address their feasibility and potential when used in latent heat thermal energy storage (LHTES) systems for a variety of potential applications. Previous studies have investigated changes into the type of PCM used in the system as well as the system configuration, ranging from boundary conditions to internal and external geometries and orientations of the system. The present study focused on conducting experiments at different inclination angles and isothermal wall temperatures with the organic PCM PureTemp37, and continued with a numerical investigation into the mushy-zone constant with respect to the aforementioned changes to system parameters. For the experiments, an acrylic enclosure was used in conjunction with a constant temperature bath that transferred heat via an aluminum heat spreader. Data collection was completed via imaging at a set interval, and these were used to determine the solid/liquid percentage of PCM in the enclosure at a specific point in time during the melt. The experiments along with a series of material properties tests were used to complete and validate numerical simulations of an identical system. To ensure numerical accuracy a variety of meshes were studied to confirm mesh independence, and methods for the simulations were selected based on standards that have been established for the field. Using the experiments as a benchmark, the numerical data returned differing trends in inclination angle and isothermal wall temperature with respect to the mushy-zone constant depending on the fineness of the constructed mesh. This led to the conclusion that more care is needed when completing mesh independence studies as false correlations of the mushy-zone constant at differing system parameters appear with more coarse models.

Table of Contents

List of Tables

Page

Table

List of Figures

Page

Figure

Nomenclature

A_{mush}	mushy-zone constant
f	liquid fraction
h_{sl}	latent heat of fusion [J / kg]
h	enthalpy per unit mass [J / kg]
c_p	specific heat [J / $kg \cdot K$]
L	latent heat per unit mass [**X**]
k	thermal conductivity [W / $m \cdot K$]
T	temperature [K]
t	time [s]
u	fluid velocity in x-direction [m / s]
v	fluid velocity in y-direction [m / s]
g	gravity [m / s^2]
d	characteristic length [μm]

Greek Letters

ρ	density [kg / m^3]
μ	dynamic viscosity [kg / $m \cdot s$]
ε	computational constant to avoid division by zero

Subscripts

s	solid or solidus
l	liquid or liquidus
m	phase-change temperature

Chapter I

Introduction

The continuing advancements in technology, infrastructure, and expansion in countries around the world over the past several decades has brought on the need for more energy. This has led to an increase in primary energy consumption, or the energy from natural resources prior to conversion for use, of 10% from 2010 to 2017 [1]. With this has come the desire to increase efficiency in various systems through the use of heat recovery systems and thermal energy storage (TES). These could maximize the energy retained, and thus available for use, in a wide range of industries.

Applications to TES are addressed in Alva et al's study with notable heat sources including solar, geothermal, fossil fuel power plants, nuclear power plants, industrial waste heat, and biomass [2]. All the listed sources are suitable candidates for energy recovery, storage, and discharge for reuse. Storage of this energy through TES would help to bridge the gaps between demand and supply commonly seen with the difference in peak and off-peak use of various systems (HVAC, electronic, etc.) at different times of the day, and would greatly reduce the amount of waste heat being output into the environment. Within the definition of TES are sensible heat thermal energy storage (SHTES) and latent heat thermal energy storage (LHTES). The former stores energy in a material's specific heat capacity and is noted as being thermally stable at higher temperatures [2], however these systems show issues with stability during the discharge processes due to the drop in temperature of the material. In contrast, the latter stores energy in the material's latent heat and is generally stable during the discharge process due to the isothermal nature of these systems.

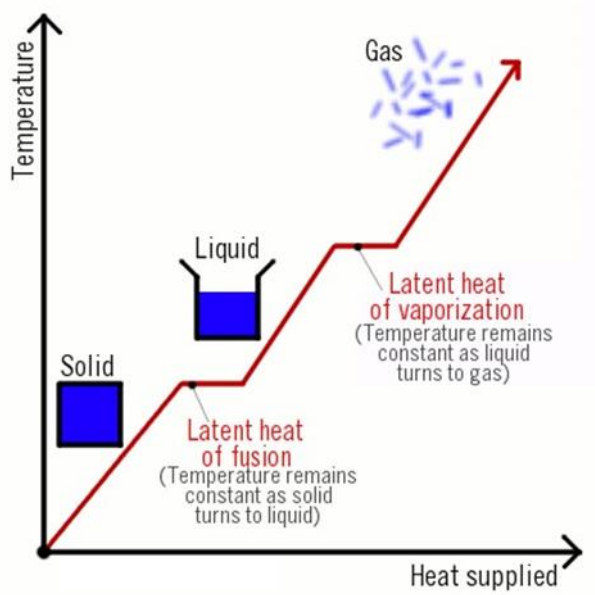

Figure 1: Sensible and latent heat graph **[3]**

LHTES systems use phase change materials (PCM) for energy storage, which most commonly uses the solid-liquid transition to charge the system. Shown in Figure 1, the latent heat displayed on the graph remains relatively isothermal during phase transition, which as mentioned ensures a stable charging and discharging processes with minor deviations until the material completely changes phase.

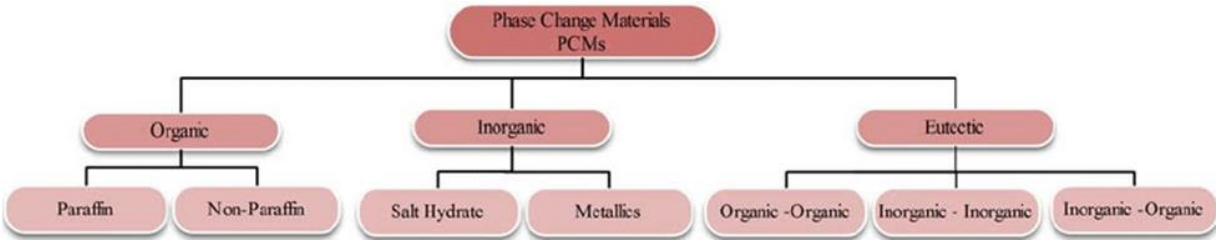

Figure 2: Types of PCM [4]

PCMs encompass a wide variety of materials including organics, inorganics, and eutectics, as shown in Figure 2. These are selected based on the application and desired melting temperature. The great selection of materials is beneficial, as alterations to a system in order to accommodate a specific PCM are not always necessary; but with this also comes the need to further study these materials experimentally and numerically to ensure the melting behavior will be as expected with relation to similar PCMs.

From this idea, many researchers have completed studies with respect to the use of PCM for real applications, including incorporation into building materials, solar cells, and various types of electronics. The addition of PCM to commercial and residential buildings through the use of bricks, shutters, or window blinds could help to regulate internal temperature throughout the different seasons [5]. Inclusion in solar systems, such as photovoltaic solar cells and solar heating for water tanks, could likewise improve efficiency and reduce waste heat of the systems [6] [7]. As another alternative for PCM in TES systems, authors have studied the potential applications of material use in small scale electronics for thermal regulation as well as lithium-ion battery systems [8] [9].

PCMs could take a greater presence in various industries for TES in the coming years. However, significant problems in the field need to be addressed before the material can easily be incorporated into residential and commercial applications. A large issue involving the study of PCM is the vast majority of materials that encompassed under that name [2]. As mentioned, two of the main groups of PCMs include organics and inorganics. The organic PCMs includes materials such as paraffins, fatty acids, esters, alcohols, and glycols. Inorganics includes salts, salt eutectics, salt hydrates, and metals [2]. Each of these could show differences when melt characteristics and melt interface

development are compared. The other main issue is the accuracy when numerically modeling the melting of these materials. Between the different software, solver methods, and selection of a value called the mushy-zone constant, studies have been conducted to assess the consequences of altering the aforementioned settings [10] [11] [12].

Of these areas of interest, conclusions have been made into effects of altering methods and software, but more research is needed to determine if there are any correlations for the mushy-zone constant when studying different PCMs. As part of the governing equations that define how the computational fluid dynamics (CFD) software solves melting and solidification problems, via the enthalpy-porosity method defined in Voller and Prakash's 1987 study [13], this constant acts as a correction factor for the numerical simulations and has been shown to speed up and slow down simulated melting by varying its value [14]. Researchers in the field have attempted to define correlations for this constant [15] and have even stated this value is completely arbitrary [16]. But the majority of authors acquire the number from either validating their numerical data to experimental data, or by taking a validated number from a previous author. In both cases authors have published works showing good validations where the experiments perfectly match the setup of the numerical simulations, and completed validations that could contain unknown levels of error due to one or more factors in the system configuration (geometry, boundary condition, internal geometry, inclination, PCM) being altered from the experimental work.

Altering the PCM would show differences in melting characteristics based on materials having different properties, and thus this would need to be avoided between the numerical models and validation work. Similarly, adjustments to the boundary condition

would affect the amount of heat the material is in contact with, and in turn could show stark differences when compared to an alternate's melt fraction and development data. The other areas of concentration, finned enclosures and inclined enclosures, have been reported to require adjustments to the selected mushy-zone constant. In Kabbara and Kheirabadi's numerical study it was noted that the addition of 1-fin and 3-fins had a significant impact on the mushy-zone constant, likely due to the effected development of the natural convection currents within their modeled rectangular enclosure [17]. They also observed that accurate mushy-zone constant data reported differences between the 0° inclined model and the 45° and 90° models, indicating that inclination angle should not be neglected when pursuing accurate models [17].

The purpose of the presented work is to experimentally analyze the melt characteristics and melt front development of the commercially available organic PCM, PureTemp 37. This material was selected because of its availability and due to the fact that only a handful of papers have been published using the manufacturer's products, none of which have studied the selected material. An isothermal wall temperature will be applied at 47°C and 57°C for inclination angles of 30°, 45°, 60°, and 90° from the horizontal. Included in the experimental part of the paper, material properties for PureTemp 37 will be collected with the given procedures and uncertainties stated to further support the validation of the numerical study. Simulations will then be run including a mesh independence study, time-step independence study, a study into the mushy-zone constant, and a full recreation of the angles and wall temperatures to match the experiments. Results between the experimental and numerical studies will be compared through both melt front versus time graphs, melt front development images.

Further simulations will be completed if necessary to evaluate the effect of inclination angle and wall temperature on the selected mushy-zone constant(s), and to determine the effects of further refinement to the meshes in order to achieve more accurate results.

When completed, the contents of this work should provide accurate experimental data to be used for validation of future numerical studies. The material properties section will include all necessary data for PureTemp 37 to be modeled using CFD software, and the melt front development images and melt fraction versus time graphs will offer multiple means of validation. The numerical work will provide insight into the effects of inclination angle and wall temperature on the melting of the selected PCM, and the critical review should state relevant factors to consider when selecting a mushy-zone constant. In the study's entirety, the melting characteristics of the commercially available PCM will be investigated with the aim to determine its potential for TES applications, and by defining the effects on the mushy-zone constant when modeling inclined enclosures a greater understanding will be developed with the aim to help guide future design of TES systems.

Chapter II

Review of the Relevant Literature

Preliminary Studies and Method Development

Preliminary studies it the field focused on obtaining a better understanding of the melt characteristics in different materials and studying the accuracy of the current numerical models. This was approached with the goal to evaluate the effectiveness and potential of using PCMs for LHTES systems. Authors such as Sparrow and Broadbent acknowledged the great difference in energy transfer when comparing melting to that of sensible heat storage in their 1982 study. Their experiments consisted of inward melting of a paraffin in a cylinder with an isothermal boundary condition. Data collected from thermocouples also informed of the significance of natural convection in the melting process, with a reported 50% deviation in energy transfers when compared to a pure conduction numerical model [18]. This confirmed the benefits that PCMs could have amongst various applications, and directly defined a problem for future studies to address.

Other works during this time, such as Sparrow, Pantakar and Ramadhyani's numerical work [19] or Gau et al's experimental work [20] furthered support behind the issue of modeling solely based on conduction. The former modeled a 2-D cylinder with outward melting by an isothermal wall using axisymmetry. They found that the thickness of the melting region was not uniform when natural convection was included in the numerical models, as compared to the conduction only model in which this region was identical regardless of the height along the cylinder [19]. The latter is the first paper of the reviewed works to investigate melting of a PCM with an isothermal boundary

condition at a different inclination. These authors studied a rectangular enclosure orientated horizontally, experiencing heating from the bottom, via the melting of a paraffin. As part of their findings an uneven melt front was reported due to the development of Benard convection cells, displayed in Figure 3, something that would not be considered in numerical modeling when using a conduction-only formulation [20].

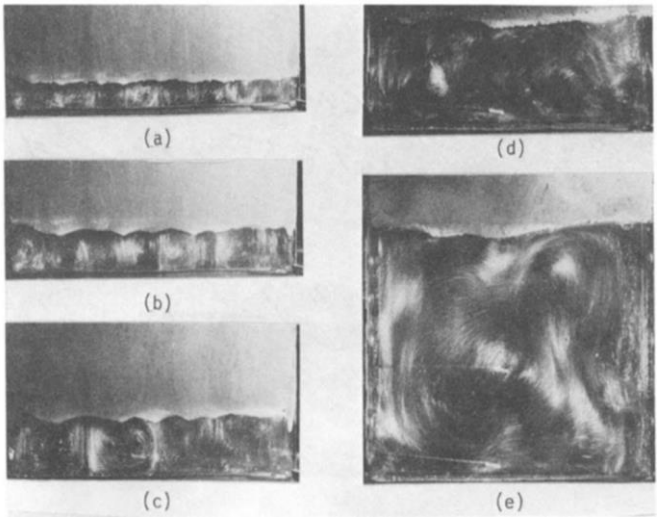

Figure 3: Development of Benard Convection Cells at different times in0 the melting process [20]

The aforementioned works all expressed the need for proper consideration of natural convection along with conduction when numerically modelling. A solution to this was proposed in Voller and Prakash's study in which a new approach, called the enthalpy-porosity method, was established [13].

$$\rho \frac{\partial h}{\partial t} = \nabla \cdot (k \nabla T) \quad (1)$$

$$h = \begin{Bmatrix} c_{ps}T & @\ T < T_m \\ c_{pl}T + (c_{ps} - c_{pl})T_m + L & @\ T \geq T_m \end{Bmatrix} \quad (2)$$

Focusing back on the earlier approach, the enthalpy formulation, the governing equations consisted solely of the energy equation (1). The enthalpy per unit mass was solved by a piecewise relation which realized if the system was liquid or solid based on the temperature. However, this approach lacked any consideration of motion within the fluid, as seen when natural convection is present. Accounting for fluid motion would require the continuity, energy, and momentum equations (3) to be considered, and would be implemented part a source term is displayed at the end of the momentum equation shown below (4) [21].

$$\rho \frac{Dv}{Dt} = -\nabla\rho + \mu\nabla^2 v + \rho g + S \quad (3)$$

$$S = -A(f)\ v \quad (4)$$

$$A(f) = \frac{A_{mush}(1-f)^2}{(f^3 + \varepsilon)} \quad (5)$$

Voller and Prakash [13] used this source term to treat the mushy-zone region as a porous medium with the ability of fluid flow. Their defined porosity function, *A(f)*, was dependent on the liquid fraction, *f*, and allowed the momentum equation to act similar to

the Carman-Kozeny equation for porous media fluid flow. In equation (4) ε is used as a constant to avoid division by zero and is set to a small value accordingly. A_{mush} refers to a constant commonly known as the mushy-zone constant, for which the proper value based on selected system parameters is still undefined [21]. As stated, this constant acts as a correction factor for the numerical simulations to help match the melting time and development of heat transfer in the system to the accompanying experimental data. The liquid fraction is described with *f* and varies based on the piecewise relation outlined in equation (6) [22].

$$f = \begin{cases} 0 & if \quad T < T_{solidus} \\ \dfrac{T - T_{solidus}}{T_{liquidus} - T_{solidus}} & if \quad T_{solidus} < T < T_{liquidus} \\ 1 & if \quad T > T_{liquidus} \end{cases} \qquad (6)$$

The 1987 study acted solely as a proposal of a new method and state specifically in their conclusions that future studies will need to investigate differences between their proposed fixed grid method and a deforming grid technique, different flow models in the mushy zone, and note that the current work lacks validation to experiments. The following year, authors Brent, Voller, and Reid published a paper to validate the enthalpy-porosity technique [23]. Numerical models were created based on the experimental work of Gau and Viskanta [24], in which gallium was simulated as the PCM in a 2-D rectangular vertical enclosure with an isothermal boundary condition. Melt front development was plotted and compared between the experiments and simulations at different times of the melt, resulting in validation of the approach as displayed in Figure 4.

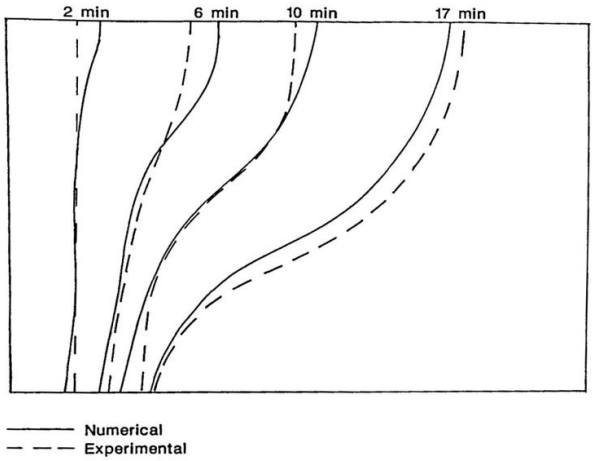

Figure 4: Numerical validation to experiments conducted by Gau and Viskanta [24] for melting of gallium [23]

Modern numerical studies apply the enthalpy-porosity method with software such as ANSYS Fluent; and implement the mushy-zone constant either through an independent study, select the value based on previous publications, or attempt to define the equation for use in their models. Figure 5 displays a mushy-zone constant independence study, comparing the numerical models at listed values for A_{mush} to experimental data for a vertically oriented rectangular enclosure. This melt fraction versus time graph acknowledges the impact of incorrect values of A_{mush}, with higher values significantly speeding up the melting process and lower values significantly slowing it down. While this method is proven to work, it comes with a greater computational expense and potential for errors at different system parameters. For example, if a study is conducted for a rectangular enclosure at two inclination angles and the mushy-zone constant is only evaluated for one of the two angles, errors could be

present due in the other to the potential change in the development of natural convection within the enclosure.

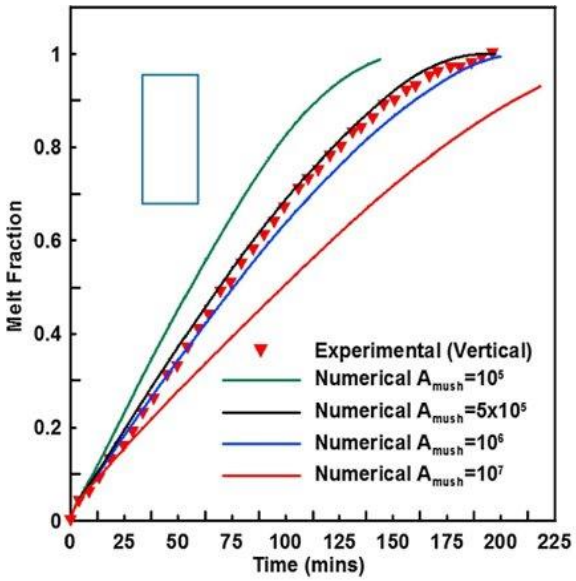

Figure 5: Mushy-Zone constant study for vertical enclosure with lauric acid and an isothermal wall boundary condition [12]

Attempts at finding the equation for the mushy-zone constant are seen in studies such as Yang et al. Equation (7) shows their given relation for A_{mush} based on viscosity of the PCM and the characteristic length (d) of the "solid microstructures within the mushy zone" [15].

$$A_{mush} = \frac{180\mu}{d^2} \tag{7}$$

While Voller and Prakash's [13] method does consider the effects of natural convection during the melting and solidification processes, it does not take into account

solid motion within the liquid. This could occur when melting a system and PCM remains attached and un-melted in a top corner/edge of the melt. As the melt would progress gravity would eventually cause this solid PCM to fall through the liquid material to the bottom of the enclosure. An example of this would be commonly seen at inclinations close to the horizontal with the heat entering the system through the bottom wall. As mentioned, when numerically modeling systems such as this the PCM would remain attached to the top of the enclosure and would not fall through the liquid [25].

Modern Experimental Studies

Modern experimental studies have built off the known issues surrounding numerical accuracy for modeling PCM and have attempted to both better define the material properties of their selected PCM and to study various materials under different system parameters.

The current study will be based on the 2013 experimental work by Shokouhmand and Kamkari, in which lauric acid was melted in a rectangular enclosure with an isothermal boundary condition [26]. As part of their investigation, the authors defined the different material properties of their PCM to form a standardized set of data for which all relevant future numerical studies could be based on. Thermocouples and a camera were used to track the melt front's development, with analysis and conclusions into the modes of heat transfer present in the system and the stages of the melt respective to those modes. The standard enclosure, shown in Figure 6, displays the 2-D proportions of the system with the thermocouple locations.

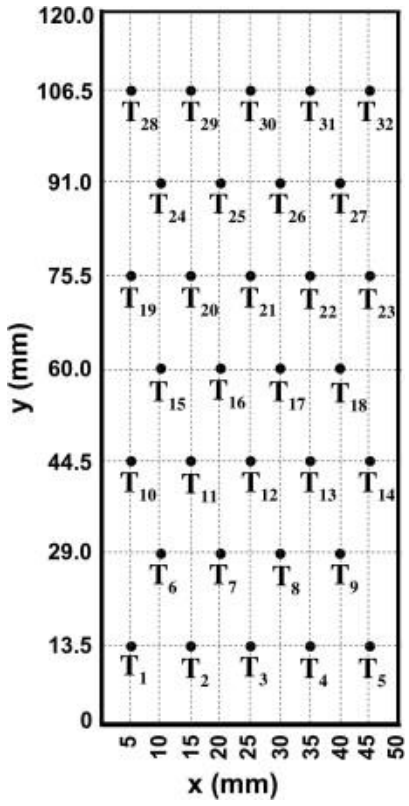

Figure 6: Standard rectangular experimental enclosure with displayed thermocouple locations [26]

This type of setup was used for various experimental investigations such as Kamkari et al's [27] study into inclination angle, with inclinations tested at 0°, 45°, and 90° from the horizontal at the same isothermal wall temperatures as Shokouhmand and Kamkari's previous paper (55°C, 60°C, 70°C). That same year Kamkari and Shokouhmand [28] published another paper investigating the melting of the same material at the same boundary condition temperatures, but with an un-finned, 1-finned, and 3-finned enclosure of the same outer dimensions. The ideas behind these two 2014 experimental studies were combined by Kamkari and Groulx [29], where the melting of lauric acid was investigated in un-finned, 1-finned, and 3-finned enclosures at inclination angles of 0°, 45°, and 90° from the horizontal, with the internal geometry alterations

displayed in Figure 7. This set of experiments would later be coupled with numerical studies, both by the aforementioned authors and by new authors, to investigate how these major changes to the system affect the simulations of the PCM, lauric acid.

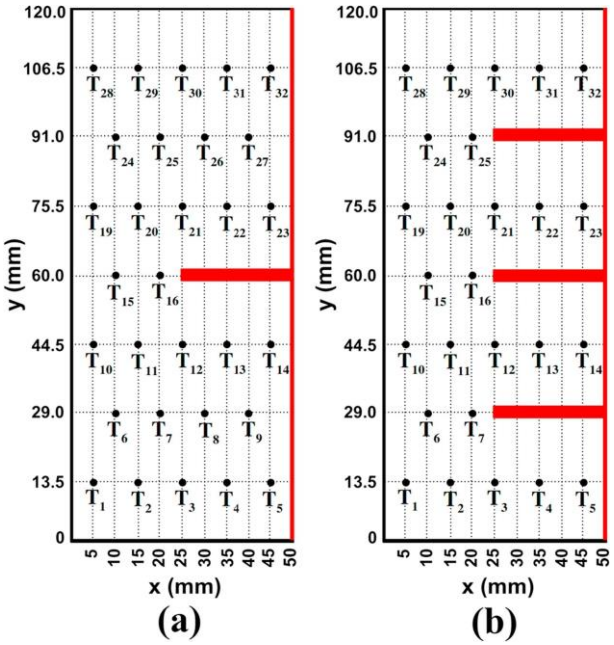

Figure 7: Standard rectangular experimental enclosure with fins and thermocouple locations displayed [29]

For these described experiments, the 2013 paper noted the initial melt governed by conduction followed by a shift to become convection dominant as the liquid built up within the enclosure. Convection currents were shown to decrease after the melt reached the wall opposite the isothermal boundary condition. This led the authors to define the melt as governed by four main stages including conduction, transition, strong convection, and weak convection [26]. The 2014 study investigating inclination angle saw the development of irregular interface shapes at non-vertical angles, likely due to the development of the convection currents and Benard convection cells discussed previously

by Gau et al [20]. The 45° inclined enclosure showed both characteristics of the 0° and 90° melts with the development of these irregular shapes along with the decreasing strength of convection at later parts of the melt, as discussed in the 2013 study. The 2014 study investigating fins saw overall melting enhancements with the presence of fins, to which the authors noted higher melting rate above the fin surfaces due to development of chaotic convective flows. The larger number of fins in the studied enclosures proved more effective towards the melting of the PCM, but increases in wall temperature showed a decrease in this effectiveness [28]. In the combined 2018 study, implementing both inclination angle and fins, the authors found that the effect of decreasing inclination angle had a greater impact on the melting of the PCM than the addition of fins to the vertical enclosure [29]. This would indicate that inclination angle of an enclosure in a potential application would have great significance to the total melt time of the system.

Other experimental investigations reviewed in the relevant literature include Mahfuz et al.'s study into the inward melting of a paraffin to simulate TES for a water heating system [7], Avci and Yazici's study into the melting of n-eicosane in a rectangular enclosure with a constant heat flux boundary condition [30], and Jiang et al.'s study into the melting of a binary nitrate salt in a rectangular enclosure with an isothermal boundary condition [31]. These three publications are not entirely relevant to this current work but display differences that will be useful to consider and understand when reviewing the numerical studies. Mahfuz's work shows a different geometry than the majority of those discussed. Annular TES systems, both with inward and outward melting, have been studied by many authors in the field and have a wide range of applications. However, when approaching validation of numerical to experimental

enclosure geometry should be considered. The internal adjustments to a rectangular enclosure from the addition of fins [29] demonstrate how convection currents can be disrupted and changed, which could greatly alter the collected results. The study of a new boundary condition, shown by Avci and Yazici, is another vital aspect to consider when selecting a validation work. Their displayed melt front images from the conducted experiments showed great differences, with much smoother interfaces, when compared to the discussed isothermal studies. Lastly, PCM selection can greatly change results of the melt, especially if the modeled PCM is of a different type entirely than that of the validation.

These three discussed numerical works further the notion that any changes to system parameters can have significant impacts on the completed melts, and help to emphasize the importance of proper validation to geometry and inclination, selected PCM, and boundary conditions.

Modern Numerical Studies and Validation Practices

Investigations into Numerical Procedure/Software

Similar to the prior discussion of the enthalpy versus enthalpy-porosity methods, authors have conducted studies to determine the effects of modeling the melting and solidification processes in different ways. Comparison of two- and three-dimensional models have been conducted to verify that the former provides accurate results [32]. This verification proves invaluable, as the negligible reported differences prove that the much less computationally expensive two-dimensional model is accurate. The authors recorded similar melt fraction contours along the 3-D models at specific times during the melt

indicating that the melting process is very close to 2-D. To further confirm this idea, they tracked the instantaneous heat flux as a function of time for both models and reported very similar data, shown in Figure 8. While this supports the claim that 2-D models can accurately replicate corresponding 3-D experiments, other authors have noted that the lack of 3-D flow structures within the natural convection can lead to melt fronts that deviate from the experiments [33]. Greater research would be needed to confirm or deny this claim and ensure the natural convection currents are being properly modeled in the simulated enclosures.

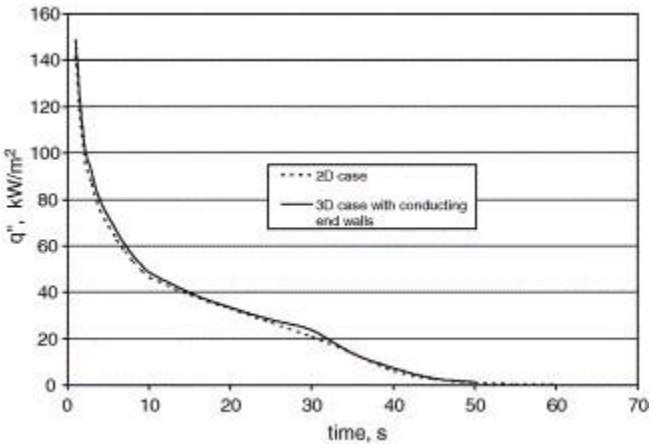

Figure 8: Numerical validation between 2-D and 3-D models [32]

The later study of Shmuelie et al [11] investigated the methods used by the CFD itself, with respect to the pressure-velocity coupling and pressure discretization schemes. Studies such as this helped establish a foundation for which all future simulations could base their setup on. For the pressure-velocity coupling schemes PISO and SIMPLE were studied, returning near identical results. However, with respect to the pressure

discretization schemes PRESTO! returned much more accurate results (within 12% error) when compared to the Body-Force-Weighted.

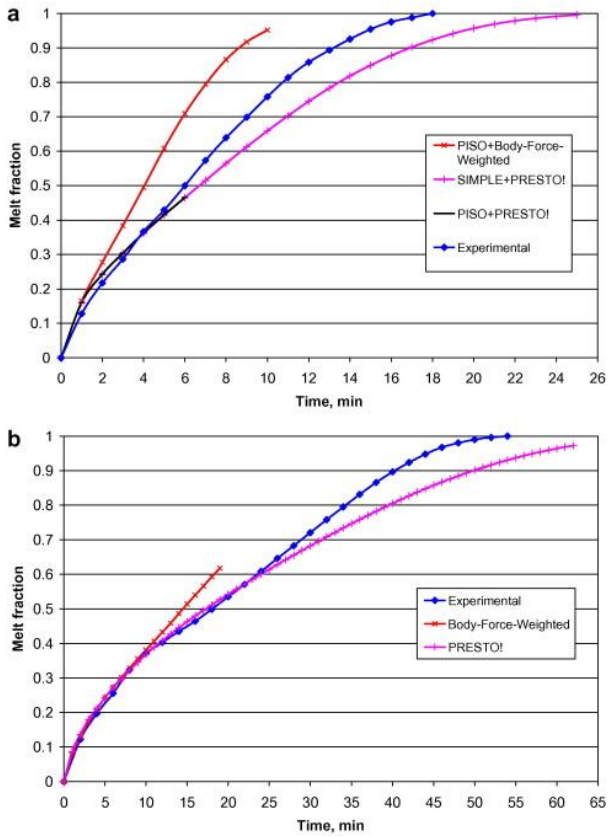

Figure 9: Investigation and experimental comparison to data from Katsman et al [34] with reference to pressure discretization schemes [11]

With multiple commercial software available comparisons between the different available CFD would be necessary to evaluate the validity of each one's results, such as the comparison between COMSOL Multiphysics and ANSYS Fluent [10]. Further comparisons have been noted and will be indirectly discussed later in the presented work, acknowledging the challenges faced when modeling inclined and finned enclosures with

COMSOL Multiphysics and validating to experiments as compared to ANSYS Fluent [12] [17] [22] [35].

The aforementioned studies help guide the field and establish which procedures and methods are valid to numerically solve phase change problems.

Investigations with Self-Validation

Some authors, albeit few, complete both experimental and numerical studies as part of their published investigation. These aim to display numerical works that match very closely, if not identically, to the experimental setup, and can consider assumptions or adjustments that were made during the experimental procedures that would otherwise have been disregarded in the numerical models (i.e. ambient temperature of the environment, potential temperature drop between heat source and heat spreader, etc.). As such, these works should provide a good starting off point for discussion into proper validation practices in the field.

In 2013, Biwole et al [36] completed a full study into the melting of the paraffin wax RT25 in a rectangular enclosure under the boundary condition of a constant heat flux through a vertical wall. Their experimental setup consisted of a 167 mm x 30 mm-large open internal cavity with a small area left open with air at the top to allow for thermal expansion. This was validated through two experimental comparisons into the melt-front development images (direct and visual comparisons at selected times of the melt), as shown in Figure 10, and stationary comparisons into the “two-dimensional velocity fields in the completely melted PCM” at four selected cross sections.

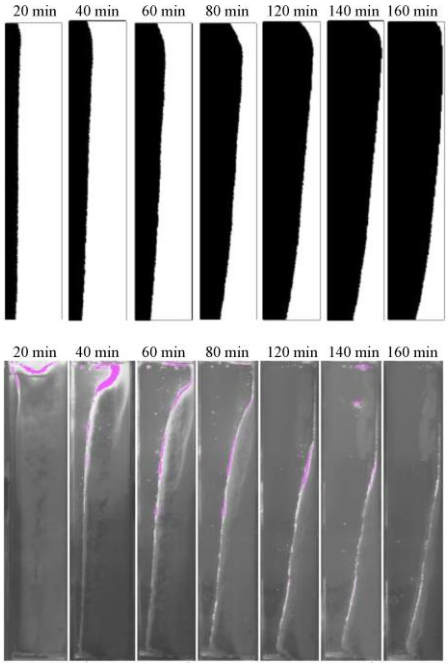

Figure 10: Completed validation for own experiment based on visual melt front interface development [36]

The authors do complete a proper validation for the initial simulations, with melt front interfaces that appear to resemble the experimental images (with the exception of the aforementioned solid-motion that is not included as part of the enthalpy-porosity technique). However, they seemingly disregard the mushy-zone constant claiming that it was selected “arbitrarily high” during the mathematical model discussion, and neglect to complete any analysis into different mushy-zone constants [36]. Their continuing models, and actual ones used for analysis and discussion in the work, stray from their experiments with the introduction of fins to the internal geometry. Discussed previously by Kamkari and Shokouhmand [28], the introduction of fins to an enclosure greatly impacts the development of convection currents in the liquid PCM, and therefore this inclusion could lead to problems with accuracy of the newly modeled systems.

Some later works go on to show the difference observed when modeling the mushy-zone constant in finned and un-finned systems, with Fadl and Eames [12] reporting a value of 5×10^5 as ideal for their un-finned model and Karami and Kamkari [22] reporting a value of 5×10^6 for their 3-finned model. These authors had similar setups with identical external geometry and PCM selection, the only difference being an isothermal wall temperature of 70°C for the former and 60°C for the later. The difference in reported mushy-zone constant proves that the addition of fins and/or the adjustment of boundary condition temperature have a notable effect on the proper selection of the mushy-zone constant, and as such making adjustments to an enclosure's geometry without proper validation could lead to errors in the collected results.

A different experimental/numerical study was completed by Arena et al [37] in which the paraffin RT35 was melted via outward melting in a finned annual enclosure, displayed in Figure 11. These authors stuck much closer to their experimental work when modeling, keeping the same geometry and number of fins. A 2-D axisymmetric assumption was made when setting up the system to reduce computation time, and the HTF flowing through the inner tube was set to be fully developed and tested as the two experimentally examined flow rates. To complete their validation, the authors graphed temperature versus time graphs during the charging and discharging processes via temperature probes set at a centered position in the PCM domain. Various mushy-zone constants were tested for both the laminar and turbulent experimental flow rates. These values were then compared to one another via melt-fraction versus time graphs and melt interface development plots to analyze the impact of the mushy-zone constant on this type of system.

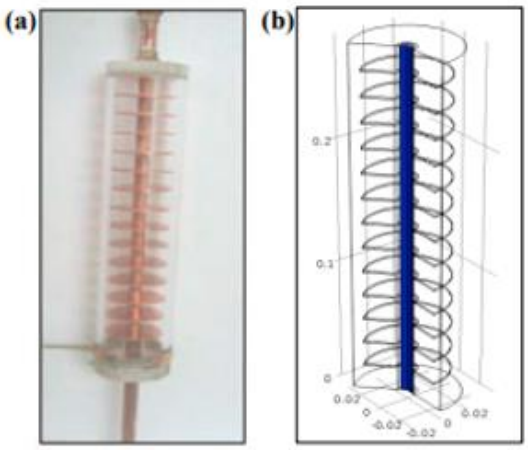

Figure 11: Annular finned heat exchanger setup [37]

The included works in this section provide reference for good and bad validation practices. When modeling an identical system to that conducted experimentally, authors should be able to recreate most every aspect of the setup and provide simulations that match near exactly to the experiments. From here, with changes to the mushy-zone constant conclusions can be established as to what parameters effect the value by referencing the previous relevant literature. However, with stark differences between the numerical and experimental work, as shown by Biwole et al [36], in an area that is known to alter the melt development, care needs to be taken to ensure accurate models are reported.

Investigations with Validation to a Standard Enclosure

Analysis and review of various pure numerical studies will offer examples of different validation practices, support the argument for proper care when validating to an

experimental system, and should help establish some further correlations of the mushy-zone constant with respect to system parameters.

Focuses on Inclination Angle

Similar to the current study, multiple numerical works have investigated the effect of inclination angle with an isothermal boundary condition and the enclosure geometry as defined in Shokouhmand et al.'s work [26], which for the purposes of this discussion will be called a "standard enclosure". The focuses of these studies have been directed at both the effect of inclination angle on the mushy-zone constant [12] [35], and the effect of inclination angle on the thermal and melting behavior of the PCM [33] [38].

The 2016 numerical investigation into the melting of lauric acid in a standard enclosure by Kheriabadi, Kabbara, and Groulx utilized COMSOL Multiphysics to model inclinations of 0°, 45°, and 90° from the horizontal in order to analyze the effect on A_{mush}. A similar work was completed in 2019 by Fadl and Eames using ANSYS Fluent and inclinations of 0° and 90° from the horizontal. The main difference found between these two papers comes with the method of validation. The former overlays melt curves at selected times to compare the melt front interface shapes between the experiments and simulations, and the latter uses melt fraction versus time curves as well as side-by-side image comparison for the melt front interface shapes. The COMSOL study notes the most accurate mushy-zone constant values for the vertical models as 1×10^6 and practically the same results between values of 1×10^4, 1×10^5, and 1×10^6 for the horizontal models [35]. In contrast the Fluent study notes the most accurate value of A_{mush} to be 5×10^5 for the vertical and $2*10^5$ for the horizontal [12]. However, it should be noted that

while Fadl and Eames reported the most accurate melt fraction versus time data at these values errors are seen in the interface shapes, especially with the horizontal simulations. Likewise, while the COMSOL horizontal simulations reported similar results for the tested mushy-zone constants, all values showed visible error when compared to the experimental data. Although the 2019 study does not investigate the effect of A_{mush} on a 45° inclined enclosure, the 2016 study shows considerable differences between the experimental and numerical melt front interface shapes at all tested values. If the systems were all set up properly and correct material property data was used, this brings into question whether or not COMSOL can accurately model inclined enclosures (specifically at the 45° inclination), and raises the question if Fluent would show similar issues modeling at this angle. This study acknowledges that the selection of the mushy-zone constant may not be able to be neglected when modeling inclined enclosures.

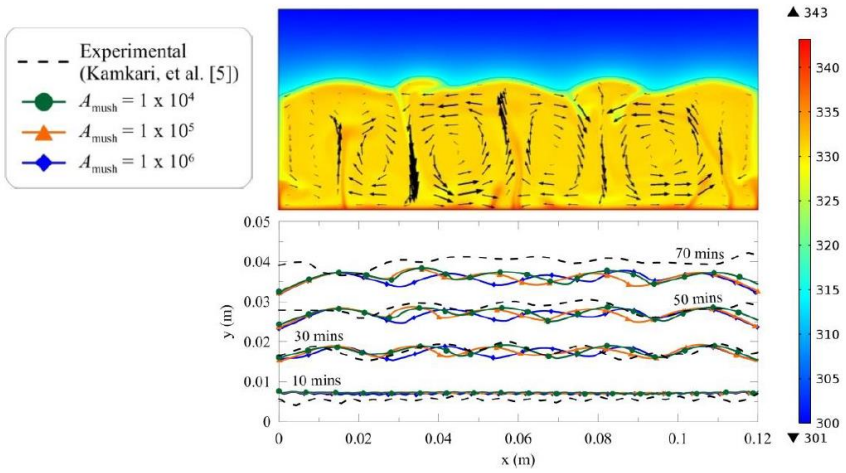

Figure 12: Validation of 0° inclined bottom heated enclosure to Kamkari et al.'s [27] experimental work [35]

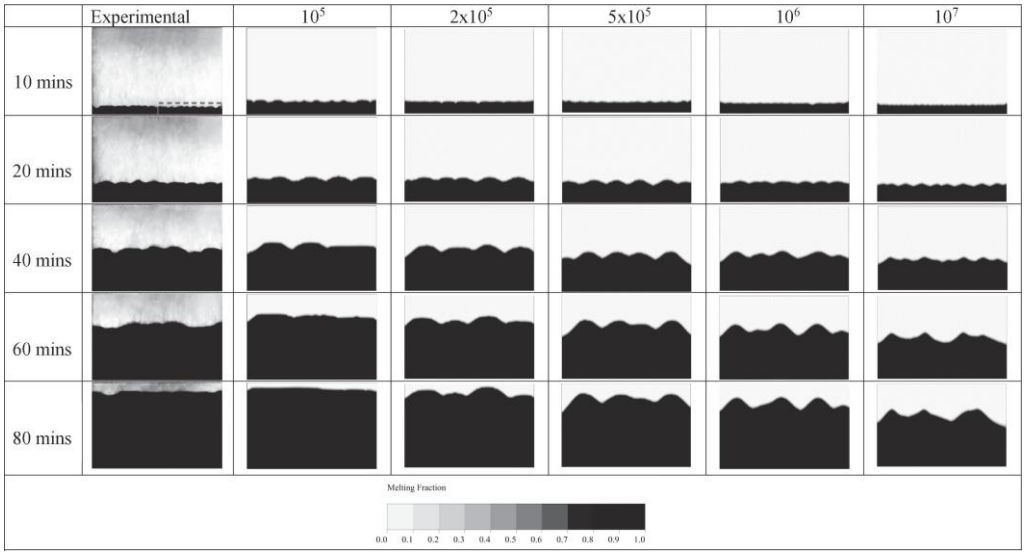

Figure 13: Comparison of Kamkari and Shokouhmand's [27] experimental work to different tested mushy-zone constants [12]

As mentioned earlier, other studies have investigated and discussed the effect of inclination angle on the thermal and melting behavior in a "standard enclosure" with lauric acid. The 2017 studies by Kamkari and Amlashi as well as Zeng et al. both use ANSYS Fluent to model their systems and validate to experimental melt fraction versus time data. Both studies used a single value of A_{mush} for all their simulated inclinations, with the former selected as 5×10^6 (without stated reasoning) and the latter selected as 10^6 (based on tested values of 1×10^5, 1×10^6, and 1×10^7). The former reported maximum deviations in melt fraction versus time of 6.5% [33], and the latter visibly looked similar but did not quantify their reported error [38]. When comparing melt front interface shapes, the results of Kamkari and Amlashi show differences between the interfaces of experimental and numerical images. This could indicate either issues in the meshes themselves, or the need for further investigation into proper validation methods to ensure accurate solid-liquid fraction as well as melt fraction interface shapes are reported. Zeng

et al. does not compare melt front interface shapes to their selected validation work, Kamkari et al.'s experimental study [27], and further goes on to introduce new differences between their presented work and the validation work. Their study greatly strays from the defined experimental inclination angles of 0°, 45°, and 90° from the horizontal, by introducing angles of 0°, 22.5°, 45°, 67.5°, and 90° from the vertical. These are completely new angles as melting is now from a top heated enclosure instead of the bottom heated shown in the experimental work. With the noted potential impact of inclination angle on the mushy-zone constant selection [12] [35], this change could very well lead to unknown levels of error in the simulated results, as the proposed angles stray completely from those that were validated to for selection of A_{mush}.

Apart from the 2017 work of Zeng et al [38], all the discussed papers in this section matched their numerical models to the experimental systems. This allowed for direct comparison and analysis into the effect of certain parameters and melt characteristics on the numerical models. In contrast, the work by Zeng et al strayed from proper validation procedures and based their results off a slightly different system entirely (with respect to modeled inclination angles). Should these variations in fact prove substantial and influential to the proper selection of the mushy-zone constant, their data could be determined incorrect. While some differences have been noted in selection of A_{mush} with respect to bottom heated inclination angles, it is unknown whether top heated inclination angles would report similar variations; and therefore, currently all that can be concluded is calling into question the accuracy of Zeng et al.'s validation methods.

Focuses on Alterations to Internal Geometry

Other numerical studies focused on the effect of the mushy-zone constant due to alterations in the internal geometry of the enclosures, and sometimes with the inclusion to different inclination angles as well. The studies in this section vary not only in aspects of the system but also the software used and selected PCM when compared to the validation experiments.

A few of the reviewed works studied both alterations to internal geometry with inclusion of different numbers of fins to the enclosure, as well as studying non-vertical inclinations. The 2016 work by Kabbara et al [17] investigated the melting of lauric acid in a "standard enclosure" in 1-finned and 3-finned configurations at a 90° inclination as well as un-finned configurations at 0° and 45° from the horizontal. These authors took care with their validation, using three different papers to match the melt front interface shapes for a vertical un-finned, vertical 1-finned and 3-finned, 45° inclined un-finned, and horizontal un-finned enclosures. Errors were noted in their COMSOL simulations, similar to those previously discussed [35], with mushy-zone constants varying the interfaces from the experimental results. While the heat transfer rate is significantly increased by the inclusion of fins to the system, the ideal values of A_{mush} for the un-finned vertical and finned vertical systems are reported as the same. It should be noted that these values do not exactly match the interface shapes with those of the experiments; and while the authors do not quantify the error, the visible difference could be enough to note potential errors either with the software or setup of the models, as displayed in Figure 14. Further acknowledgement into the limitations of the enthalpy-porosity model is visible in

the reported graphs, with solid PCM remaining at a higher point in the vertical enclosure due to the lack of modeling solid motion in the governing equations [21].

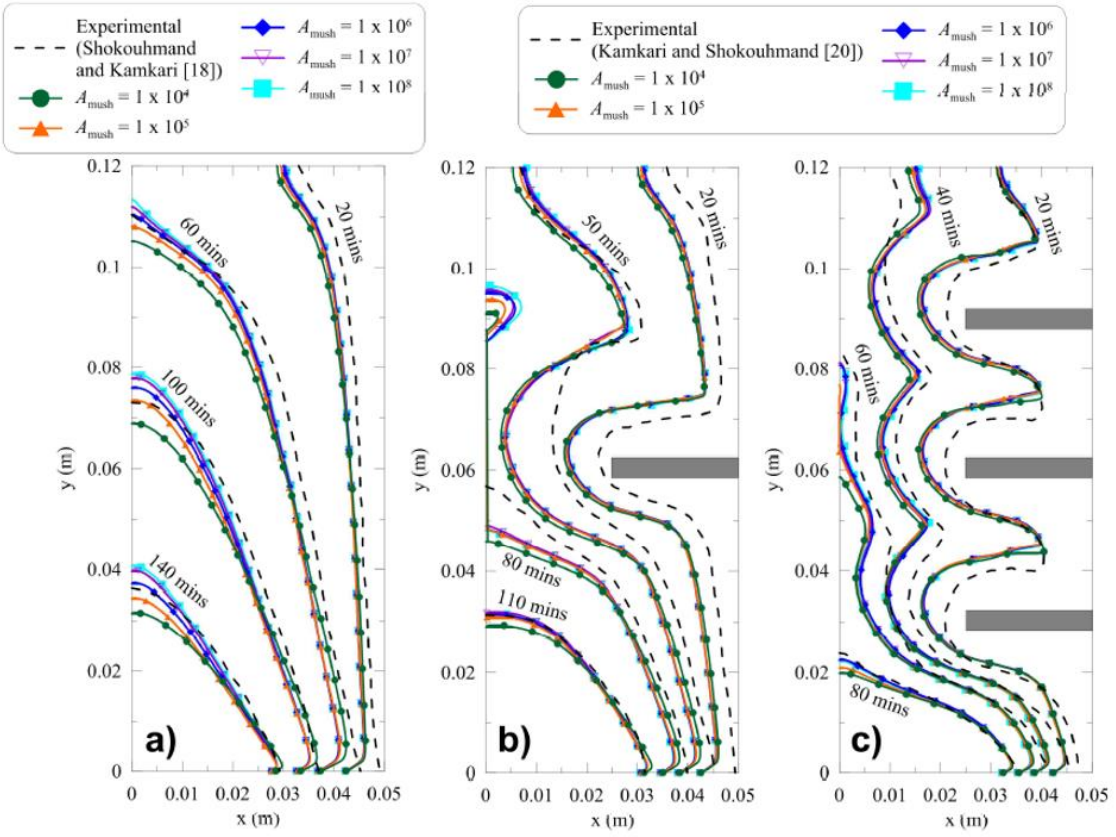

Figure 14: Validation of Experimental works of Shokouhmand and Kamkari [26] and Kamkari and Shokouhmand [28] to completed numerical models of Kabbara et al [17]

Different authors went on to simulate the melting of lauric acid in a standard enclosure using ANSYS Fluent with those of Abdi et al [25] as well as Karami and Kamkari [22]. The former authors investigated the effect of variation in the number of fins for a bottom heated enclosure, with 1-finned, 3-finned, and 5-finned modeled systems of varying lengths. Validation is completed to an un-finned horizontal enclosure with bottom heating, which could call into question whether the inclusion of fins would

affect proper selection of a mushy-zone constant for this configuration. While the effect of A_{mush} has been studied in the vertical finned enclosure, the differing development of the natural convection flows in a horizontal enclosure could lead to potential differences when correctly selecting a value, as shown in the previously discussed un-finned studies [12]. Although Fadl and Eames [12] show that the difference in the correct values for A_{mush} in vertical and horizontal enclosures is not incredibly large, the displayed melt fraction versus time results indicate that it could have serious implications on the accuracy of the simulations if improperly selected. Furthermore, visible errors in the solid motion are displayed in Abdi, Martin, and Chiu's [25] melt fraction contours, with solid being suspended in the liquid PCM and not falling due to gravity.

Karami and Kamkari [22] model 1-finned and 3-finned systems at inclinations of 0°, 45°, 90°, 135°, and 180° from the horizontal. These authors validate to the previous experimental work of Kamkari and Groulx [29] which investigated the melting of lauric acid in a standard enclosure at inclinations of 0°, 45°, and 90° from the horizontal in 1-finned and 3-finned enclosures. Validations of the melt front interface shapes show visible similarities, however, with the new investigated angles of 135° and 180° it is unknown whether these would affect selection of A_{mush}.

The desire to explore the impact of fin size and shape was continued with focus to fin aspect ratio [39], fin position and shape [40], and investigations into upward and downward stepped fins [41]. These works all note the effect of thermal behavior and melting characteristics on their given changes to a simple finned system, but without proper accompanying experimental data for validation these could contain errors due to

variation in development of convection currents and thus impact the accuracy of the melt front interface.

The vertical orientation for un-finned and straight-rectangular finned enclosures has been noted to have different ideal mushy-zone constant values [12] [22], leading to the belief that even with validation to straight-rectangular finned experimental data errors could be present in the reported data due to changes in the flow of natural convection currents within the enclosures; however, as previously mentioned differences in selected boundary condition temperature of the cited works could prove significant enough to change the accurate mushy-zone constant value. Although these authors provide interesting insight into the effect different fin configurations has on the melting characteristics within the enclosure, without properly ensuring that the phase change and natural convection are being modeling correctly melt times and interface shapes could likely contain inaccuracies.

Greater errors in validation procedures are visible in the works of Biwole et al. [42] and Tang et al [43]. The former work goes on to validate their numerical model by recreating experiments completed by Shokouhmand and Kamkari [26] as well as comparing to a numerical benchmark set by Betrand et al [44]. With the correct system adjustments and material property setup, these validations could confirm that their numerical procedure is accurate. However, given the great differences compared to their respective validation works it would not confirm whether or not their numerical data is accurate to an experimental counterpart.

The former does note that the selected mushy-zone constant is based on a past work by Biwole, Eclache, and Kuznik [36]; however, when reviewing this paper the

authors state that the “value is chosen arbitrarily high”, and no further analysis is completed in comparison to the experiments. It has been shown in all of the previously discussed works that small variations in the value of A_{mush} can have great effect on the accuracy of reported numerical results and choosing this value should not be at random with no reference to experiments for validation [12].

The later authors, Tang et al [43], also seem to validate their numerical process without validating the actual system that is being modeled. They recreate the experimental study and match the solid-liquid interface with that of Shokouhmand and Kamkari’s previous work [26]. This system uses a different PCM as well as a different geometry entirely, as rectangular instead of shell-and-tube. Further temperature analysis and validation is completed to a previous shell-and-tube study by Longeon et al [45], however this study uses a different PCM than that seen in Tang et al.’s paper. The last major issue with this study comes in the selection of their mushy-zone constant. The authors state the value was collected from a previous work by Ye et al [46], however this study uses a material with different reported properties than the RT50 selected by Tang et al. With the PCM itself having great impact on the accurate selection of the mushy-zone constant, the differences in validation and the numerical model are not trivial and could again lead to significant errors in the reported melt front interface and total melt time data.

Focuses on Differing Boundary Conditions

Few of the reviewed works investigated the effects of a constant heat flux boundary condition, only one of these validated primarily to experiments that used a standard enclosure. The work of Fadl and Eames [14] studied the effect of different constant heat flux boundary conditions on the melting of lauric acid using ANSYS Fluent. While the authors note melting characteristics of the simulations, they validated to the experimental work of Shokouhmand and Kamkari [26] which instead uses an isothermal boundary condition. From the reviewed literature it is unknown whether this difference in boundary conditions would directly impact proper selection of the mushy-zone constant, but it very well could have significant effect.

Significance of the Discussed Validation Works

Many studies have been referenced and analyzed with respect to their validation procedures and accuracy, some of which can be found in the following table with reference to the author's found values of A_{mush} and accompanying validation works. The goal of this was to address the significance of proper selection of the mushy-zone constant and justify why correlations and understanding of how different changes to system parameters (geometry, inclination, boundary condition) affect this value. As mentioned, some of these still do not have a defined relation as to whether they will affect the value's selection. However, future studies into how changes in the system alter the accuracy of the models will hopefully help to establish more accurate simulations that will not require accompanying experiments to ensure proper validation.

Moving on into the significance of this in the presented work, numerical simulations were completed with accompanying experimental and material property data collection for validation. The study of a new PCM, PureTemp 37, was used with a standard enclosure at differing inclination angles and isothermal wall temperatures to directly compare the collected results to those of the previously discussed lauric acid studies. From a validation standpoint, this study should help define the significance of validating with the proper PCM and give further understanding of how mushy-zone constant selection is impacted by inclination and wall temperature.

Study	Type	PCM	Geometry	Boundary Condition	Amush	Validation
Sparrow 1982	Experimental	Paraffin Wax	Cylinder	Isothermal wall	X	X
Gau 1983	Experimental	n-Octadecane	Rectangular	Isothermal wall	X	X
Gau 1985	Experimental	Gallium	Rectangular	Isothermal wall	X	X
Shokouhmand 2013	Experimental	Lauric Acid	Rectangular	Isothermal wall	X	X
Kamkari 2014	Experimental	Lauric Acid	Rectangular/Finned	Isothermal wall	X	X
Kamkari 2014	Experimental	Lauric Acid	Rectangular/Inclined	Isothermal wall	X	X
Kabbara 2016	Numerical	Lauric Acid	Rectangular/Finned/Inclined	Isothermal wall	Varying based on setup	Shokouhmand 2013
Kheriabadi 2016	Numerical	Lauric Acid	Rectangular /Inclined	Isothermal wall	Varying based on setup	Skhouhmand 2013
Zeng 2017	Numerical	Lauric Acid	Rectangular /Inclined	Isothermal wall	$1*10^6$	Kamkari 2014
Kamkari 2018	Experimental	Lauric Acid	Rectangular/Finned	Isothermal wall	X	X
Fadl 2019	Numerical	Lauric Acid	Rectangular	Constant heat flux	$5*10^5$	Shokouhmand 2013
Abdi 2019	Numerical	Lauric Acid	Rectangular/Finned	Isothermal wall	$1*10^6$	Kamkari 2014
Fadl 2019	Numerical	Lauric Acid	Rectangular/Inclined	Isothermal wall	$5*10^5$	Shokouhmand 2013 and Kamkari 2014
Karami 2019	Numerical	Lauric Acid	Rectangular/Finned	Isothermal wall	$5*10^6$	Kamkari 2018
Nakhchi 2020	Numerical	Lauric Acid	Rectangular/Stepped Fins	Isothermal wall	$5*10^6$	Kamkari 2018 and Karami 2019
Bhattacharjee 2021	Numerical	Lauric Acid	Square	Isothemral wall	$1*10^5$	Shokouhmand 2013
Oliveski 2021	Numerical	Lauric Acid	Rectangular/Finned	Isothermal wall	$1*10^{11}$	Kamkari 2014
Tang 2021	Numerical	Rubitherm 50	Cylinder/Finned	Isothermal wall	$1*10^5$	Shokouhmand 2013

35

Chapter III

Methodology

Experimental Setup

Figure 15 shows a schematic of the setup used for all the tested cases in this study. The system consisted of acrylic rectangular enclosure, a constant temperature bath (Anova Model A40), an aluminum heat spreader, and a computer and camera. The rectangular enclosure had interior dimensions of 50×120×120mm, to house the PCM PureTemp 37 (PureTemp LLC, Minneapolis, MN), and 25mm thick walls (Figure 15). To confirm all walls of the enclosure acted as adiabatic foam insulation was placed on all walls around the enclosure, excluding the one facing the camera.

Within the system, two loops were added to circulate fluid in and out of the constant temperature bath, indicated by the red lines in Figure 16. The flow through the system is shown by the arrows on the flow loops. At the start of each experiment this was used to ensure the bath reached the desired test temperature prior to flowing the heat transfer fluid through the heat spreader. After the desired temperature was reached, the outer loop was turned on by means of two three-way L-port valves to allow flow through the heat spreader and melting of the PCM to commence.

The camera was mounted on the experimental apparatus in a stationary position that would remain constant for all melts. As shown in Figure 16, the camera was facing the one side of the PCM container, perpendicular to the heat transfer flow from the heat spreader to the PCM. This allowed for imaging of the melt development. In accordance with past literature, and the later accompanying numerical simulations, this flow and melt

front was assumed to be two-dimensional with little variation along the length of the PCM container [32].

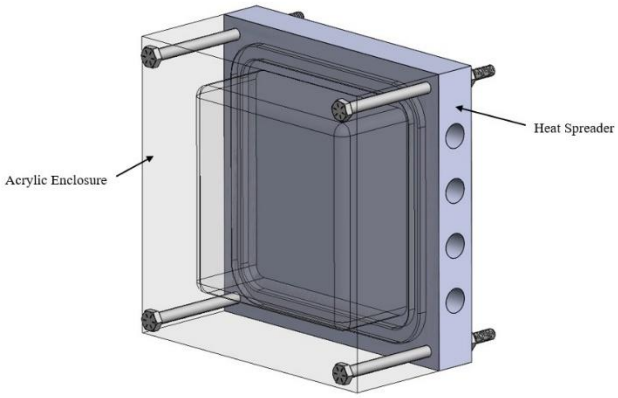

Figure 15: Experimental Enclosure and Heat Spreader Model

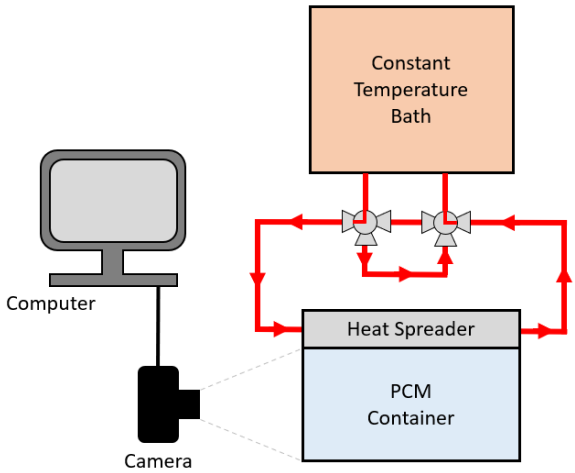

Figure 16: PureTemp 37 Experimental Setup

A prior series of tests were completed to verify the assumed isothermal wall boundary condition was accurate, to verify the sensor in the constant temperature bath

was accurate, and to determine any other potential causes of error during the experiments. Four type T thermocouples were used at the stated locations in Figure 17, with a determined accuracy of ± 0.1°C. The accuracy of the temperature display on the bath was confirmed with the T4 thermocouple, given it was very close to the bath itself and minimal heat loss to the environment through the plastic tubing would be experienced as this position in the system. Data was reported within 0.1°C to that of the bath's internal sensor, and with constant ambient temperature reported during the test via T2 the temperature display on the bath was confirmed accurate. Thermocouples were placed at the inlet and outlet of the heat spreader, shown with T1 and T3, to determine if there was any temperature drop across it. This would determine whether an isothermal boundary condition could be assumed. Differences were minimal, reporting less than 0.1°C, verifying the use of an isothermal boundary condition. The T1 thermocouple was also used to determine temperature loss to the environment via the plastic tubing. It was determined that a 1°C temperature drop occurred between the constant temperature bath and the inlet of the heat spreader. To account for this all the conducted melts were set 1°C higher than the desired test temperature (to 48°C and 58°C).

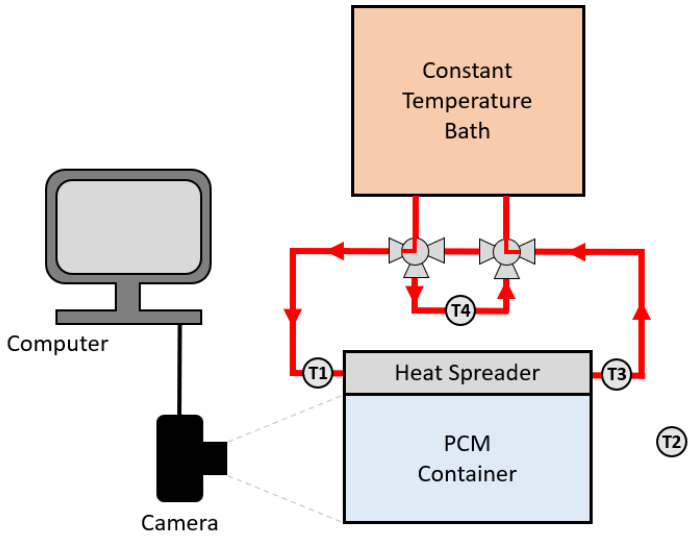

Figure 17: PureTemp 37 Initial Experimental Setup with Thermocouples

The main area of error seen in the experiments was glare on the face of the enclosure due to changes in ambient lighting conditions. Differences were minimal, but to remedy this issue a small photo booth was added around the system to reduce these lighting variations.

Initial Setup for Melts

Prior to the melts, solid PureTemp 37 was placed into a beaker and melted in an oven. This was then poured into the rectangular enclosure. This was left to solidify at the defined inclination angle of 180° to ensure not PCM leaked from the container. Once completely solidified, a chemical resistant Viton o-ring was placed in the gland of the enclosure and it was bolted onto the aluminum heat spreader. The o-ring ensured that no PCM would leak from the PCM container during the melting and solidification processes. The bath was turned on, with flow through the outer loop, and was set to 57°C. This was aimed at relocating any air in the enclosure to the top corner opposite the camera and heat

spreader. Although the amount of air in the system was minimal, if the air was left in its original position differences in total melt time were noticed. To adjust the enclosure and ensure uniformity for future melts, the intended corner was elevated to a selected height for this and all future melts. Once the remaining air in the system was relocated to the correct corner of the enclosure, melts and data collection were ready to begin.

Experiments were completed at inclination angles 30°, 45°, 60°, and 90° at both 47°C and 57°C. The inclination angle θ is defined in Figure 18, with the isothermal heat spreader indicated by the red line. Based on the displayed setup, gravity would be acting downward and perpendicular to the horizontal line (θ = 0°) in Figure 18. In preparing the melts the enclosure was oriented on the adjustable experiment apparatus to the desired angle and checked with a digital angle gauge (Wixey Model WR300 Type 2). An accuracy of ±1° was allowed, with resolution of the selected angle gauge reported at 0.1°. In adjusting the experimental apparatus, the heat spreader, PCM container, and camera all moved in unison which ensured standardization of the imaging throughout all tested inclinations.

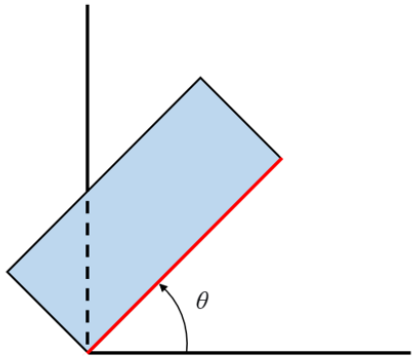

Figure 18: Experimental Angle Definition

Experimental Procedure

Experiments were started by setting the bath to the desired temperature and inclination angle, with flow running through the inner loop. Upon reaching the test temperature the camera and computer were turned on and set up to start data collection at five-minute intervals for all completed melts. This interval value was selected to ensure sufficient resolution for the melt fraction versus time curves were achieved without the over collection of data. The flow was then switched to run through the heat spreader via the outer loop and data collection was started. This process was let to continue autonomously until phase change of all the material was complete. At this point, the data collection was stopped, the bath was turned off, and the selected corner of the enclosure was elevated to properly place any air in the system for the following melt. The PCM was let to cool and solidify, and a visual inspection was completed to confirm correct placement of any air in the system. Following this a new melt was started with the selected testing conditions. This process was repeated for all inclination angles at 47°C and 57°C.

Experimental Post-Processing

To complete post-processing of the images MATLAB R2020a was used. Figure 19 displays the steps for post processing, from the original image taken by the camera to the returned solid percentage. Images were loaded into the workspace (1) and were cropped and altered to only show the area of the enclosure with PCM (2). A function was then used to convert the images into black-and-white based on the determined mask value (3). This value varied for each melt based on the present ambient conditions and was

determined through selecting a photo at the start of the melt (100% solid), the end of the melt (100% liquid), and at least two images during the melt (approximately 50% liquid). Values were tested to verify that the generated images were accurately representing the solid and liquid regions. With a clear distinction between solid and liquid in the images, an average was taken to determine the fraction of liquid and solid in the container corresponding to black and white pixels, respectively. This value represented the solid fraction at each interval in the melt (4). The determined cropped dimensions of the image and mask value were then used with MATLAB's image batch processor app to collect liquid fraction data for all images throughout the given melt. This tool allowed for the output of solid fraction and respective time data to Microsoft Excel. The data was then be converted to liquid fraction by subtracting the solid fraction from one and melt fraction (liquid fraction) versus time graphs were created.

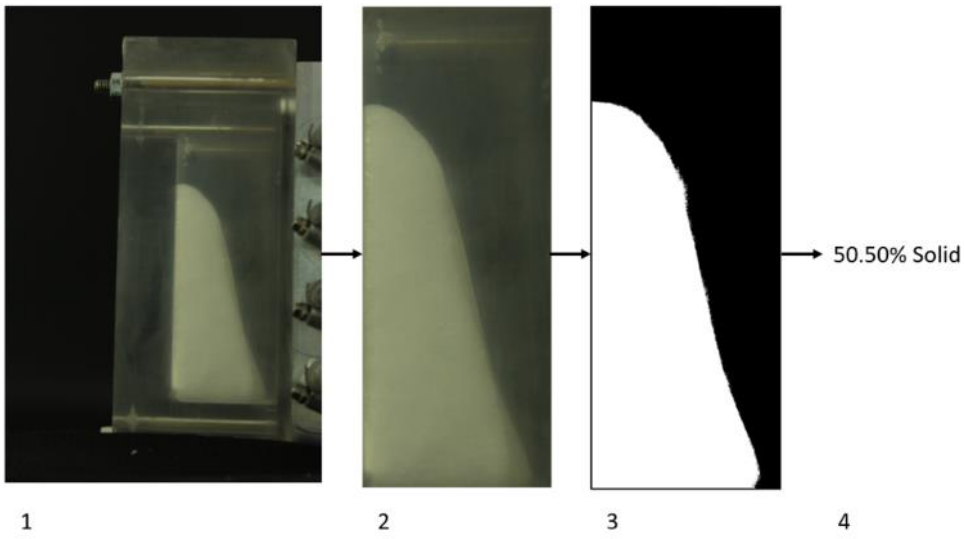

Figure 19: Experimental Image Processing Steps

This process was repeated, and the same crop dimensions and mask value could not be used for all melts, as there were some slight differences in ambient conditions and camera setup between the melts. Although the experimental apparatus adjusted the whole system together, small variations between the angle of the camera with reference to the PCM container as well as distance between the camera and PCM container were observed.

Material Properties

Table 1 contains much of the collected material property values for PureTemp 37, excluding the liquid density data and the viscosity data. This data can be found in Figure 20 and Figure 22, respectively. In the material property table, the subscripts “s” and “l” represent the solid and liquid states of the material.

Table 1: PureTemp 37 material property data

T_s/T_l	310.6/315 K
h_{sl}	195960 J/kg
ρ_s	910 kg/m^3
cp_s/cp_l	2400/3090 J/kg-K
k_s/k_l	0.233/0.194 W/m-K

Solid Density

Testing for solid density was completed with an attachment for the Mettler Toledo Analytical Balance. The weight of the sample in air was compared to the weight of the sample in an auxiliary liquid, in this case distilled water, to determine the solid's density. Following the formula shown below, with *A* representing the weight of the sample in air,

B representing the weight of the sample in distilled water, ρ_o representing the density of distilled water (at 21°C, the ambient temperature) in accordance with a provided table and given air density of 0.0012 g/cm^3 as provided in the given documentation for the balance. A total of five tests were completed, and the average of the collected solid density values is shown in Table 1.

$$\rho_s = \frac{A}{A-B} \times (\rho_o - \rho_l) + \rho_l \quad (8)$$

Liquid Density

Temperature dependent liquid density data collected with a pycnometer and a microbalance through a collaboration with the University of Cincinnati. Their corresponding collected data for the liquid density is shown in Figure 20.

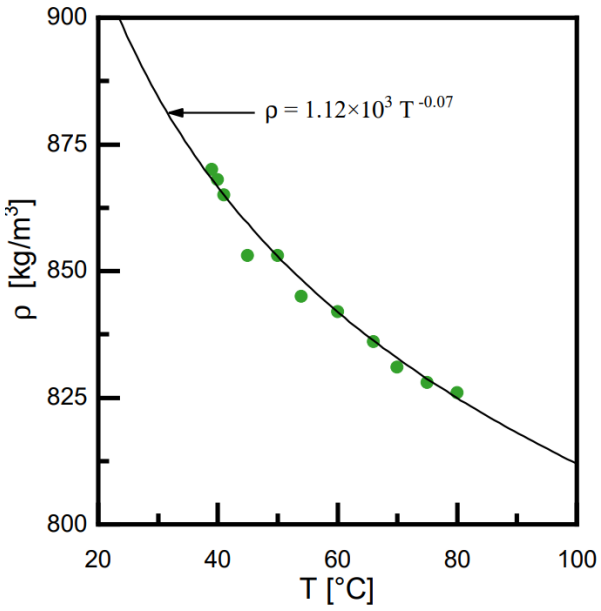

Figure 20: Temperature dependent density data collected by the University of Cincinnati

Solid Thermal Conductivity

Solid thermal conductivity of the PCM was measured using the Thermtest TLS-100 portable meter and standard 100mm needle probe, which follows ASTM D5334-14 “Standard Test Method for Determination of Thermal Conductivity of Soil and Soft Rock by Thermal Needle Probe Procedure”. In this method approximately 200mL of PCM was melted and poured into a hollow aluminum cylinder with a diameter of 5.08cm and a height of 10.16cm. The probe was inserted into the liquid PCM and left until the PCM fully solidified and reached ambient temperature. A total of five measurements were then completed and the average of the collected solid thermal conductivity values is shown in Table 1.

Liquid Thermal Conductivity

The liquid thermal conductivity was measured using a transient plane source (TPS) by Hot Disk Instruments (specifically the TPS 2500S) with a kapton-insulated sensor and a liquid sample holder with an insert for liquid bath. Liquid PCM was inserted into the sample holder via one of the three tubes until the chamber was full. The sample holder and insert were then placed into a constant temperature bath at the temperature 55°C. A thermocouple was placed on the sample holder to confirm when it reached steady state, matching the bath's temperature. The sensor was connected to the TPS and the environment temperature was set to 51°C, accounting for some heat loss to the room from the top of the sample holder. Five tests were completed, allowing the system twenty minutes of rest time between each, and the average of collected liquid thermal conductivity values is shown in Table 1.

Properties Collected from Differential Scanning Calorimetry

The melt temperature in terms of onset and endset temperatures, the latent heat of fusion, and solid and liquid specific heats for PureTemp 37 were determined through the use of a DSC (DSC 3 STARe, Mettler Toldeo, Columbus, OH). ASTM E1269, "Determining Specific Heat Capacity by Differential Scanning Calorimetry" was followed with adjustments to the heating rate. A small sample of PCM was placed in a 40µl aluminum crucible. A method was followed wherein the sample was initially held at 10°C for 10 minutes and then heated to 80°C at a rate of 2°C/min. This temperature was held for 10 minutes. This method was repeated a second time to ensure the PCM properly situated in the bottom of the crucible without any gaps affecting the thermal contact and overall results of the test. The collected results for the DSC are displayed in Figure 21.

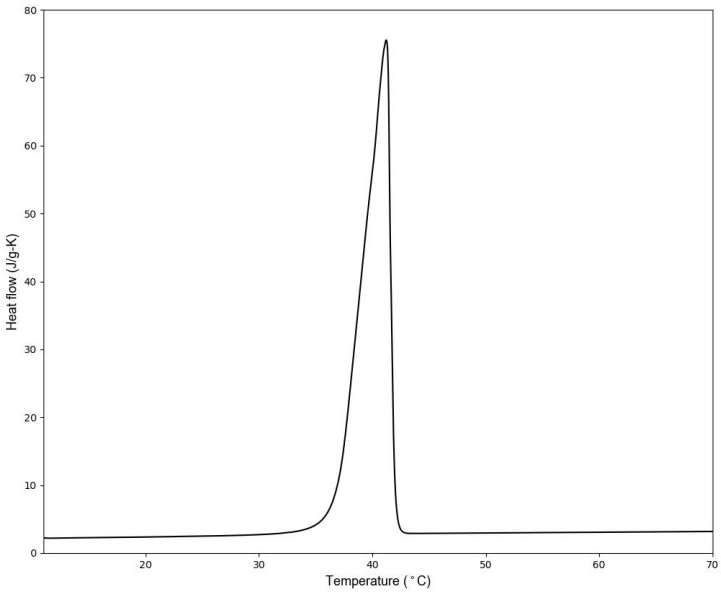

Figure 21: DSC Curve of PureTemp 37

Temperature Dependent Viscosity

Temperature dependent viscosity data collected with a Ubbelohde viscometer (Cannon Instrument) according to ASTM D445 through a collaboration with the University of Cincinnati. The corresponding collected data for the dynamic viscosity is shown in Figure 22. This data was collected and determined through measured kinematic viscosity and density data and converted to dynamic viscosity data prior to input into the numerical software.

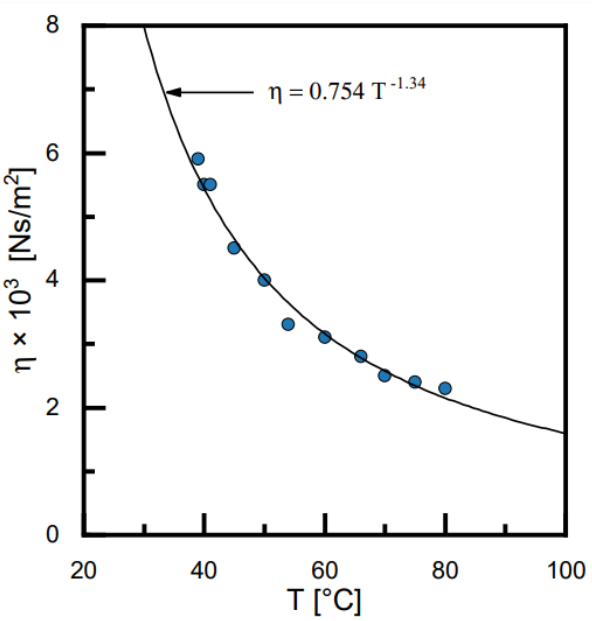

Figure 22: Temperature dependent viscosity data collected by the University of Cincinnati

Numerical Setup

Governing Equations

Through ANSYS Fluent, the enthalpy-porosity technique was used in modeling the melting process of the PCM in accordance with the different orientations and temperatures completed in the experiments. Instead of explicitly tracking the melt interface, this method determines the liquid fraction of each cell, between values of 1 (liquid) and 0 (solid) within the mesh to determine the melt front progression. The modeled PCM was assumed to be incompressible with constant thermophysical properties at both its solid and liquid states. The modeled enclosure was assumed to be completely full of PCM, neglecting any volume changes upon phase transition to liquid. The governing equations for the 2-D transient laminar models are defined below. Equations (10), (11), (12), (13), (14), and (15) correspond to the continuity, x-momentum, y-momentum, energy, and source terms for the x-momentum and y-momentum equations, respectively.

$$\frac{\partial u}{\partial x}+\frac{\partial v}{\partial y}=0 \tag{10}$$

$$\rho\left(\frac{\partial u}{\partial t}+u\frac{\partial u}{\partial x}+v\frac{\partial u}{\partial y}\right)=-\frac{\partial P}{\partial x}+\mu\left(\frac{\partial^2 u}{\partial x^2}+\frac{\partial^2 u}{\partial y^2}\right)+\rho g\cos(\theta)+S_x \tag{11}$$

$$\rho\left(\frac{\partial v}{\partial t}+u\frac{\partial v}{\partial x}+v\frac{\partial v}{\partial y}\right)=-\frac{\partial P}{\partial y}+\mu\left(\frac{\partial^2 v}{\partial x^2}+\frac{\partial^2 v}{\partial y^2}\right)+\rho g\sin(\theta)+S_y \tag{12}$$

$$\frac{\partial(\rho H)}{\partial t}+\frac{\partial(u\rho H)}{\partial x}+\frac{\partial(v\rho H)}{\partial y}=\frac{\partial}{\partial x}\left(k\frac{\partial T}{\partial x}\right)+\frac{\partial}{\partial y}\left(k\frac{\partial T}{\partial y}\right) \tag{13}$$

$$S_x = -\frac{(1-f)^2}{f^3+\varepsilon} A_{mush} u \quad (14)$$

$$S_y = -\frac{(1-f)^2}{f^3+\varepsilon} A_{mush} v \quad (15)$$

Meshing Setup

The meshes were created using a structured grid in Pointwise V18.4R2. Cells were set with a 1:1 aspect ratio, following much of the reviewed literature, and the system was oriented as shown in Figure 23. Two wall conditions were selected with the two vertical sides and the top being grouped as one boundary condition, and the bottom wall being set as the other. These would represent the adiabatic and isothermal wall boundary conditions, respectively. Figure 23 shows a visual of the boundary conditions. It should be noted that all created meshes and models were 2-D, based on previous studies into the effects of modeling 2-D versus 3-D [32], and based on much of the reviewed simulations using the standard enclosure.

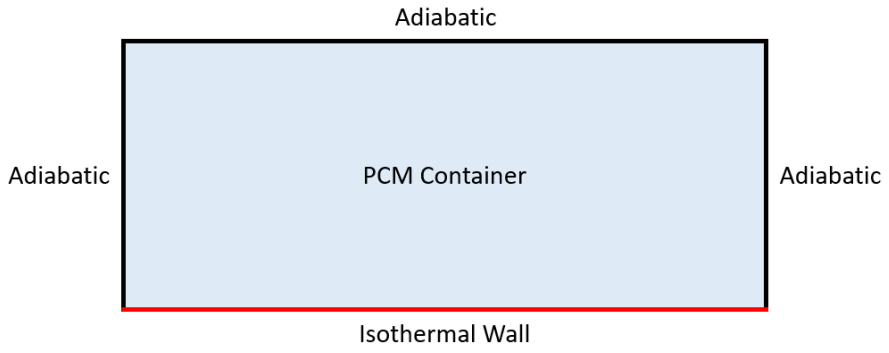

Figure 23: Numerical boundary condition setup

Initial meshes were created and tested with 15,360, 24,000 and 34,560 nodes. These provided accurate results in terms of melt fraction versus time graphs, when modeled, but displayed very linear interfaces when comparing the numerical melt front development curves to the experimental melt front images. In order to improve these results, finer meshes were created at 96,000 nodes; and this change and variation will be discussed further in the Numerical Results section.

Model Setup

The models were run using ANSYS Fluent 2020R2 on Embry-Riddle Aeronautical University's Cray CS400 supercomputer (Vega) to solve the aforementioned equations. Models were set to laminar flow with melting and solidification turned on. This software uses the enthalpy-porosity method [13] to model solidification and melting, and as such different mushy-zone constants were tested in comparison to the experiments to determine the most accurate choice. A new fluid material was added and modified to the collected material property data for PureTemp 37, outlined in Table 1. The pressure-velocity coupling was set to the SIMPLE scheme and the spatial discretization used least squares cell based for the gradient, PRESTO! for pressure, second order upwind for momentum and energy, and first order implicit for the transient formulation. Residuals were set to 1×10^{4}, 1×10^{6}, 1×10^{6}, and 1×10^{9} for continuity, x-velocity, y-velocity, and energy, respectively. The boundary conditions were adjusted, according to Figure 23, setting the adiabatic walls to a heat flux of zero and the isothermal wall to the respective test temperature in Kelvin. Given the orientation

of the enclosure within the mesh, x- and y-components of gravity acting on the enclosure were set relative to the desired orientation.

Mesh Independence Study

Mesh independence was evaluated by comparing the melt fraction versus time curves of the different sized meshes at an isothermal wall temperature of 57°C and inclination angle of 90°. These system parameters were selected and used for the mesh independence study, time-step independence study, and initial investigations into the mushy-zone constant, as in the reviewed literature the vertical orientations showed the best match to experimental data and the higher wall temperature allowed for a quicker computation time. Initially, the study was tested using the meshes displayed in Figure 24, and returned average percent differences of 2.8% between the 15,360 node mesh and the 24,000 node mesh, and 1.8% between the 24,000 node mesh and the 34,560 node mesh. These values were considered acceptable to state that mesh independence had been achieved, and the 24,000 node mesh was determined fine enough to proceed with further simulations at different angles and temperatures.

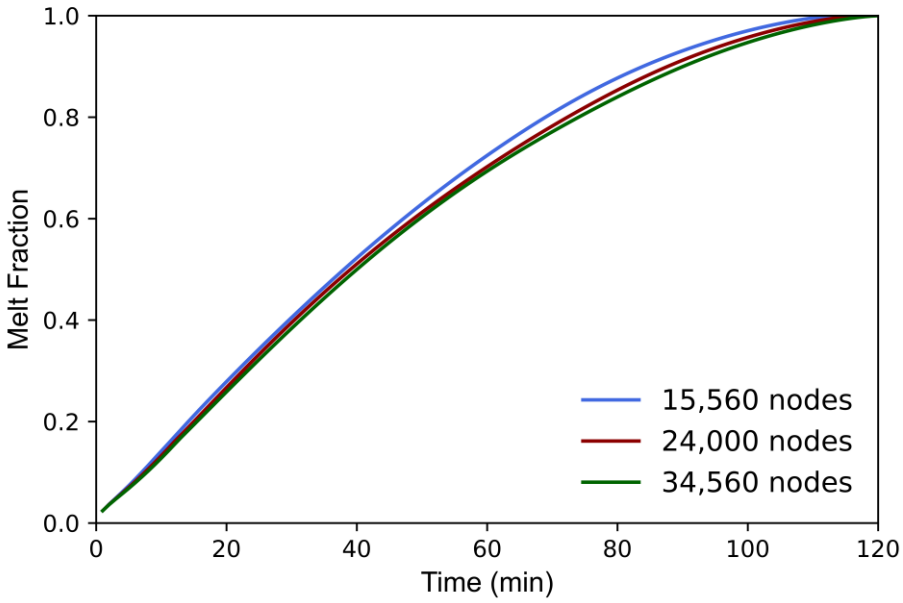

Figure 24: Mesh independence study

Time-Step Independence Study

Given the system was modeled as transient, a time-step independence was also necessary. Based on the mesh-independence study, the 24,000 node mesh was used to test time steps at 0.01, 0.05, and 0.1 seconds (with system parameters of 57°C and 90° inclination) through melt fraction versus time graph comparisons. These results are displayed in Figure 25. Analysis returned average percent differences of 0.01% between the 0.01 and 0.05 second time steps and 1.09% between the 0.05 and 0.1 second time steps. These values confirmed that time-step independence was achieved, and due to the minimal difference in computational expense the 0.05 second time step was selected and used for all the following simulations.

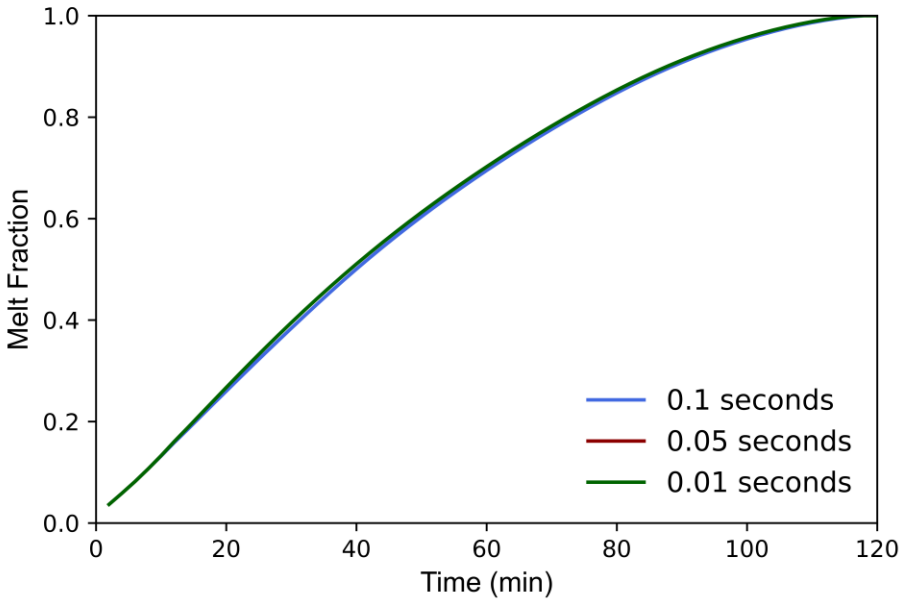

Figure 25: Time-step independence study

Numerical Procedure

Models with the previously discussed methods, mesh, and time-step were created at the 57°C wall temperature and 90° inclination to evaluate the most accurate value of the mushy-zone constant. At the 24,000 node mesh, values of 1×10^{5}, 1×10^{6}, 1×10^{7}, 5×10^{7}, 1×10^{8}, and 1×10^{9} were evaluated by changing the mushy-zone parameter input value within the solidification and melting tab in ANSYS Fluent. Initial comparisons and validation to the experiments was completed by solely using melt fraction versus time data.

Following the discussed literature, the most accurate value was then use for all the remaining test cases. These were created by varying the x- and y-components of gravity in the General tab in ANSYS Fluent, and by changing the constant temperature value setting for the isothermal boundary condition.

In order to run the simulations on Vega, batch and journal files were created to initialize and run each model. Limitations were present, as to complete each simulation the models needed to run for multiple days, requiring the continuation and editing of the journal files in accordance with the 24-hour limitation on the normal queue of the supercomputer.

It should be noted that initialization temperature of all the models was set to the room temperature in which the experiments were run (295 K), using the ambient T2 thermocouple data that had been previously collected. Also, the data was set to output a .dat file every 60 second of melt time. This would ensure smooth graphs were achieved for good comparisons to the experimental data.

Numerical Post-Processing

For each completed model, numerical post processing was completed using CFD-Post 2020 R2. The final .dat file was read and a melt fraction contour was taken to ensure the interior area was completely liquid. Once confirmed, an area average melt fraction was plotted over time, which could later be used for validation to the experimental data. The results were exported to Microsoft Excel where initial graphs and analysis were completed, followed by final graph construction in Python.

Further analysis into the melt front interfaces was completed by taking images of the melt fraction at different points in time. This was achieved by using the melt fraction contour and confirming the liquid percentage, after which an area average of the melt fraction was taken at that specific point in the melt. In the following Numerical Results

section, collected melt front images at 25%, 50%, and 75% liquid fraction for each of the completed models are compared to the experimental counterparts, respectively.

Chapter IV

Results

Experimental Results

The unedited experimental melt fraction versus time graphs shows three distinct regions of the melt. Displayed in Figure 26, specifically for the 47°C and 45° inclination case, the initial portion of the melt time shows minimal change in the overall melt fraction of the system. In all of the completed models this is followed by a near constant melting rate for the majority of the simulation time, and a gradual decrease as the majority of the PCM in the enclosure changes phase to liquid. These three regions on the following graph are separated by the two vertical black lines.

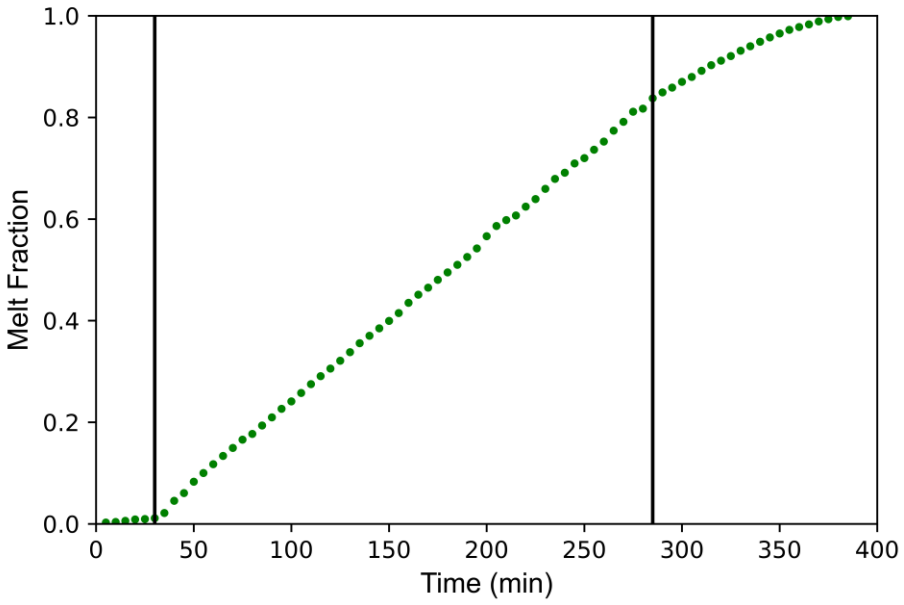

Figure 26: Unedited melt fraction versus time graph for 47°C at 45° inclination

The initial region is attributed a period of sensible heating until the PCM along the isothermal boundary condition reaches the melting temperature of the material

(37°C). The following linear portion contains both a short period of pure conduction until a small liquid region of PCM is established between the boundary condition and the remaining solid PCM. As this region grows so do the convection currents within the enclosure, leading to the melt being driven mainly by natural convection. The final discussed portion represents the weakening of convection currents, as the remaining PCM in the enclosure diminishes until the entire contents of the enclosure are liquid.

Since the period of sensible heating was not reproduced in the numerical simulations, this period of the experimental melts was excluded and melt fraction versus time comparisons started with the second region on the graph. In analyzing the linear region of the melt fraction versus time graph, Figure 27 shows melt front development images of the 47°C at 45° inclination at the given times from the start of the melt. The initial period of conduction in this region is illustrated with the earlier melt time images; and the displayed images start at 30 minutes to ignore the initial region of sensible heating during the melt.

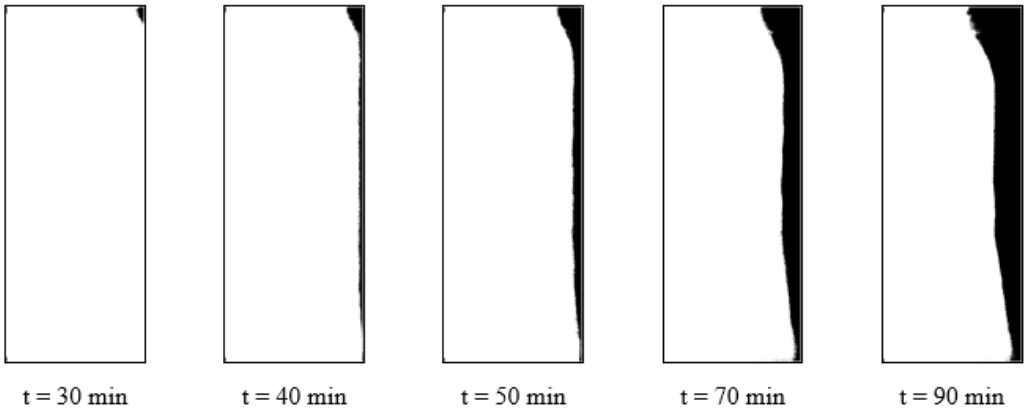

Figure 27: Conduction and convection identification for 47°C at 45° inclination

As the melt progresses the increased presence of natural convection currents are observed, with the later images showing a more uneven interface. This is a result of the liquid PCM being heated along the isothermal boundary condition, shown in Figure 28 by the red line, and being circulated within the enclosure, shown by the blue line. As this liquid is forced along the solid-liquid interface, more heat is dispersed into the upper portion of the enclosure causing an uneven melt front. Adjustments to the inclination of the enclosure, based on the given test case, also have drastic impact to the development of these convection currents and thus melt front interface shapes.

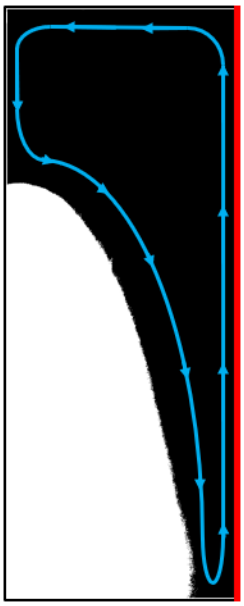

Figure 28: Natural convection circulation within enclosure

Figure 29 and Figure 30 show the final collected experimental data at all the studied inclinations for 47°C and 57°C, respectively. In agreement with the reviewed literature, increasing the temperature and/or reducing the inclination angle from the horizontal is shown to reduce the overall melt time.

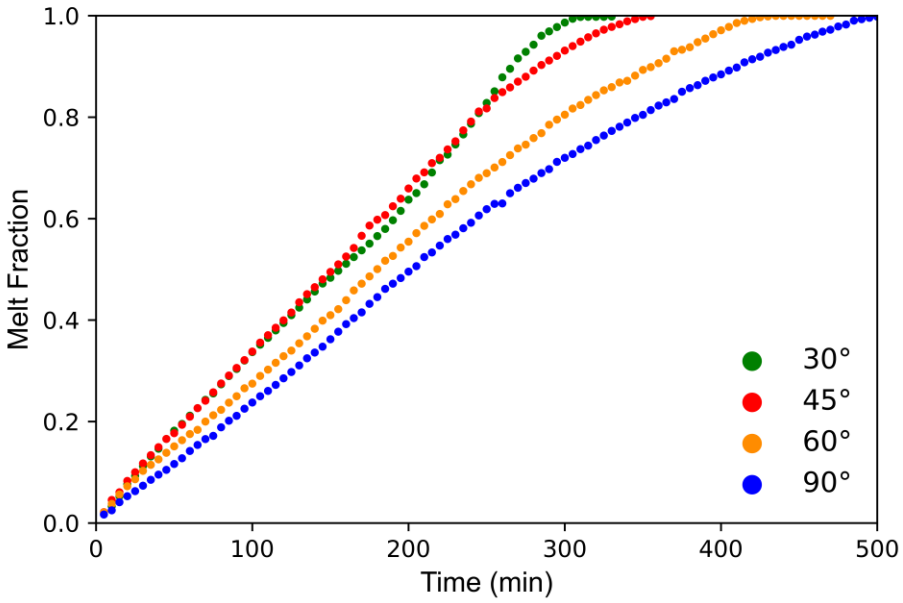

Figure 29: All experimental melt data at 47°C

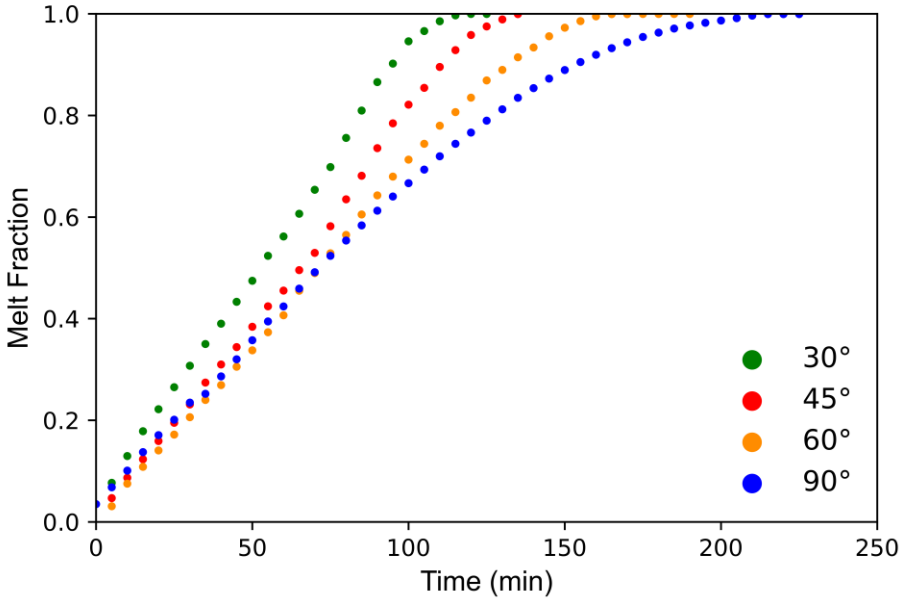

Figure 30: All experimental melt data at 57°C

As mentioned, adjustments into the inclination angle show significant impacts into the melt front interface shapes. Figure 31 and Figure 32 display the melt front images at 25%, 50%, and 75% liquid for all the tested angles and wall temperatures of 47°C and 57°C, respectively. As the angle becomes more horizontal, the observed solid-liquid interface becomes more nonuniform. This is easily observed in the 75% liquid images at 30° and 45° for both temperatures. The nonuniform interface is attributed to the development of natural convection driven vortices within the enclosure. The developments will serve as another good validation method when evaluating the melting of this material numerically.

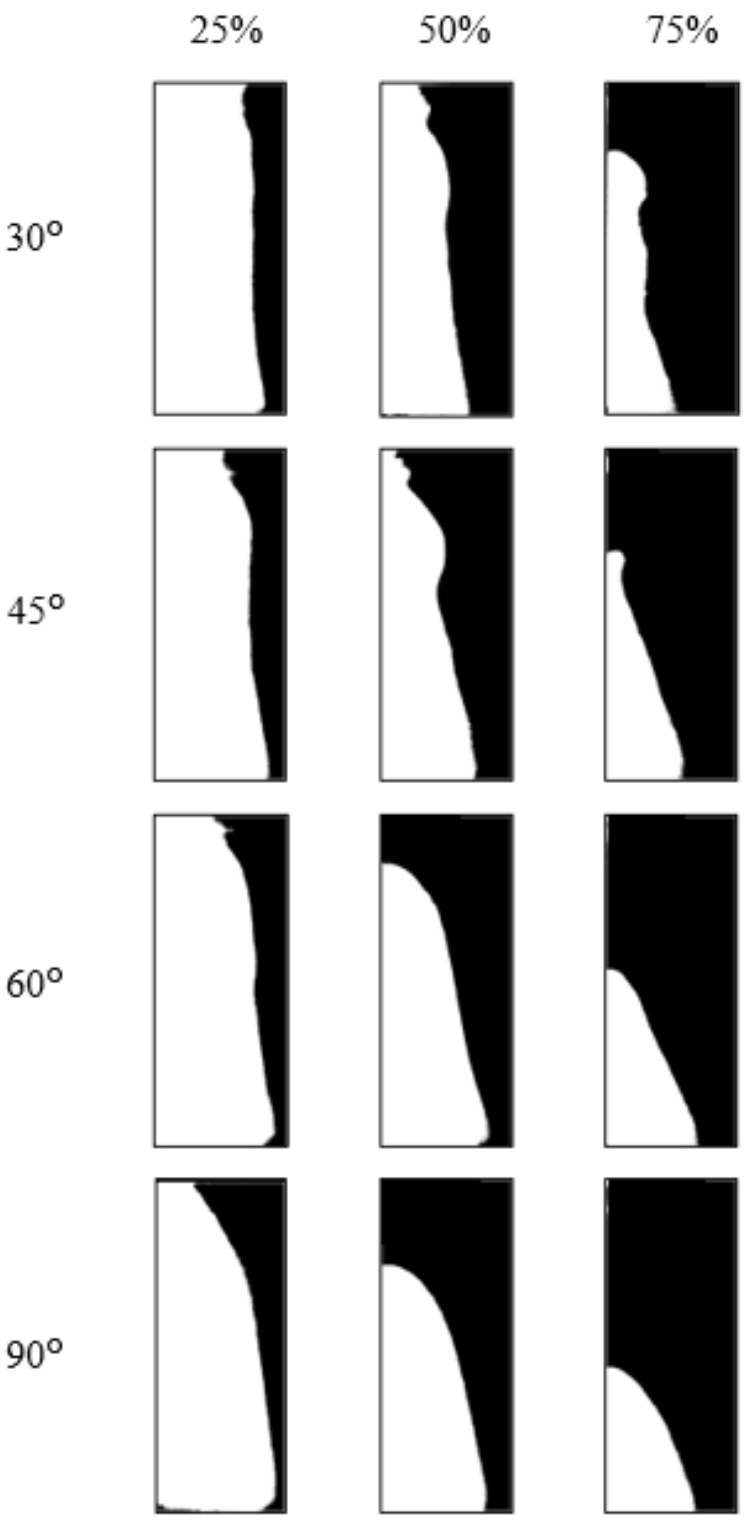

Figure 31: Melt front interfaces at liquid percentages at 47°C

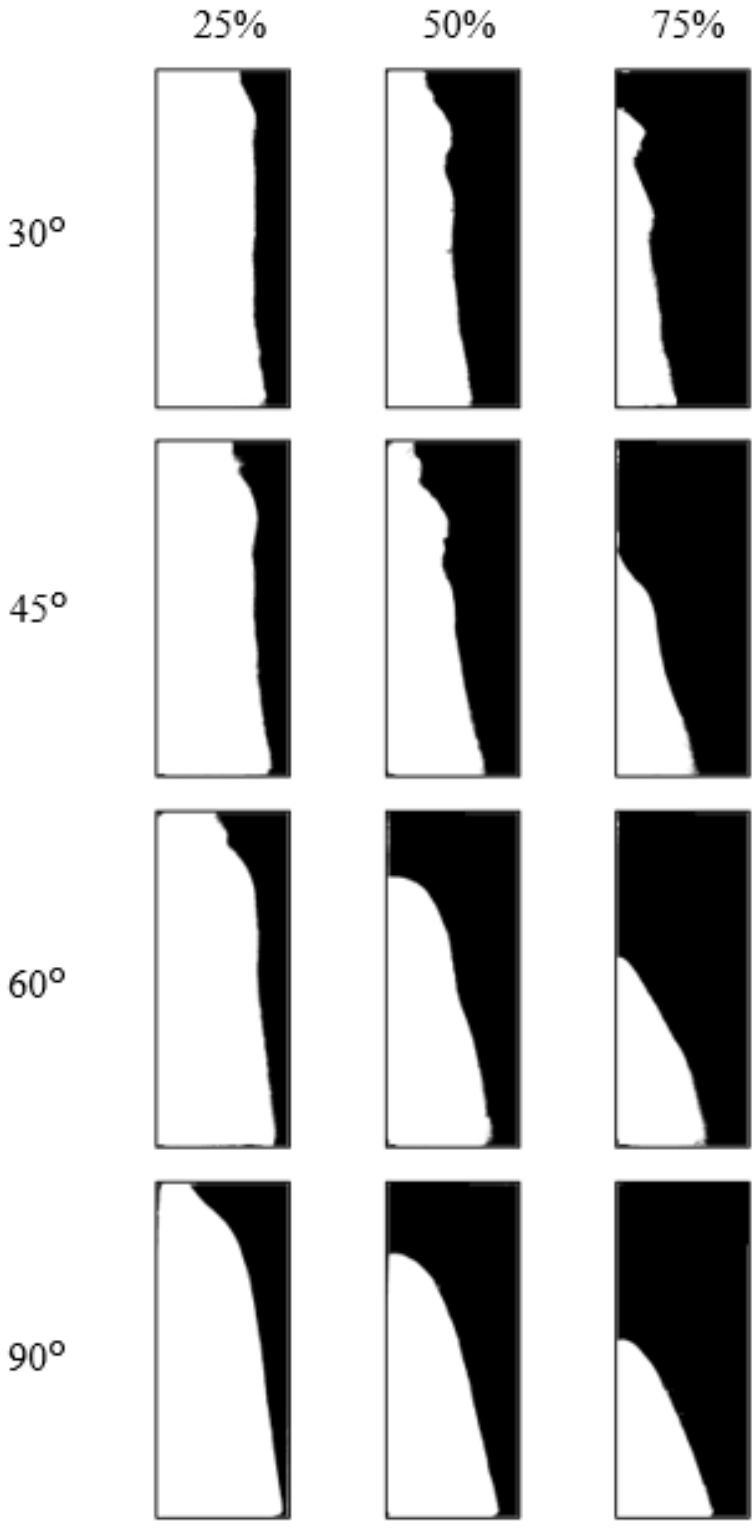

Figure 32: Melt front interfaces at liquid percentages at 57°C

Numerical Results

Discussed in the Mesh Independence Study section, two different sets of meshes were created and tested for comparison to the experimental data to evaluate impacts of setup variation. More specifically the mushy-zone constant and mesh fineness were explored when attempting to accurately numerically model at different inclinations and wall temperatures.

Initial Model Testing at 24,000 Nodes

Initial testing of the mushy-zone constant was completed at various values under the system parameters of 57°C and 90° inclination for the 24,000 node mesh, as seen in Figure 33. Average precent differences between the experimental and numerical melt fractions are provided in Table 2 for all tested mushy-zone constant cases. The data showed somewhat conflicting results. Greater accuracy for the melt fraction curves at a value of 5×10^7 with regards to total melt time was observed, in comparison to a lower average percent difference at 1×10^7 for much of the convection dominant middle region of the melt. Both values were selected for the setup of models and run at the various angles and wall temperatures. The aim of this would be to prove the sensitivity of this value, and as such how selection based on one system configuration would not be ideal for all system configurations.

Table 2: Mushy-zone constant study percent difference at stated A_{mush} values

A_{mush}	% Difference
$1*10^5$	40.86%
$1*10^6$	21.05%
$1*10^7$	4.46%
$5*10^7$	12.62%
$1*10^8$	14.82%
$1*10^9$	16.73%

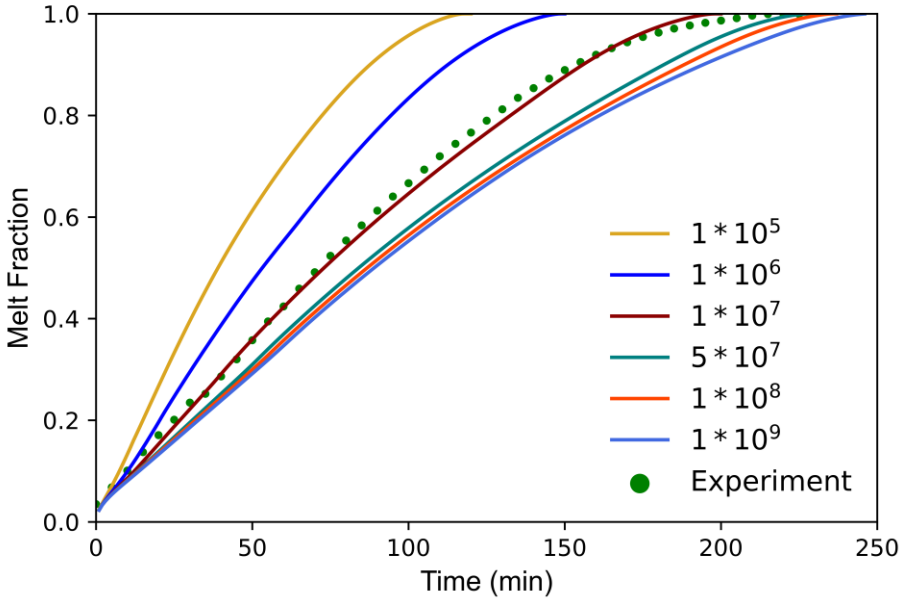

Figure 33: Mushy-zone constant study at 57°C and 90° inclination for 24,000 node mesh

The following tables and figures provide melt fraction versus time comparison of the two tested mushy-zone constant values against the experimental data for the for the 24,000 node mesh at all angles and wall temperatures. Percentages listed in the tables are average percent difference between the experimental and numerical results.

Table 3: Melt fraction versus time average percent difference comparison for 24,000 node mesh at 47°C

Angle	A_{mush}	% Difference
30°	$1*10^7$	38.62%
	$5*10^7$	11.90%
45°	$1*10^7$	8.57%
	$5*10^7$	23.77%
60°	$1*10^7$	9.90%
	$5*10^7$	7.89%
90°	$1*10^7$	14.97%
	$5*10^7$	5.00%

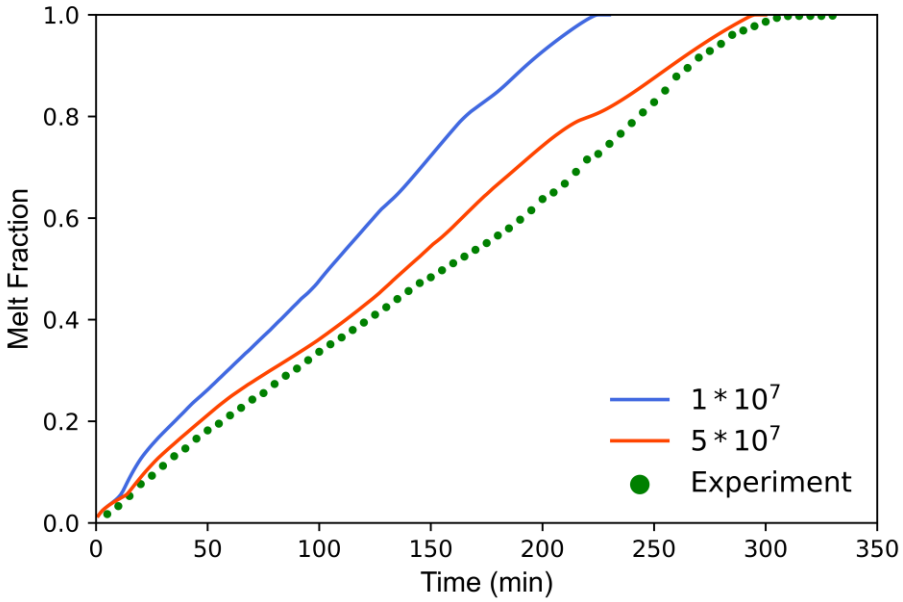

Figure 34: Melt fraction versus time comparison at 47°C and 30° inclination for 24,000 node mesh

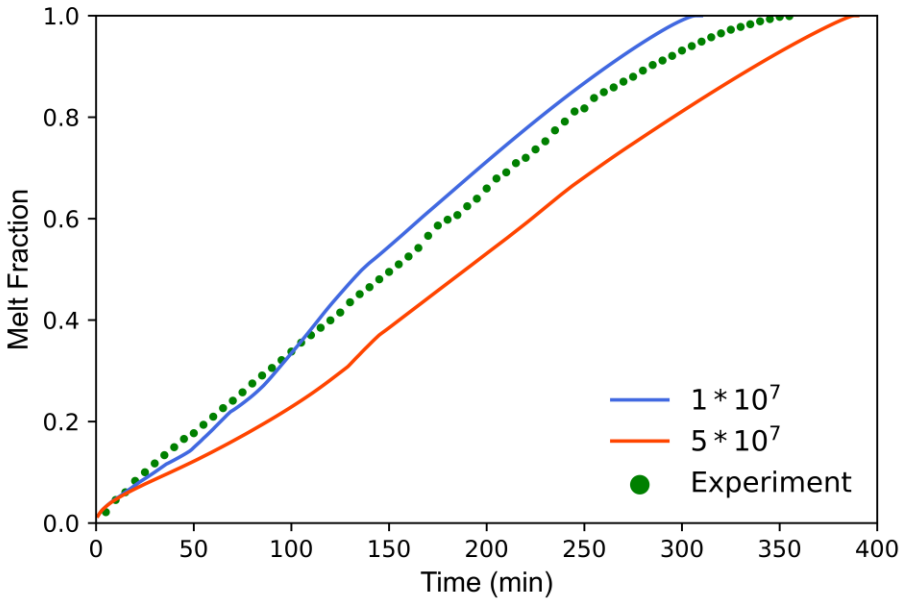

Figure 35: Melt fraction versus time comparison at 47°C and 45° inclination for 24,000 node mesh

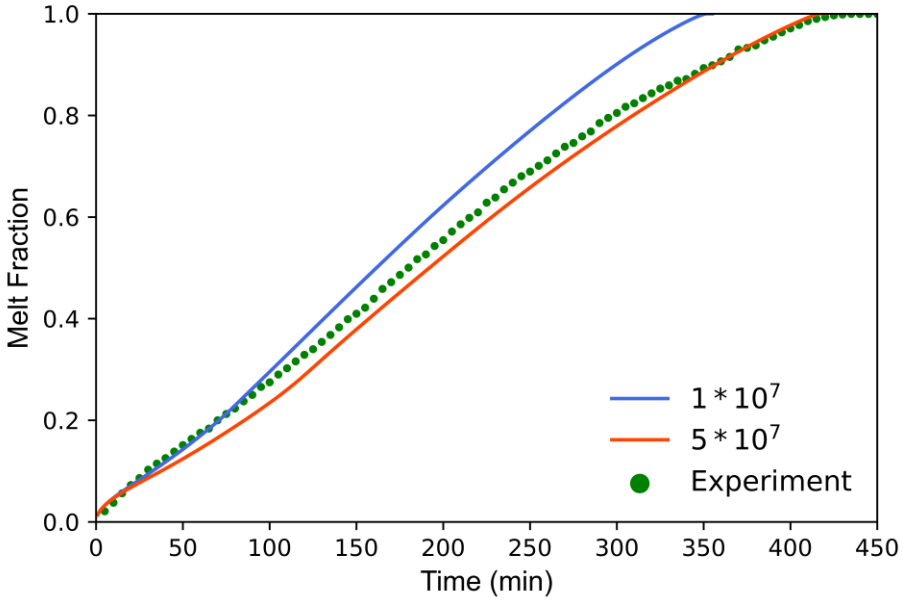

Figure 36: Melt fraction versus time comparison at 47°C and 60° inclination for 24,000 node mesh

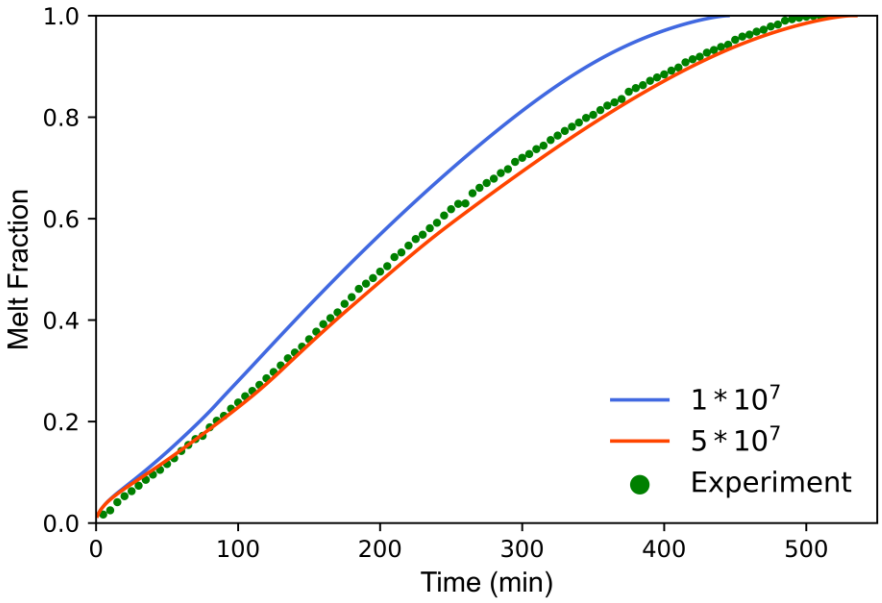

Figure 37: Melt fraction versus time comparison at 47°C and 90° inclination for 24,000 node mesh

Table 4: Melt fraction versus time average percent difference comparison for 24,000 node mesh at 57°C

Angle	A_{mush}	% Difference
30°	$1*10^7$	25.33%
	$5*10^7$	7.27%
45°	$1*10^7$	12.77%
	$5*10^7$	18.06%
60°	$1*10^7$	11.70%
	$5*10^7$	10.10%
90°	$1*10^7$	5.50%
	$5*10^7$	7.48%

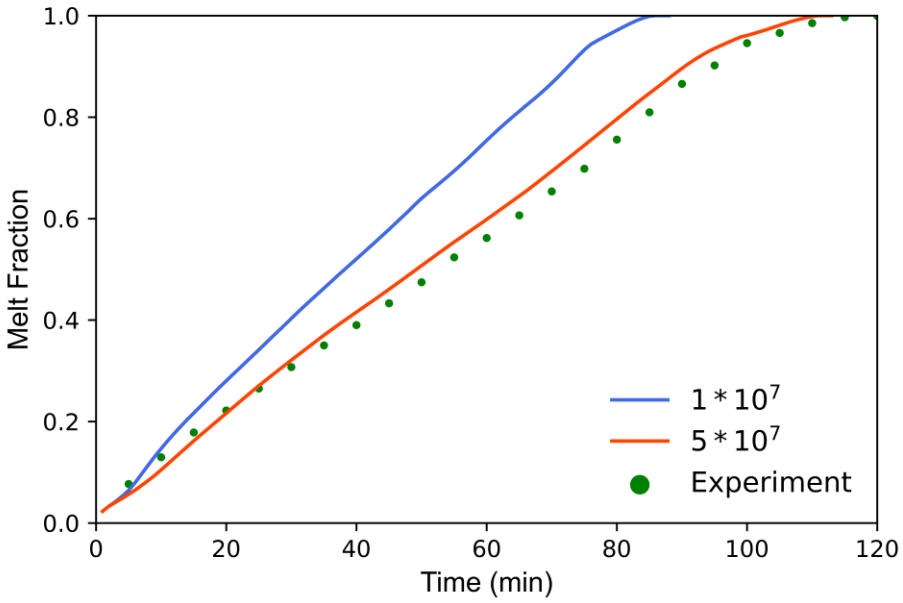

Figure 38: Melt fraction versus time comparison at 57°C and 30° inclination for 24,000 node mesh

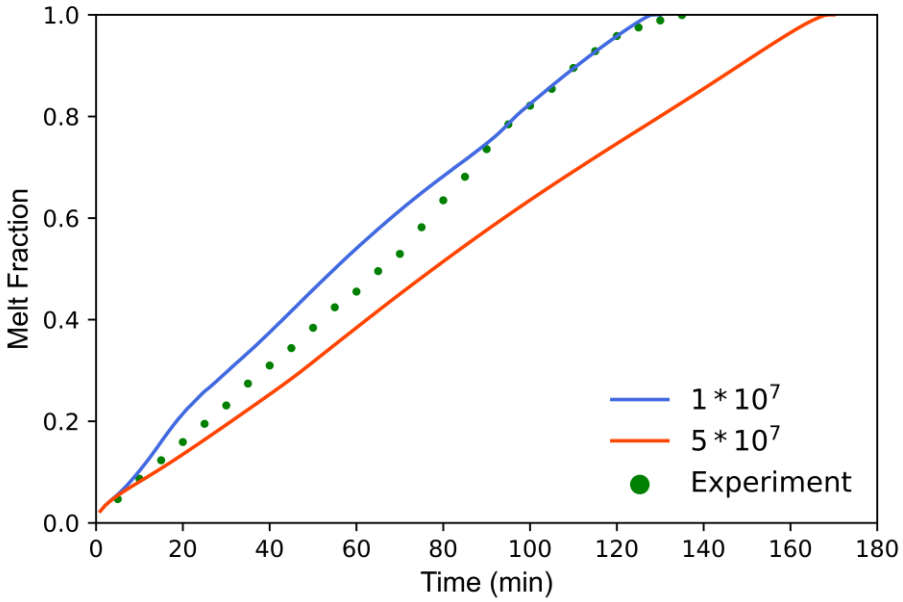

Figure 39: Melt fraction versus time comparison at 57°C and 45° inclination for 24,000 node mesh

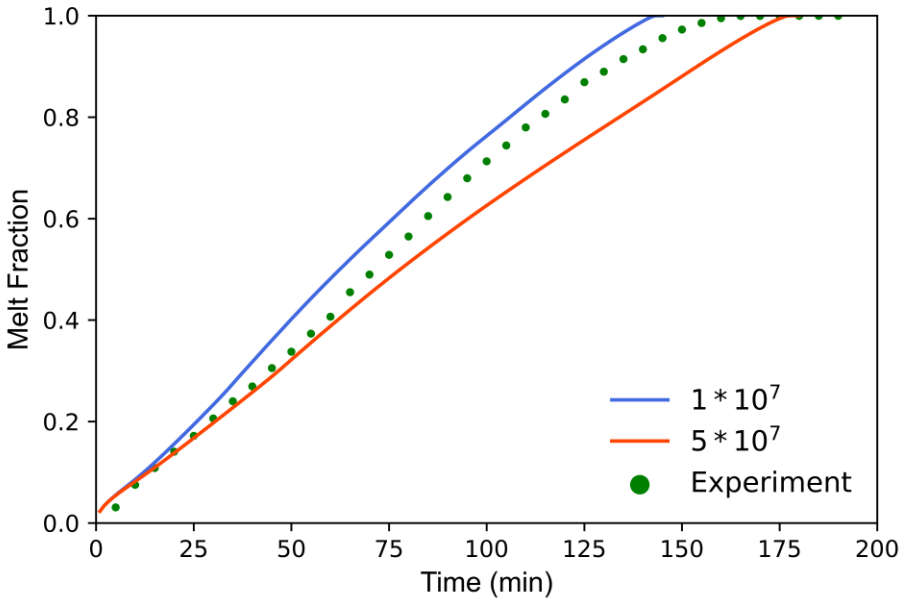

Figure 40: Melt fraction versus time comparison at 57°C and 60° inclination for 24,000 node mesh

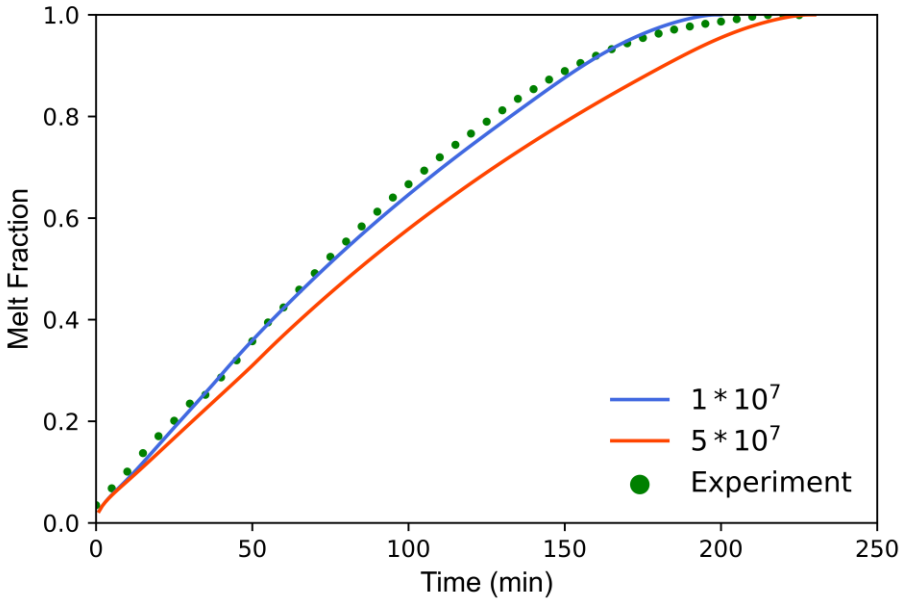

Figure 41: Melt fraction versus time comparison at 57°C and 90° inclination for 24,000 node mesh

Some trends are observed with the 47°C data, with all results except the 45° inclination reporting the value of 5×10^7 as the most accurate to the experiments. This lower temperature data also shows a gradual increase in average percent difference as the inclination angle of the enclosure is reduced. In other words, the software is more accurately modeling the vertical orientation, which is corroborated by the previously discussed literature. Issues have been noted in the past when modeling a 45° inclination numerically, which could prove at this angle an alternate mushy-zone constant could be required to accurately replicate the natural convection currents in the system. Ignoring the outlier of the 45° orientation, the increased average percent difference could confirm that higher values of the mushy-zone constant would be required to accurately model lesser angles, and thus the mushy-zone constant would be dependent on the inclination angle.

The 57°C studies showed little trend with lower average percent differences in the 30° and 60° orientations at an A_{mush} value of 5×10^7, and lower average percent differences in the 45° and 90° orientations at an A_{mush} value of 1×10^7. Similar to the 47°C wall temperature, issues arise when modeling the 45° inclination at the higher temperature; however, for the higher temperature as displayed in Figure 39 a different slope is observed between the experimental and numerical data.

Without a definitive trend of the mushy-zone constant and issues arising specifically at the 45° inclination, visual inspection of the melt front interface images was completed for all numerical cases to their experimental counterparts. This method serves as the other main means of validation in the field and should provide some information as to whether the software is accurately simulating the developing convection currents.

To introduce the discussion of visual image comparison for the melt front development, Figure 42 repeats that which was discussed in Figure 33 by showing the melt fronts at 25%, 50%, and 75% liquid for 24,000 node mesh at 57°C and 90° inclination. At the stated values of A_{mush}, it is observed that in the vertical orientation increasing the mushy-zone constant helps to more accurately replicate the experimental images. It is observed that this goes against the main method of validation for the field, melt fraction versus time comparison for A_{mush} selection, with a continuing visual improvement in the solid-liquid interface as the mushy-zone constant increases. Should this method solely be used for validation, a A_{mush} value with a higher average percent difference when compared to the experimental data via melt fraction versus time curves would be observed as optimal. However, some notice is given to the linear aspects of the higher mushy-zone constant models; where the software fails to accurately replicate the smooth interface and rather splits it into two separate lines with a sharp corner.

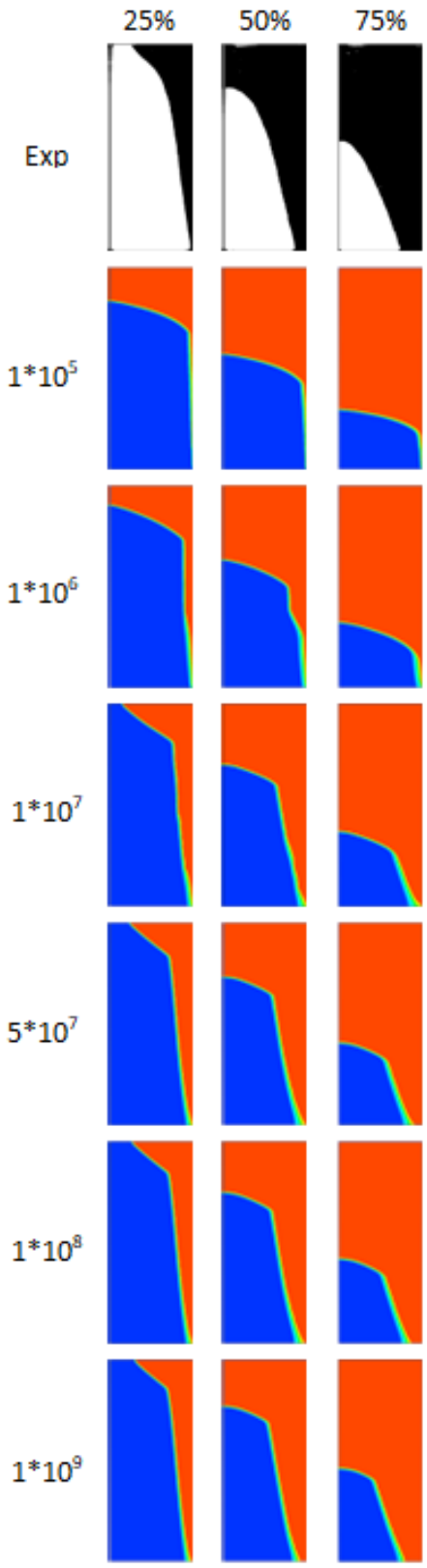

Figure 42: Melt front development images at 57°C and 90° angle for 24,000 node mesh

The following series of figures compares the melt front development visually between the experiments and numerical simulations at two studied mushy-zone constants, simulated temperatures, and simulated angles. Melt front images were again taken at 25%, 50%, and 75% for comparison during the convection driven region of melting, as this part of the melts would likely have the greatest differences due to the development of currents in each given system.

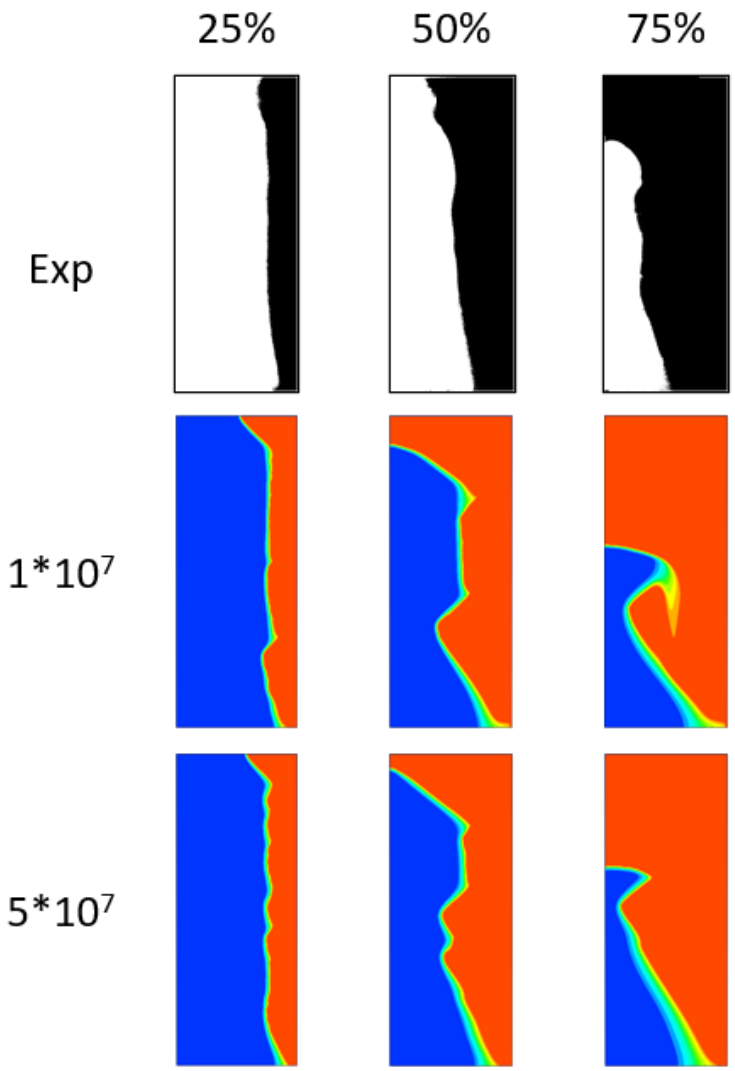

Figure 43: Melt front development images at 47°C and 30° angle for 24,000 node mesh

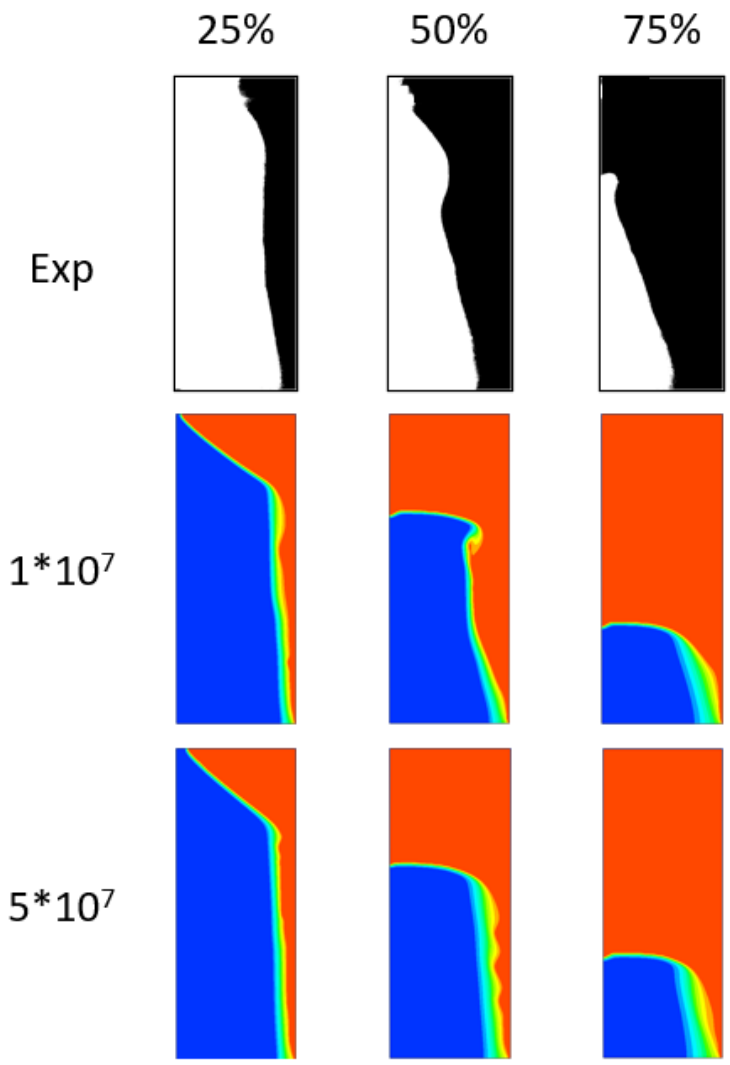

Figure 44: Melt front development images at 47°C and 45° angle for 24,000 node mesh

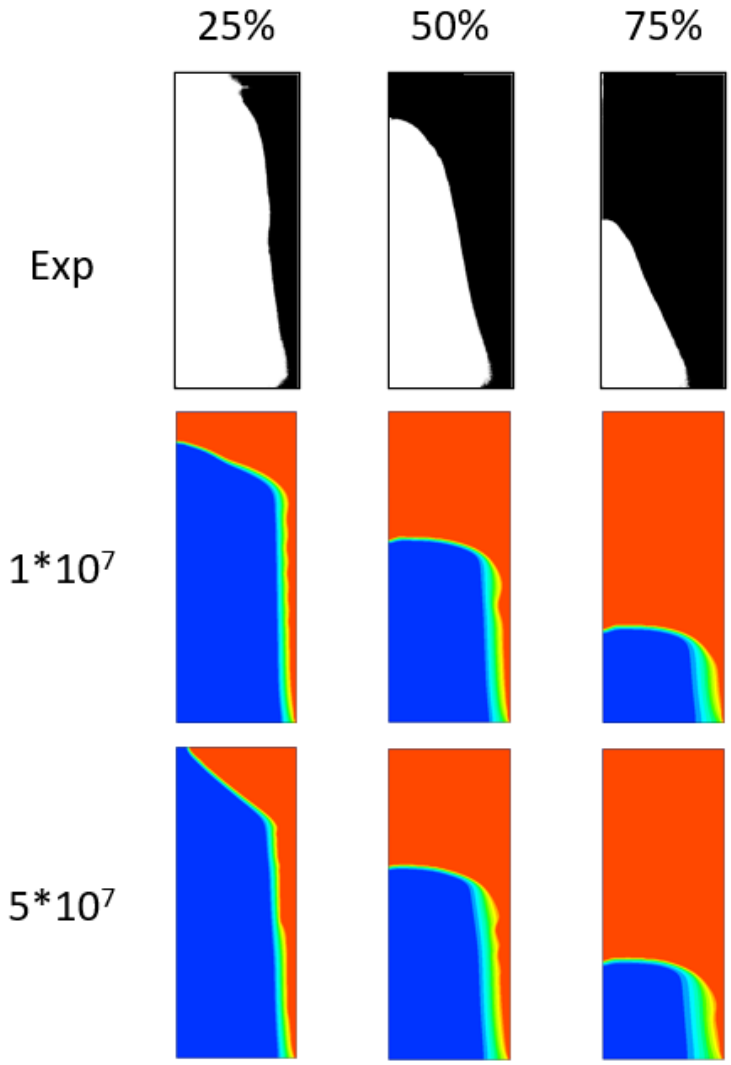

Figure 45: Melt front development images at 47°C and 60° angle for 24,000 node mesh

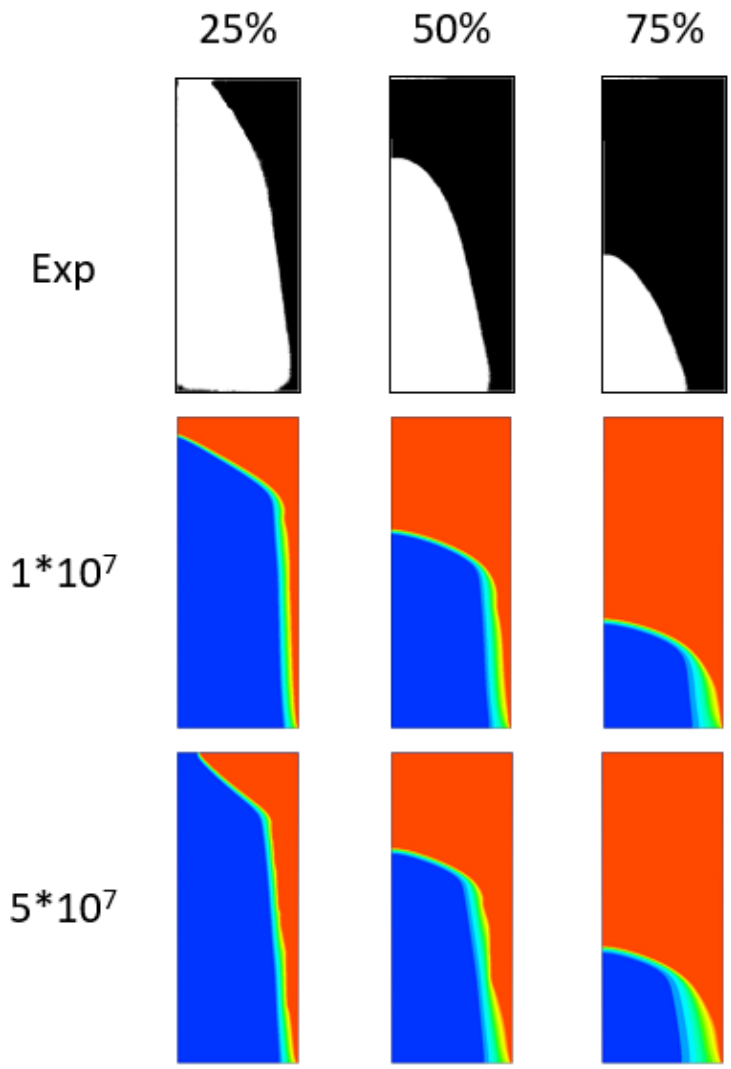

Figure 46: Melt front development images at 47°C and 90° angle for 24,000 node mesh

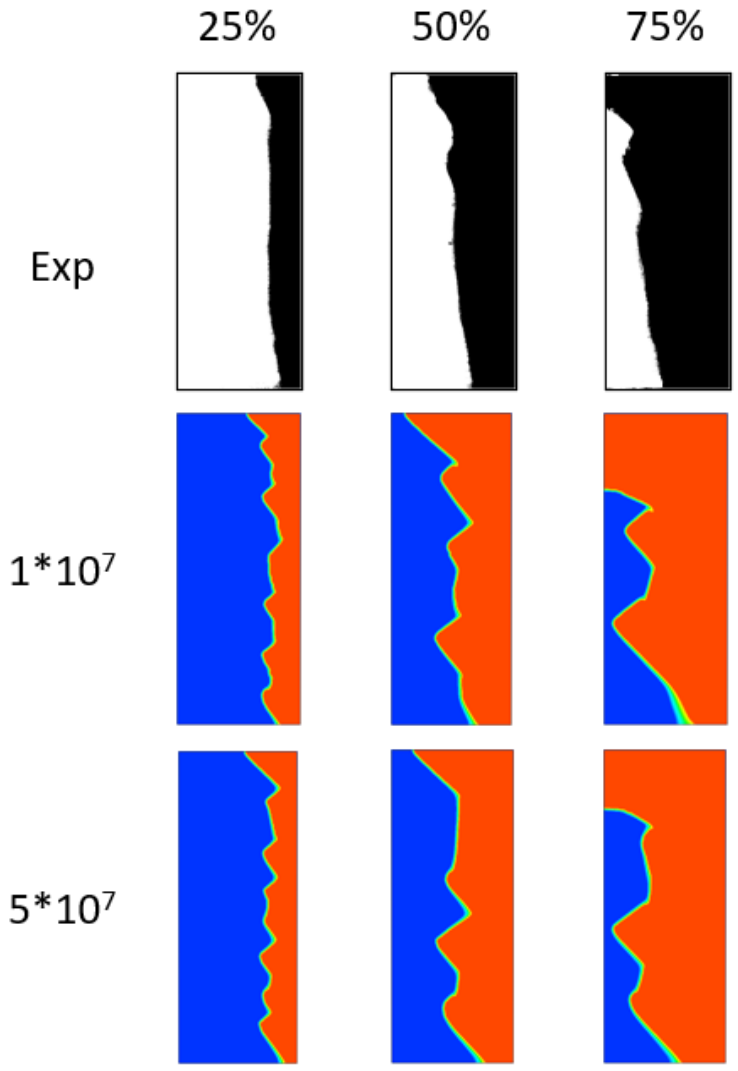

Figure 47: Melt front development images at 57°C and 30° angle for 24,000 node mesh

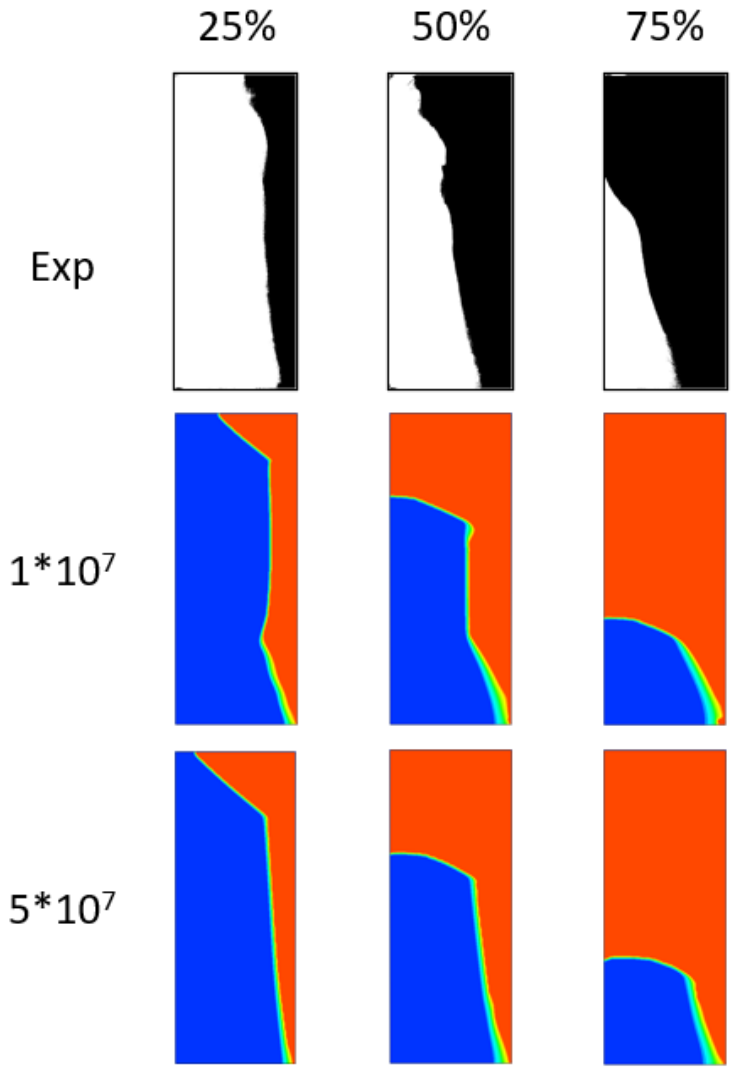

Figure 48: Melt front development images at 57°C and 45° angle for 24,000 node mesh

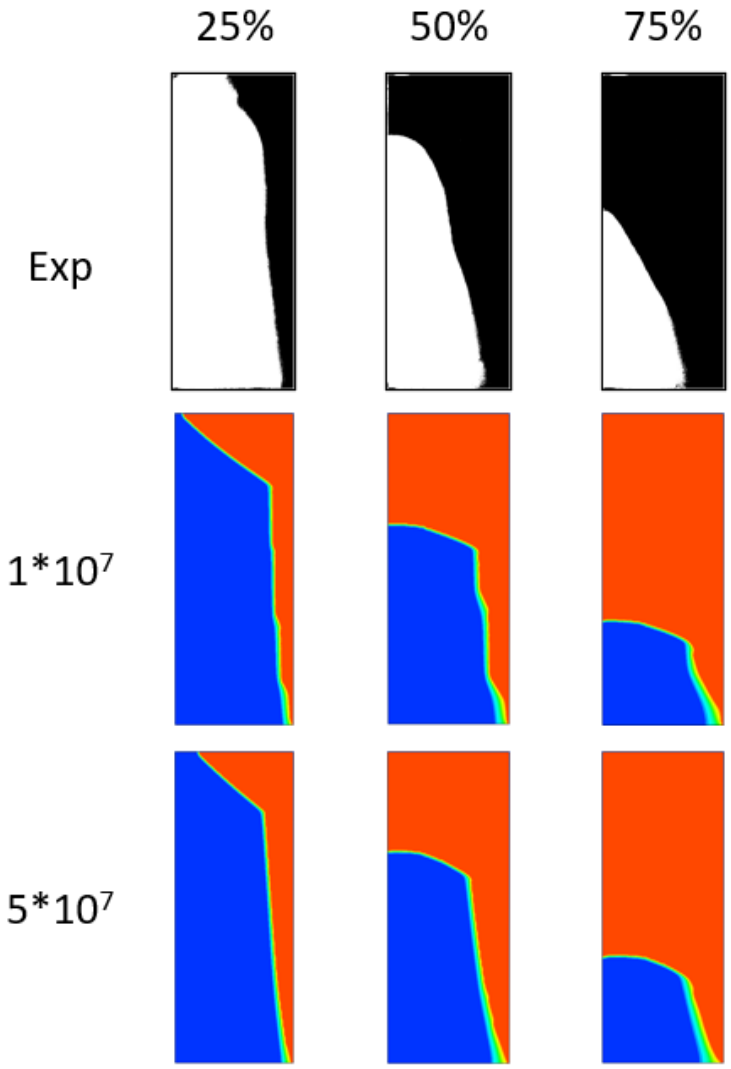

Figure 49: Melt front development images at 57°C and 60° angle for 24,000 node mesh

The collected images visually show a better accuracy at the greater angle melts. Although the images do not appear to replicate exactly what was completed in the experiments, they do show the general trend. The main differences are observed with the greater amount of PCM at the bottom of the enclosure, rather than those of the experiments which are more spread out along the wall opposite the boundary condition.

Based on Figure 42, with the study into various values of A_{mush} at a constant orientation, increasing the mushy-zone constant could help to better replicate the interface shape; however, following the analysis completed for Figure 33, this change would also likely increase the total melting time and thus increase the average percent difference between the melt fraction versus time curves.

This issue illustrates one of the main problems in validation for modeling solidification and melting with CFD. Of the two main methods of validation, if comparing experimental results to numerical models by means of melt fraction versus time graphs an accurate replication of the liquid-to-solid ratio of PCM in the enclosure could be obtained over time, given constant system conditions (time, inclination, etc.). However, validating solely to this method would likely result in inaccurate interface shapes in the numerical models. More so, by following the main methods of validation stated in the literature, where in a single system configuration is studied and mushy-zone constant is determined for use in all other configurations, even greater errors could be present not only in melt front development images over time but also in the melt fraction versus time comparison.

Finer Model Testing at 96,000 Nodes

In an attempt to remedy these issues, meshes of greater fineness were studied to try and better replicate the development of natural convection within the enclosure. Mesh sizes at 96,000 nodes were studied, in accordance with the previous discussion of the Mesh Setup section. The following figures provide melt fraction versus time graphs comparing the 96,000 to the previously discussed more coarse meshes and experimental

results. The following tables provide average percent differences at the stated inclination angles and wall temperatures. After a similar mushy-zone constant study at the 57°C and 90° inclination, initial models studied at this finer mesh size were completed at an A_{mush} value of 5×10^7 as this value showed the most accurate results for the majority of the completed simulations.

Table 5: Melt fraction versus time average percent difference comparison for 96,000 node mesh at 47°C

Angle	% Difference
30°	12.85%
45°	28.83%
60°	9.56%
90°	3.16%

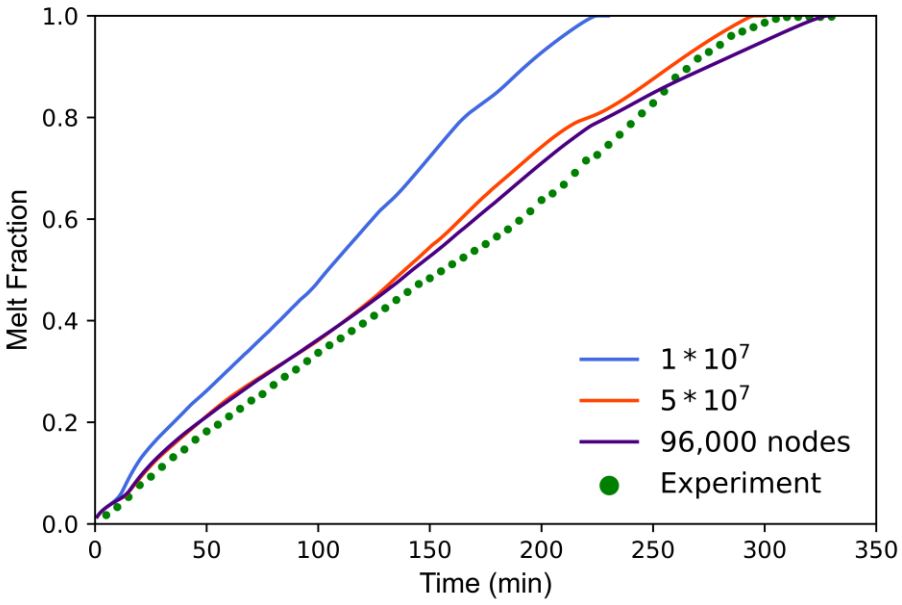

Figure 50: Melt fraction versus time comparison at 47°C and 30° inclination for 96,000 node mesh

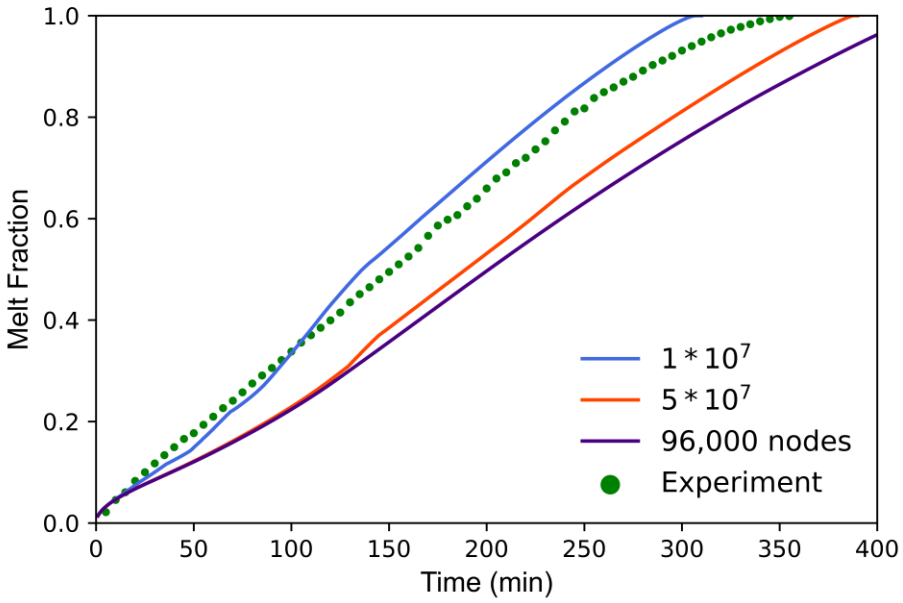

Figure 51: Melt fraction versus time comparison at 47°C and 45° inclination for 96,000 node mesh

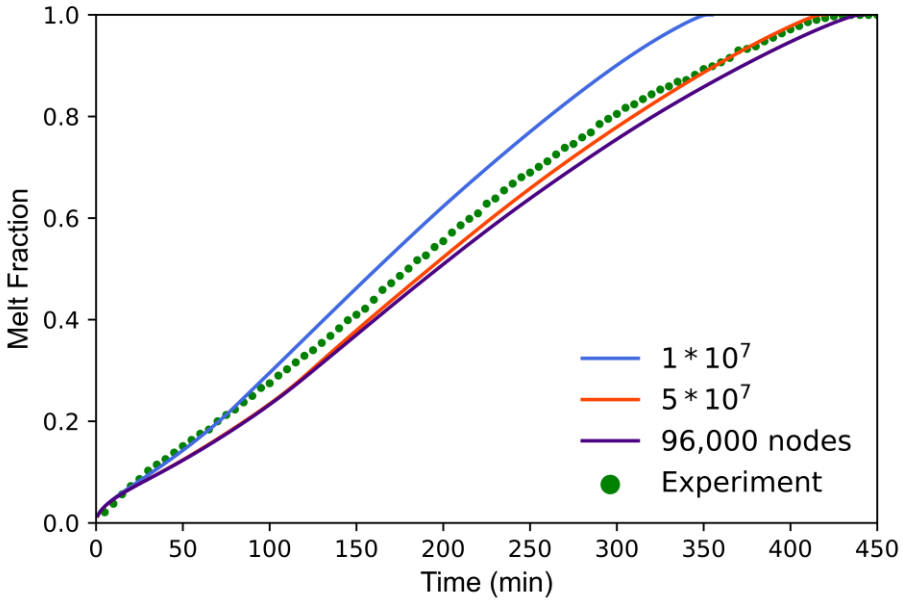

Figure 52: Melt fraction versus time comparison at 47°C and 60° inclination for 96,000 node mesh

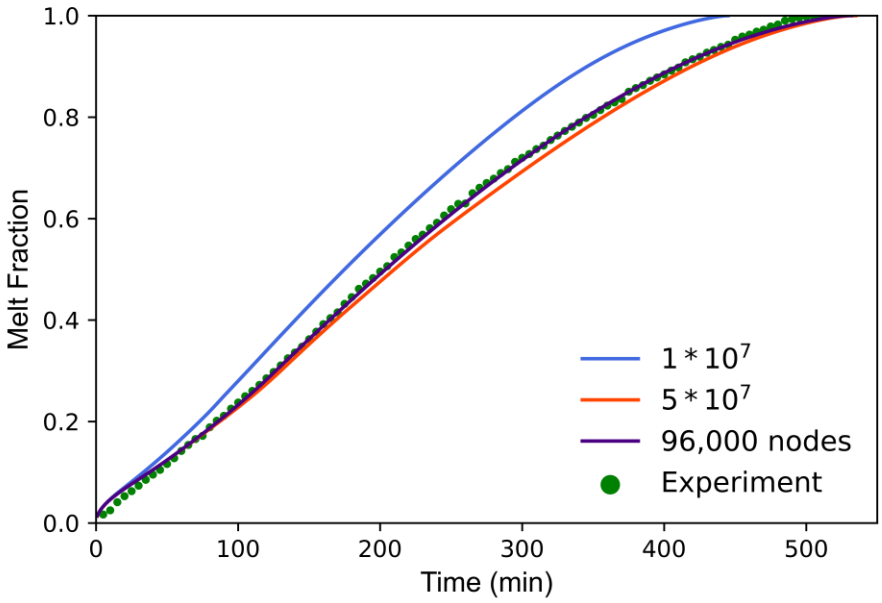

Figure 53: Melt fraction versus time comparison at 47°C and 90° inclination for 96,000 node mesh

Table 6: Melt fraction versus time average percent difference comparison for 96,000 node mesh at 57°C

Angle	% Difference
30	4.10%
45	12.68%
60	6.10%
90	4.06%

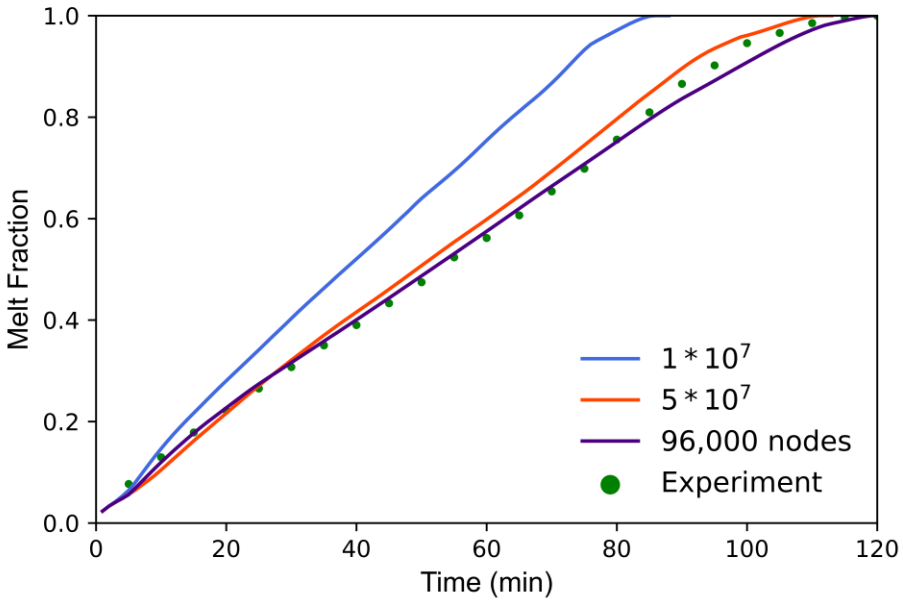

Figure 54: Melt fraction versus time comparison at 57°C and 30° inclination for 96,000 node mesh

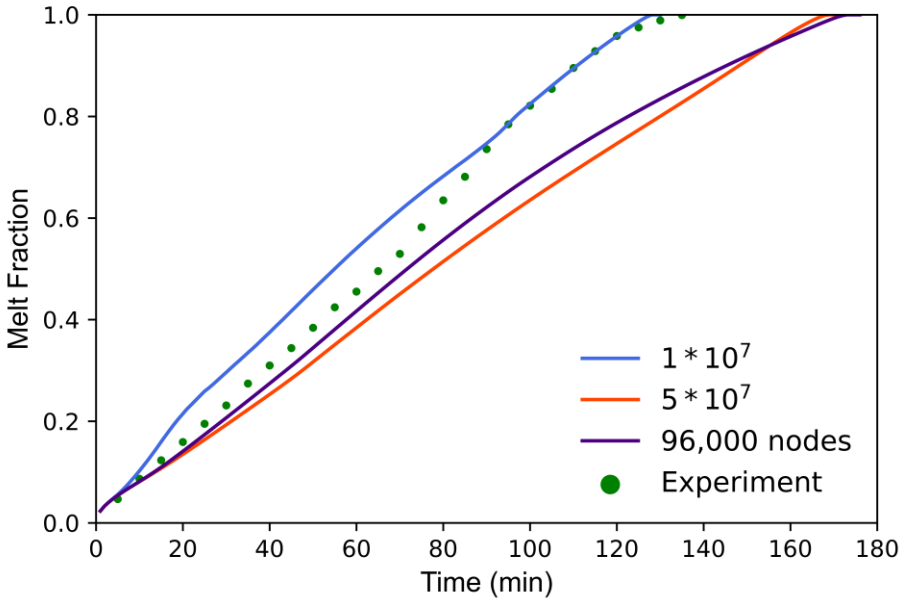

Figure 55: Melt fraction versus time comparison at 57°C and 45° inclination for 96,000 node mesh

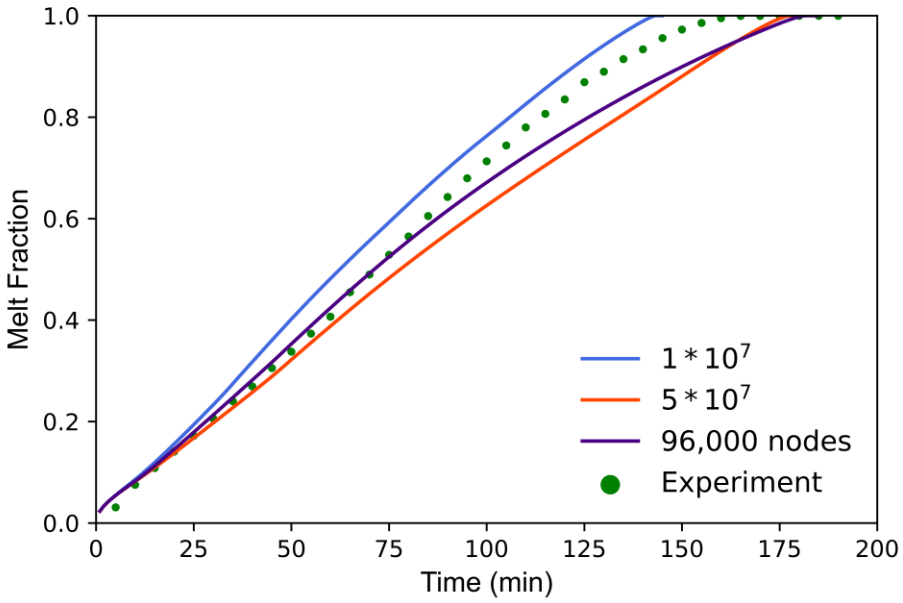

Figure 56: Melt fraction versus time comparison at 57°C and 60° inclination for 96,000 node mesh

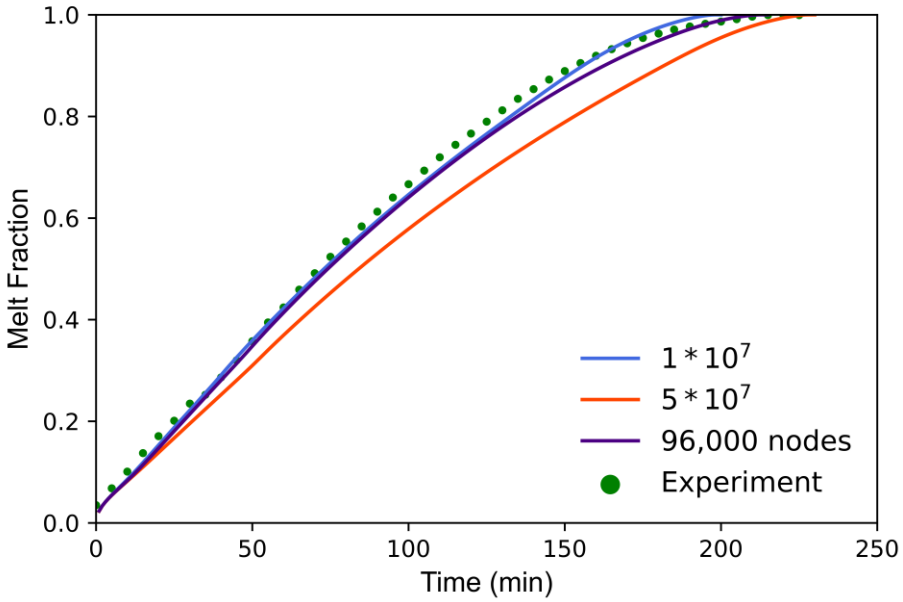

Figure 57: Melt fraction versus time comparison at 57°C and 90° inclination for 96,000 node mesh

The adjustment to a finer mesh had good agreement with the melt fraction versus time graphs with average percent differences near or below 10% for all but the 45° inclination at both tested temperatures. These finer models showed improvements when compared to most of the 24,000 node models but did show worse average percent differences at the lower angles. Previous studies have acknowledged CFD software has had issues when accurately modeling at a 45° inclination angle, noting a significant lag behind the experimental results [35]. Similar to the previous analysis, a difference in slope is observed between the experimental and numerical data at the 57°C wall temperature. To better understand this discrepancy and evaluate whether or not increasing the number of cells within the mesh had an impact on the interface development, the following figures were created to analyze the melt front development at the stated temperatures and inclination angles. Comparisons are shown to the experimental images as well as the 24,000 node meshes completed with a mushy-zone constant value of 5×10^{7}, as this would allow for direct comparison of the more coarse to more fine meshes without any variation in A_{mush}.

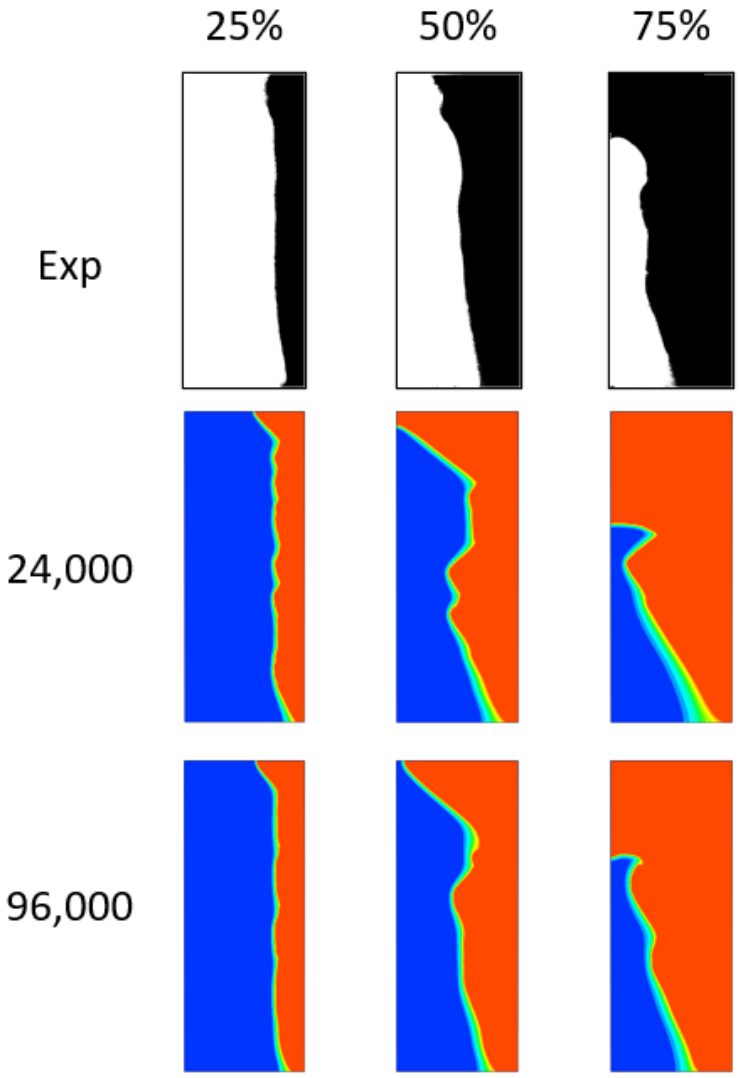

Figure 58: Melt front development images at 47°C and 30° angle for mesh sizes

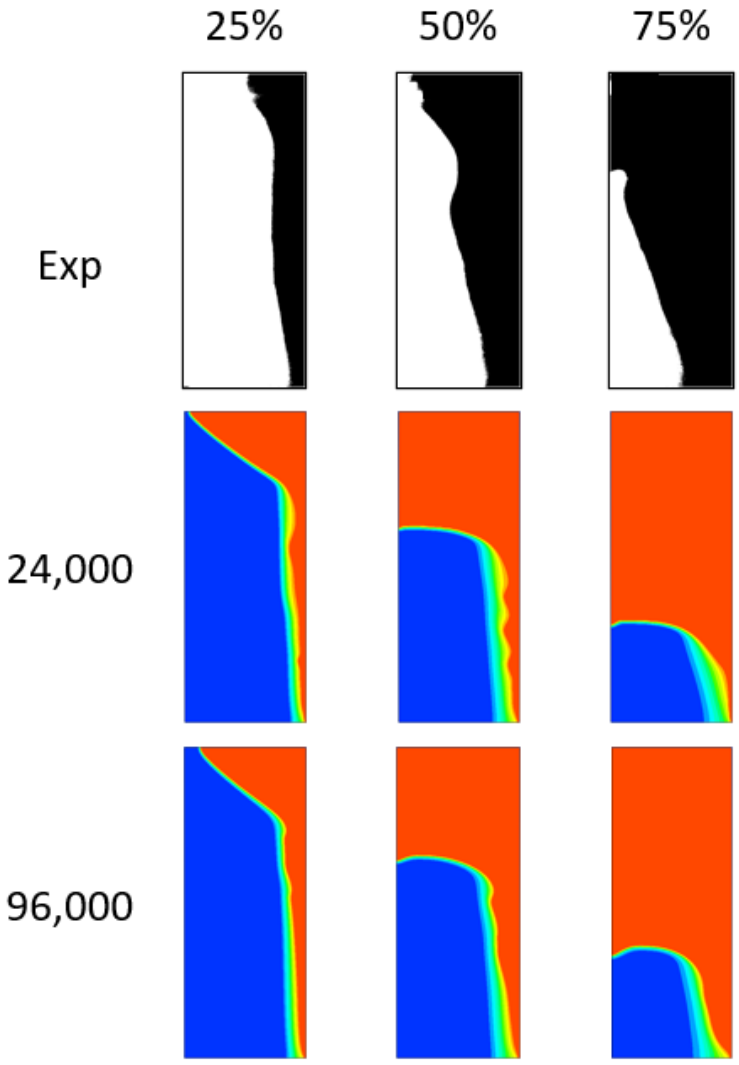

Figure 59: Melt front development images at 47°C and 45° angle for mesh sizes

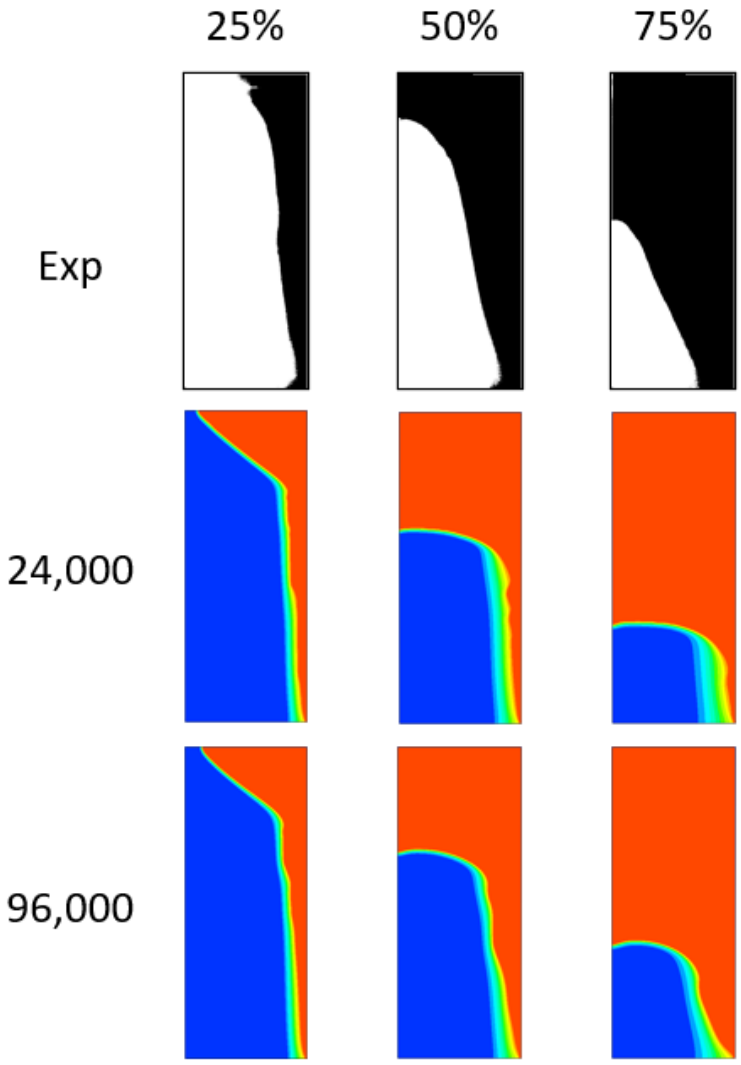

Figure 60: Melt front development images at 47°C and 60° angle for mesh sizes

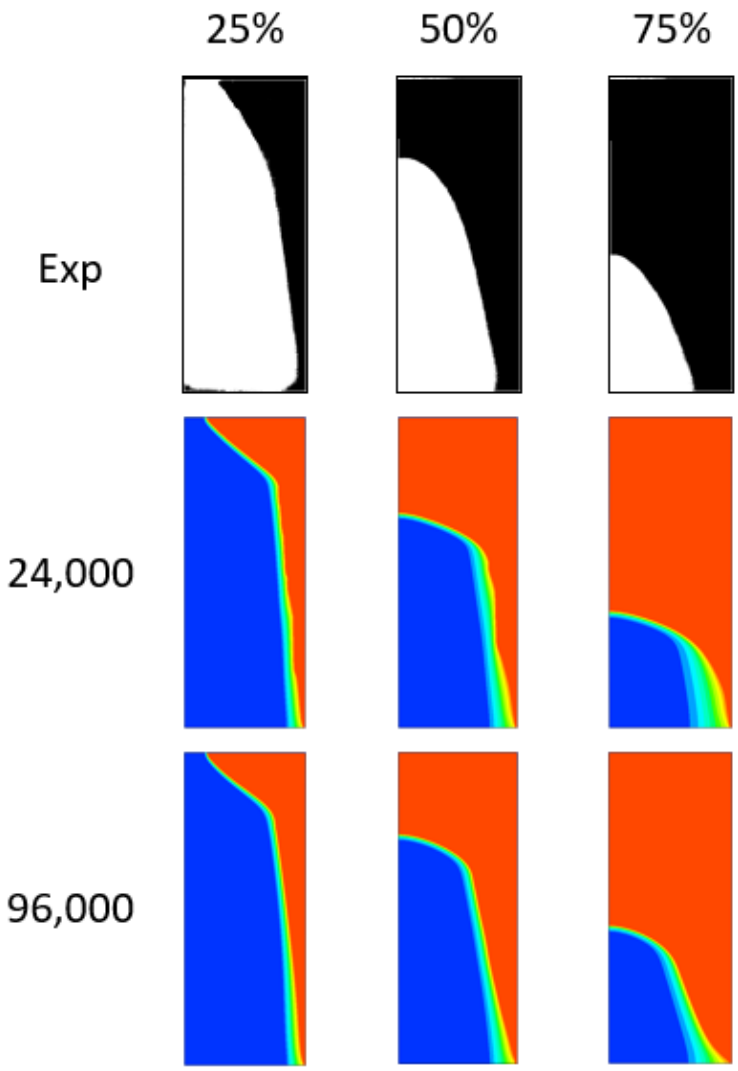

Figure 61: Melt front development images at 47°C and 90° angle for mesh sizes

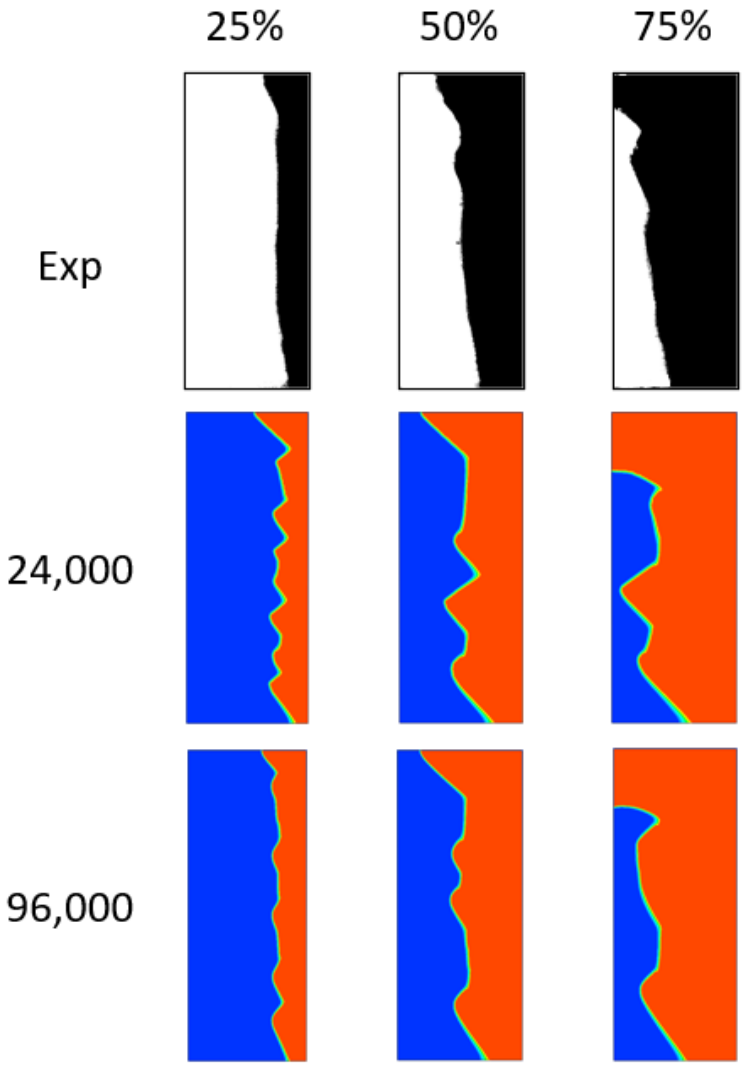

Figure 62: Melt front development images at 57°C and 30° angle for mesh sizes

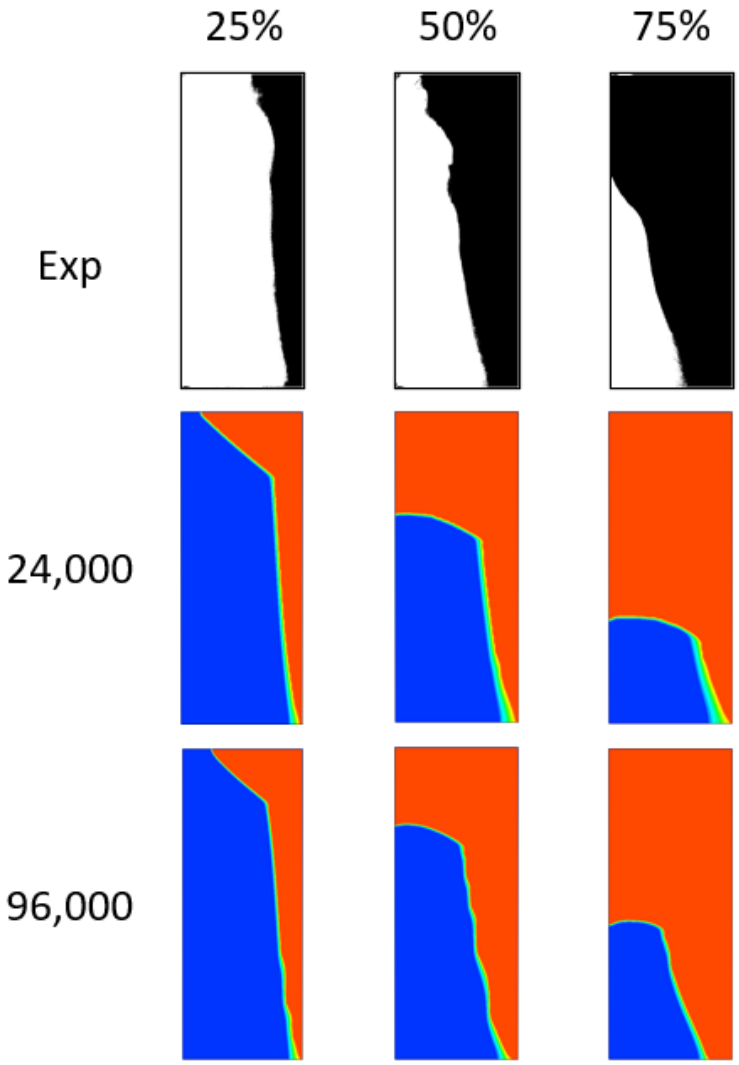

Figure 63: Melt front development images at 57°C and 45° angle for mesh sizes

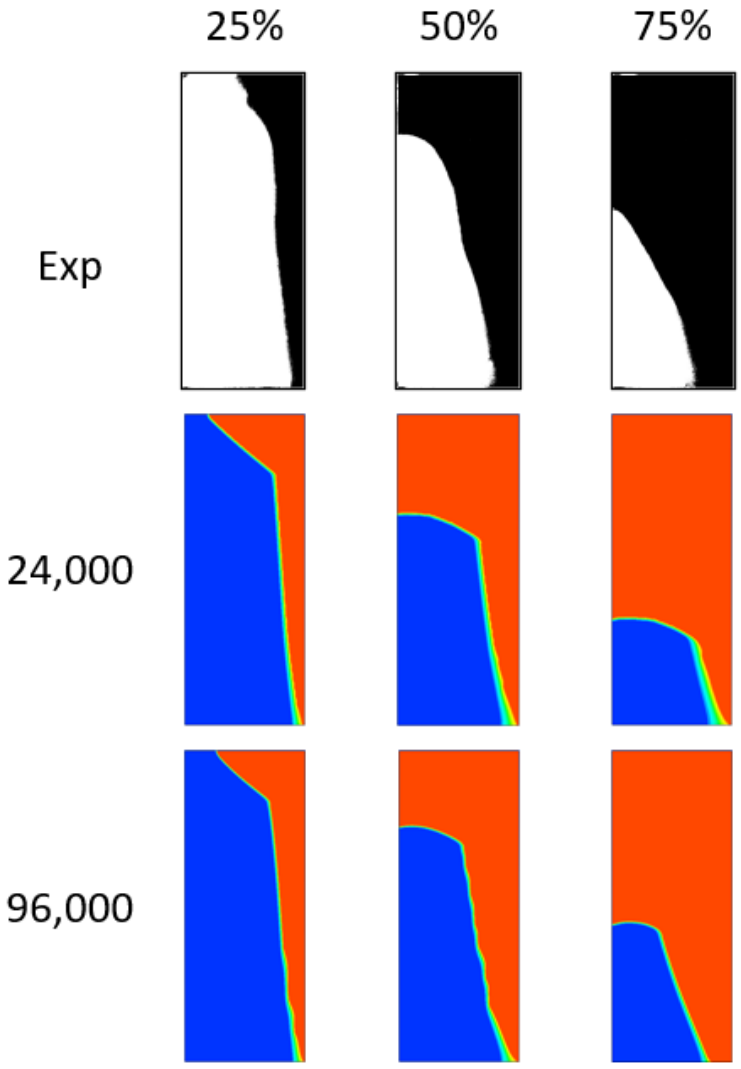

Figure 64: Melt front development images at 57°C and 60° angle for mesh sizes

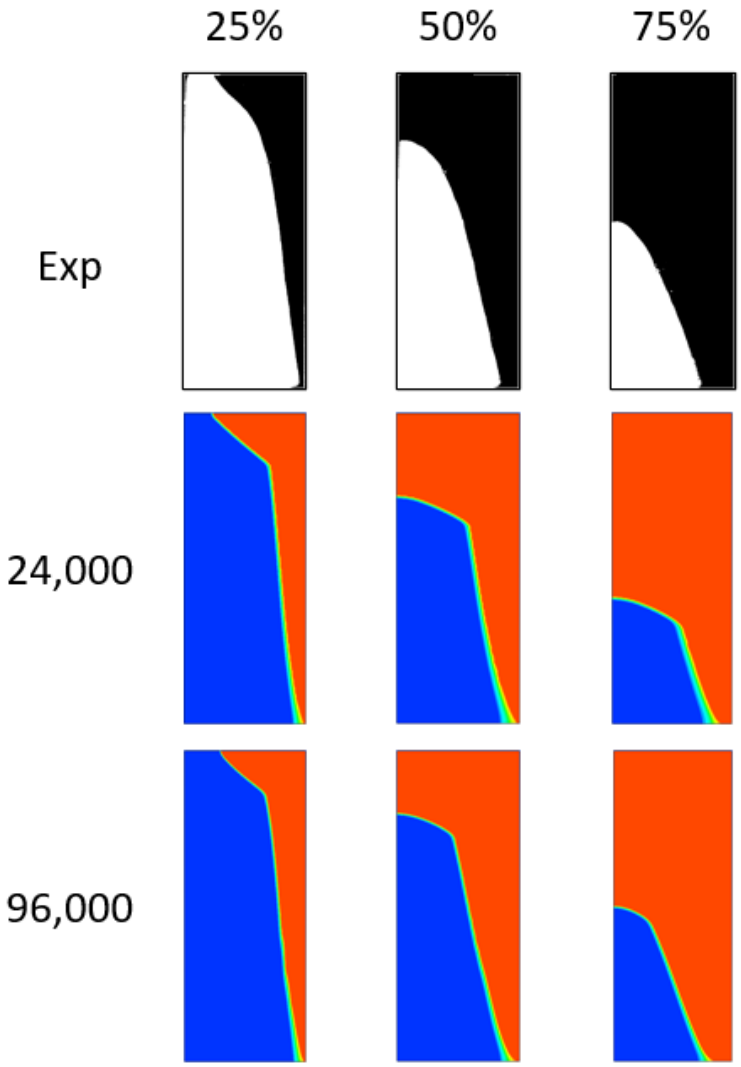

Figure 65: Melt front development images at 57°C and 90° angle for mesh sizes

Increasing the total number of cells in the mesh has had significant visual impact on the melt front development image comparison. The finer mesh appears to more accurately reproduce the smoother curvature of the solid-liquid interface at the greater angles. Both the lesser angles at the 24,000 and 96,000 node meshes display the dents into the interface, as visible in Figure 62. These are likely due to the development of vortices within the enclosure; however, the simulations appear to model a greater number

and magnitude of vortices as evident in the respective melt front images. Based on the previously discussed images at the 24,000 node mesh as well as the current images for the 30° angles, it is thought that increasing the mushy-zone constant and/or the fineness of the mesh could further help to resolve these issues.

Similar to the 24,000 node mesh, a trend can be seen with an increase in average percent difference when looking at the melt fraction versus time graphs at the 47°C models, again with the exception of the 45° inclination. However, unlike the more coarse mesh the higher wall temperature shows very close average percent differences for all of the angles, excluding the 45° inclination, at the tested mushy-zone constant of 5×10^{7}.

Further Model Investigations

In an attempt to finally define the effects of inclination and wall temperature as well as the discovered discrepancies of differences in mesh size and validation methods on the mushy-zone constant, further models were created a run at lower mushy-zone constants for the 45° inclined melts as well as finer meshes with a node count of 384,000. The adjustments to the 45° inclined enclosure aimed at determining what reduction to the mushy-zone constant would be necessary to bring the graph closer to the experimental data, and the average percent difference more in line with those of the other tested angles. The finer meshes were completed at only the 57°C wall temperature as an initial evaluation, with plans to study the lesser temperature prior to any other form of publication. These are focused at determining what would be required to produce more accurate melt front development images, especially with the great observed differences at the lesser angles of the 57°C models.

The following tables and figures provide average percent difference values and graphical comparison of the 96,000 node mesh at the stated mushy-zone constant values and respective wall temperatures. The lower temperature melt follows similarly to the 24,000 node mesh with the best achieved value of A_{mush} reported as 1×10^{7}. For this temperature, decreasing the value showed significant impact in adjusting the numerical models to more accurately replicate the experimental data. The higher temperature melts also showed better agreement with reduction to the mushy-zone constant value. However, unlike the 47°C models the 57°C models showed improvement with even greater reduction to the constant, reporting the lowest average percent difference at 1×10^{6}. Although it was not tested, an assumption could be made that the more coarse mesh could have displayed a similar trend. Either way, the reduction of the value at the 45° inclination seemed necessary to improve the numerical accuracy, thus proving that at least at the 45° angle variation of the mushy-zone constant cannot be ignored.

Table 7: Melt fraction versus time average percent difference comparison for 96,000 node mesh at 47°C and 45° inclination with different mushy-zone constants

A_{mush}	% Difference
$5*10^{7}$	28.83%
$1*10^{7}$	13.33%
$1*10^{6}$	18.62%

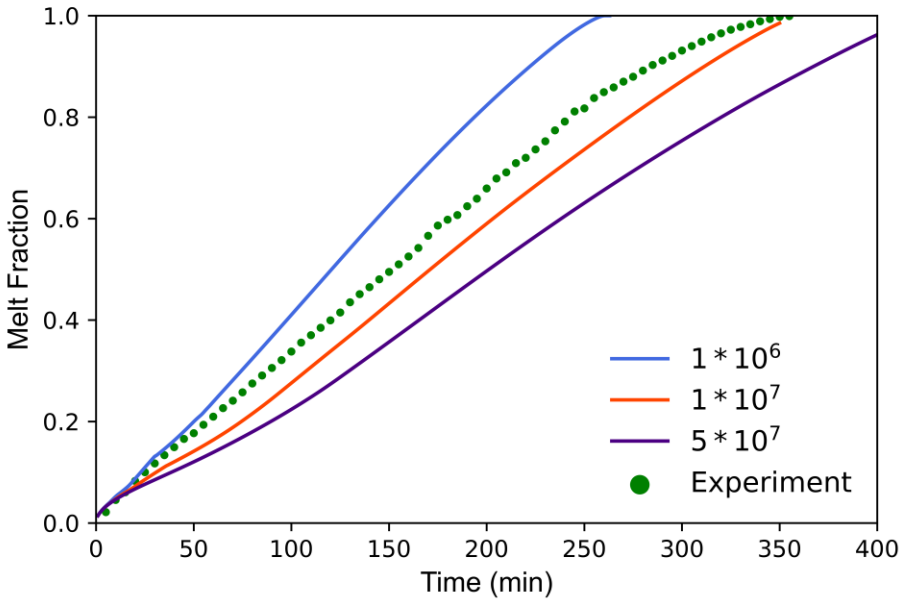

Figure 66: Melt fraction versus time comparison at 47°C and 45° inclination and different mushy-zone constants for 96,000 node mesh

Table 8: Melt fraction versus time average percent difference comparison for 96,000 node mesh at 57°C and 45° inclination with different mushy-zone constants

A_{mush}	% Difference
$5*10^7$	12.68%
$1*10^7$	8.24%
$1*10^6$	7.47%

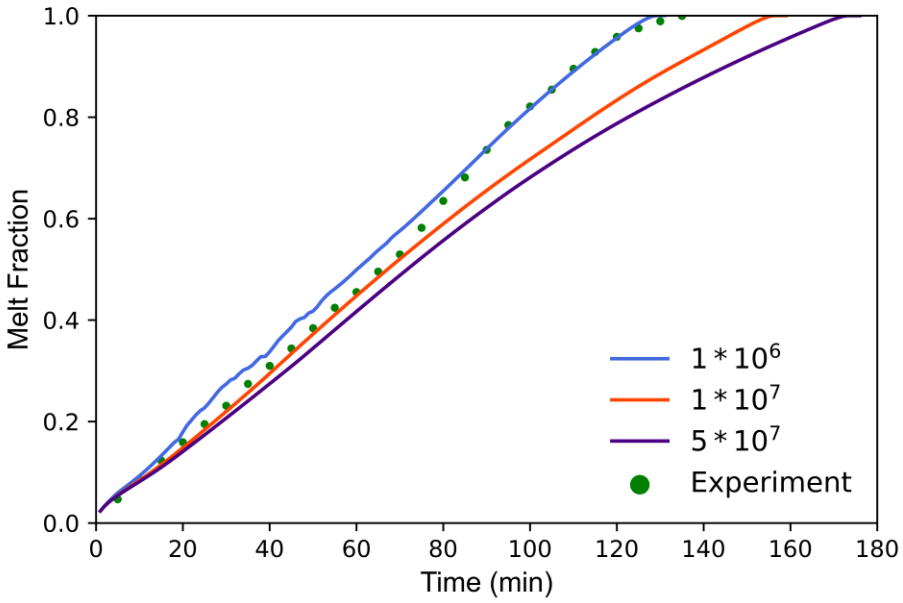

Figure 67: Melt fraction versus time comparison at 57°C and 45° inclination and different mushy-zone constants for 96,000 node mesh

Although reduction to the mushy-zone constant provides better melt fraction versus time graphs with a lower average percent difference and a more accurate slope of the numerical data, as previously seen with the more coarse meshes lowering this value has a negative effect on the melt front interface shapes at different percentages of liquid fraction. To evaluate this impact, the following figures compare melt fraction development images of the experiments to the different mushy-zone constant values tested with the 96,000 node meshes. Similar to previous analysis, lowering the mushy-zone constant reduces the accuracy of the melt front interface at the 25%, 50%, and 75% liquid fraction when compared to the experiments.

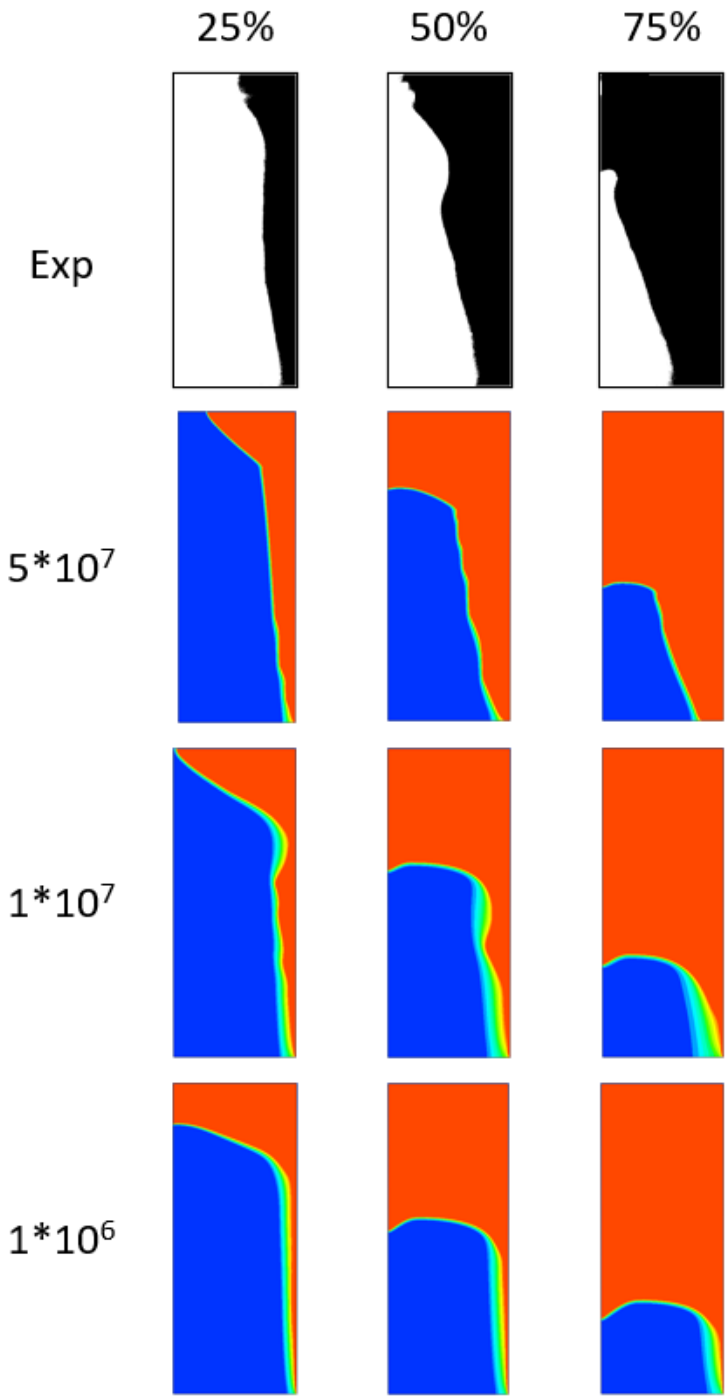

Figure 68: Melt front development images at 47°C and 45° angle for different mushy-zone constants

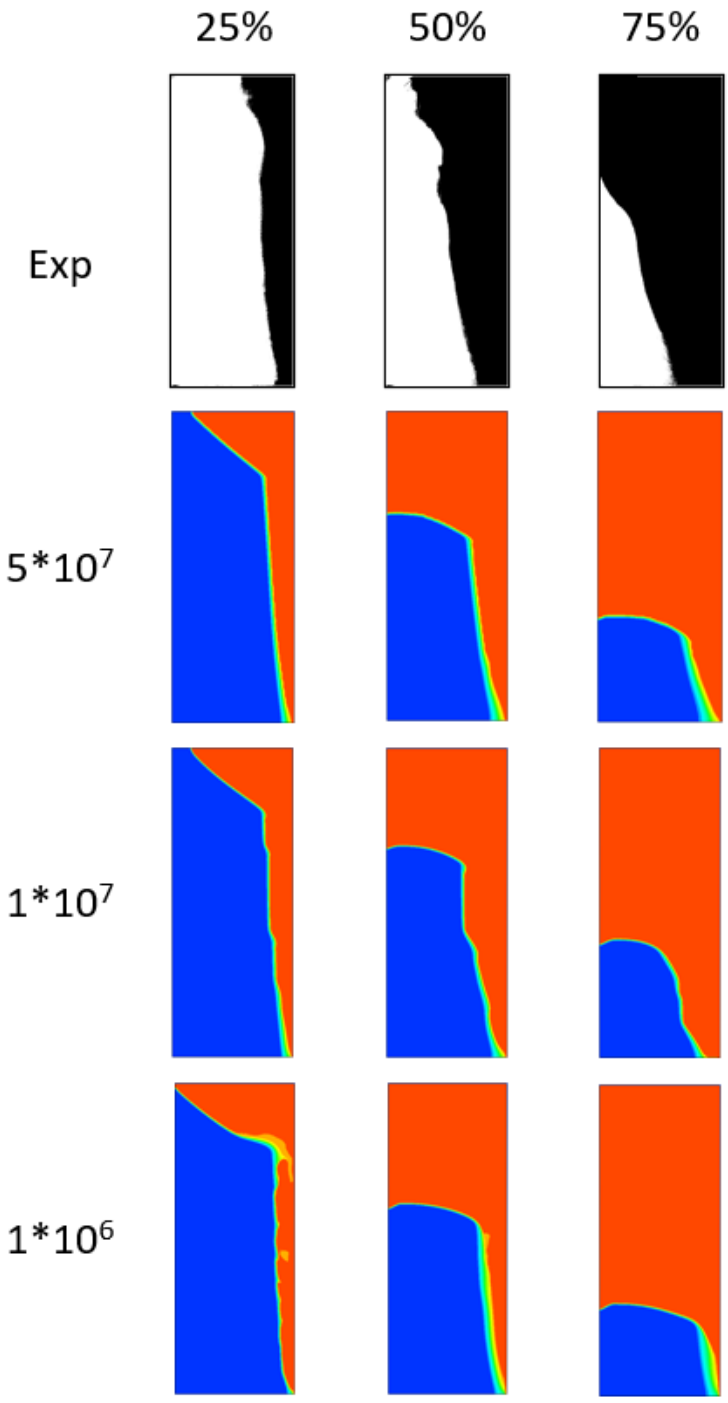

Figure 69: Melt front development images at 57°C and 45° angle for different mushy-zone constants

The following figures provide graphical comparison of the three studied mesh sizes with a set mushy-zone constant of 5×10^7, and the accompanying table shows average percent differences of the 384,000 node mesh to the experimental data at the studied angles. The melt fraction versus time data reports more accurate numerical results with all angles but the 90° inclination when compared to both the 24,000 node mesh (Table 4) and the 96,000 node mesh (Table 6). It is thought that increasing this value to 1×10^8 or 1×10^9 would even more accurately replicate the results to the experiments, but since the average percent difference was below 10% the achieved results were deemed acceptable.

Table 9: Melt fraction versus time average percent difference comparison for 384,000 node mesh at 57°C and stated angles with an A_{mush} value of $5*10^7$

Angle	% Difference
30	3.83%
45	5.94%
60	5.01%
90	9.15%

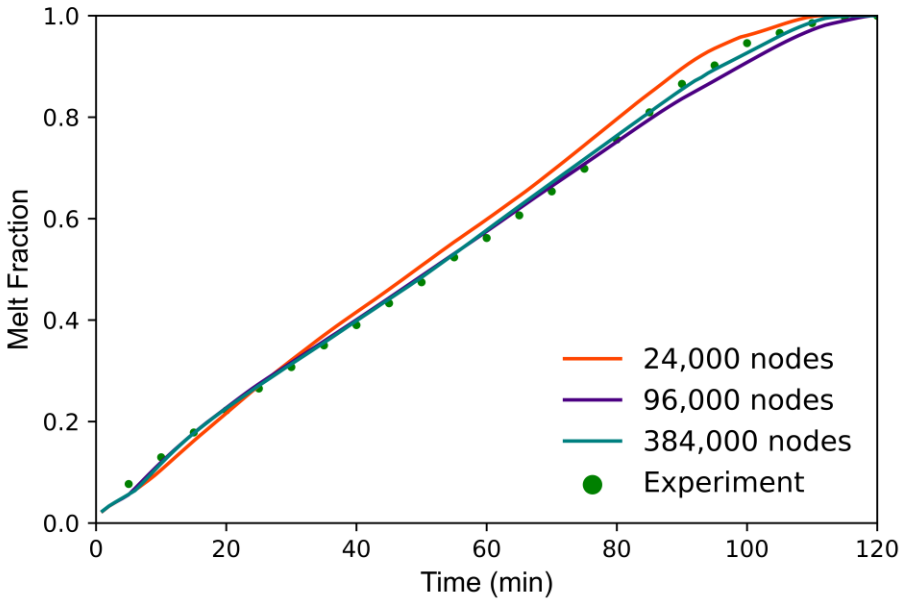

Figure 70: Melt fraction versus time comparison at 57°C and 30° inclination at various mesh sizes and a mushy-zone constant value of 5×10^7

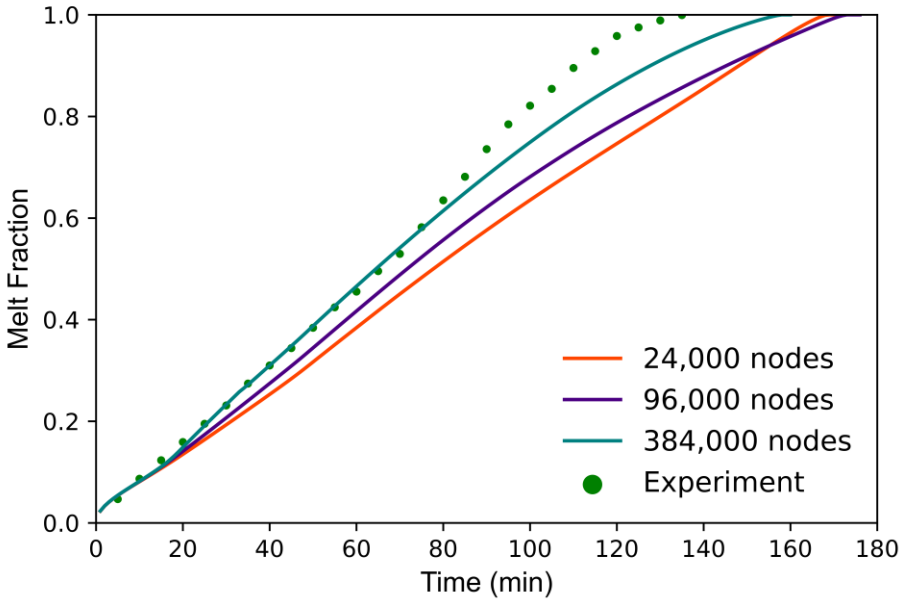

Figure 71: Melt fraction versus time comparison at 57°C and 45° inclination at various mesh sizes and a mushy-zone constant value of 5×10^7

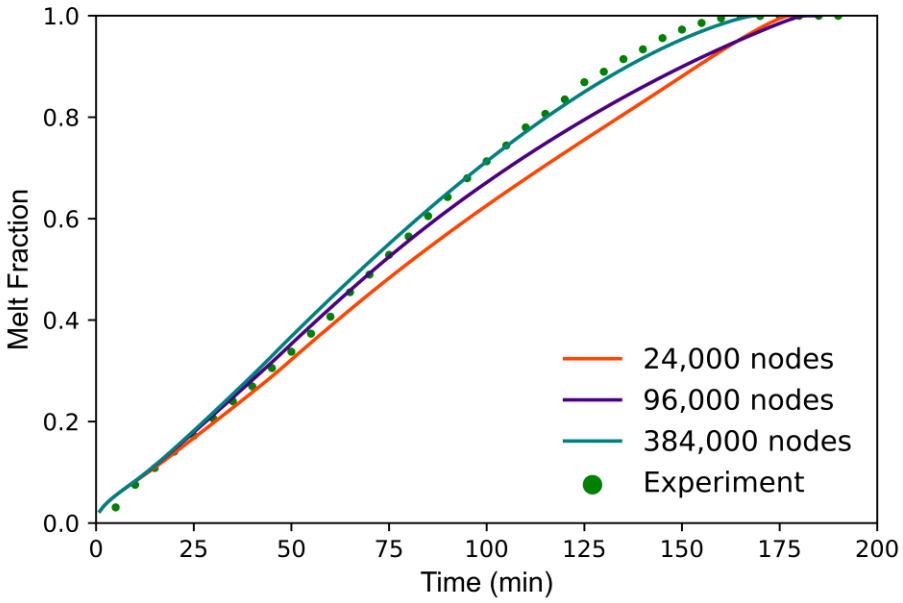

Figure 72: Melt fraction versus time comparison at 57°C and 60° inclination at various mesh sizes and a mushy-zone constant value of 5×10^7

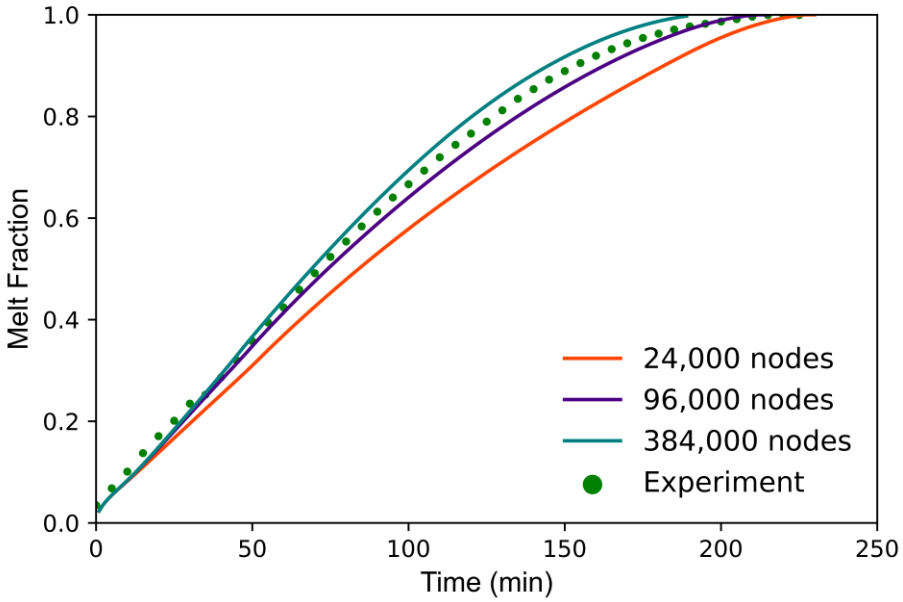

Figure 73: Melt fraction versus time comparison at 57°C and 90° inclination at various mesh sizes and a mushy-zone constant value of 5×10^7

In completing analysis on the other main means of validation, the following figures show melt front development images at 25%, 50%, and 75% comparing the experimental data to the stated mesh sizes, all at a constant mushy-zone constant value of 5×10^{7}. In all completed models, the greater mesh size did show a smoother and more accurate interface shape. At the lesser angles the finer meshes even began to show better replication of the vortex shapes and number within the enclosure. They still appear to be of a greater magnitude than the experiments; however, it is thought that given the trend observed in effects of mesh size greater refinement may show even more accurate results when focusing on the image comparison.

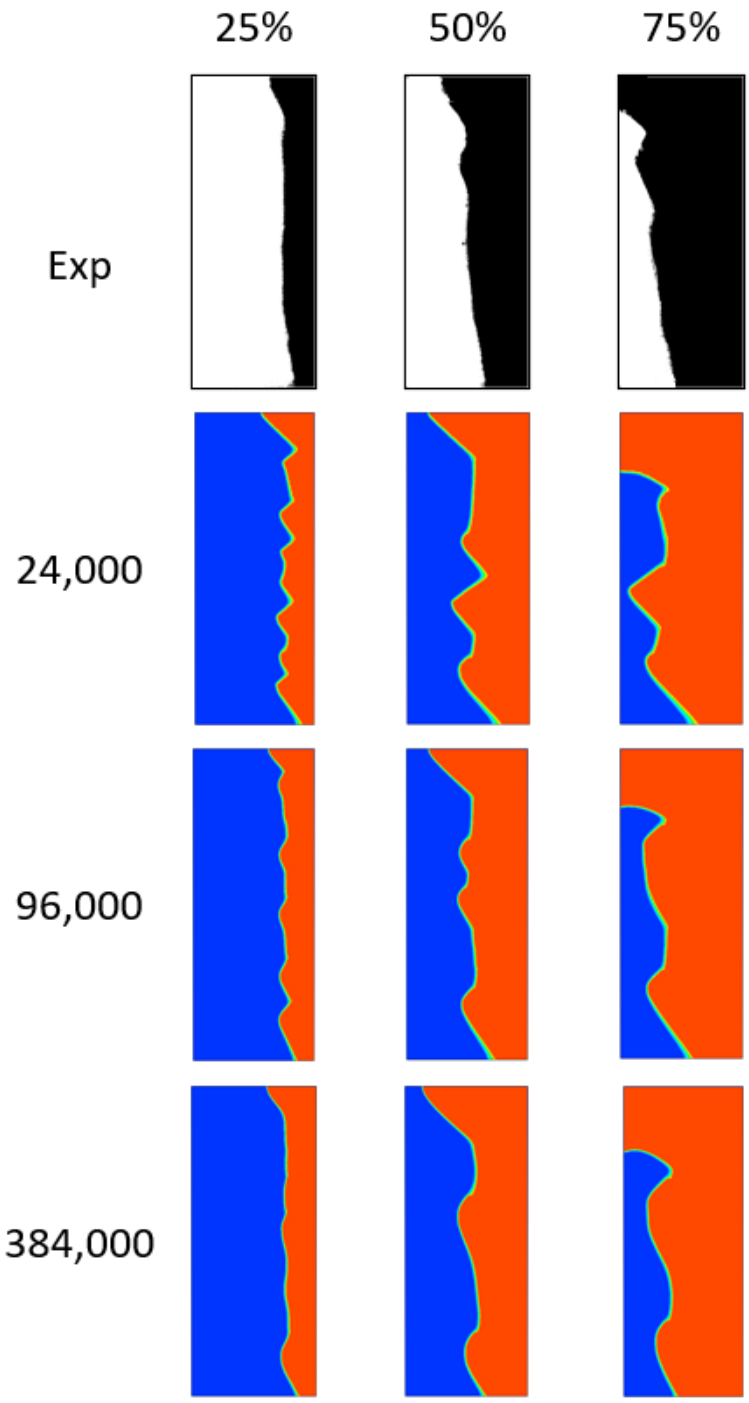

Figure 74: Melt front development images at 57°C and 30° angle for different mesh sizes

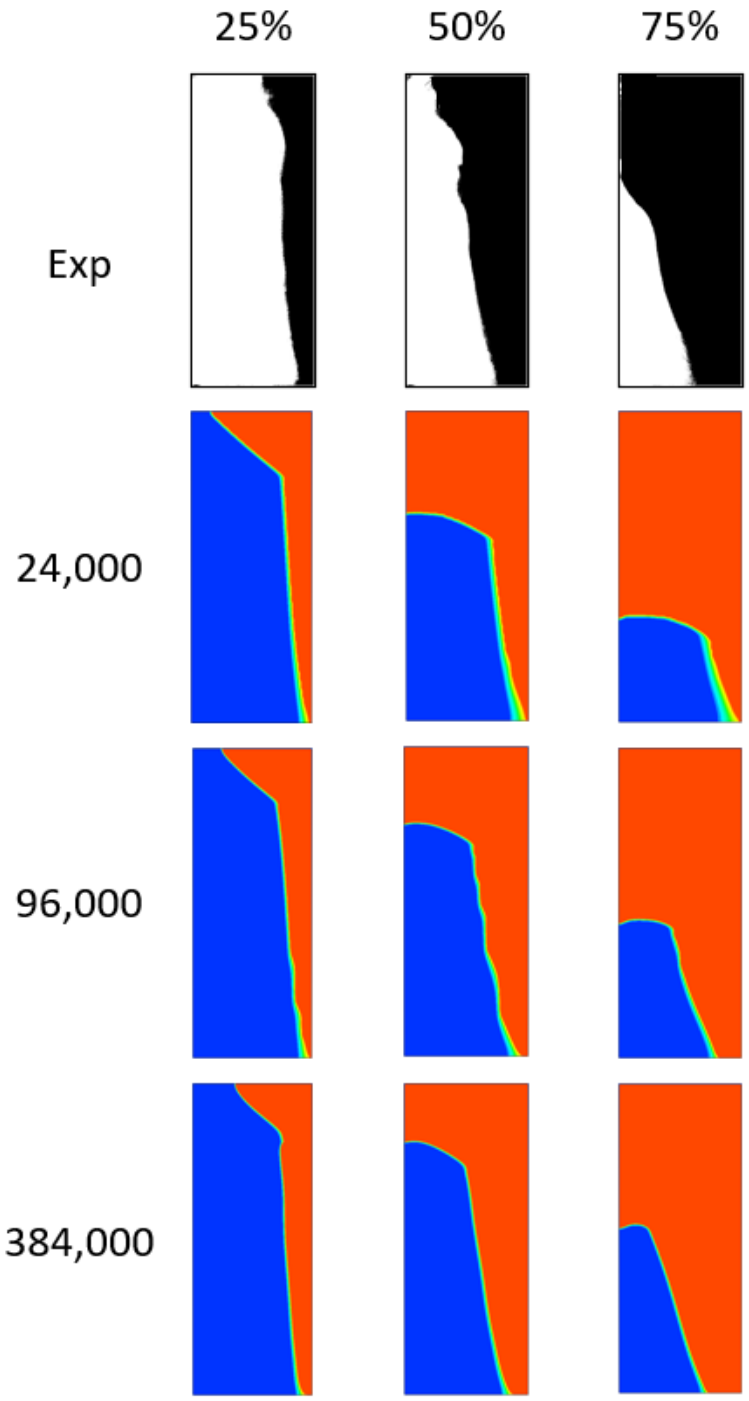

Figure 75: Melt front development images at 57°C and 45° angle for different mesh sizes

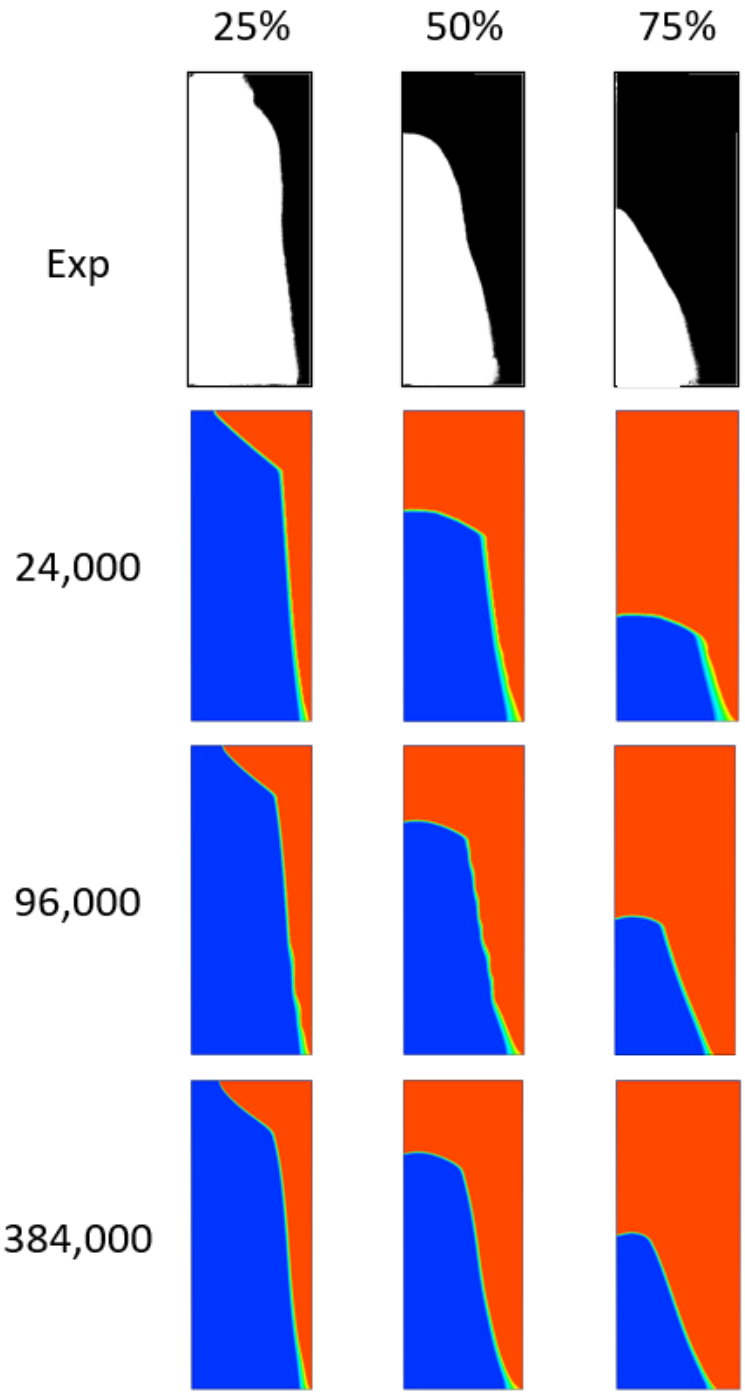

Figure 76: Melt front development images at 57°C and 60° angle for different mesh sizes

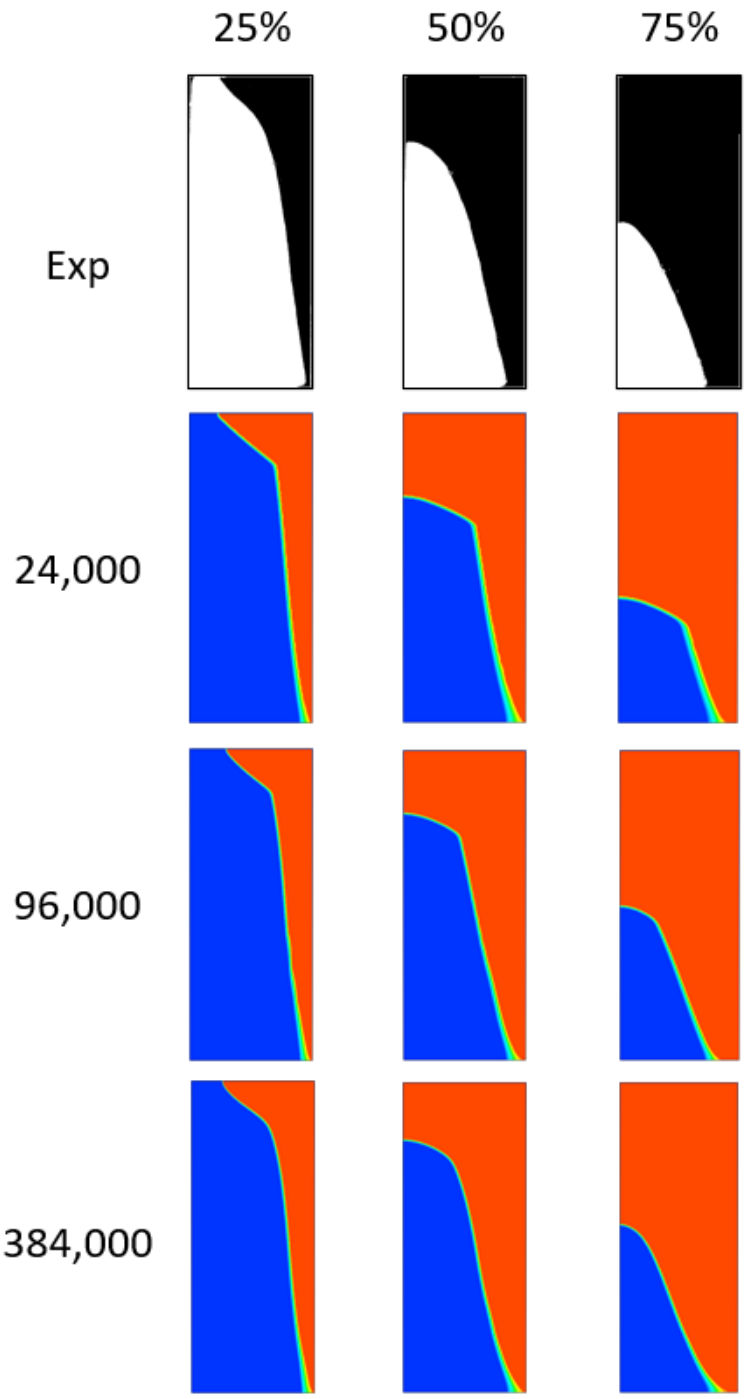

Figure 77: Melt front development images at 57°C and 90° angle for different mesh sizes

Even with the achievement of mesh independence, the 24,000 and 96,000 node meshes, much finer meshes are required to achieve proper validation to both the melt front interface shapes as well as the melt fraction percentage over the duration of the melt.

With regards to melt fraction percentages, lesser sized models completed at 24,000 nodes and 96,000 nodes appear to show some trend at the lower isothermal wall temperature of 47°C, with a gradual increase in the percent difference from the 90° to 60° to 30° inclination angles. Both size meshes reported great errors in the 45° inclination that would require a different mushy-zone constant to reduce this average percent difference. Looking at the higher wall temperature (57°C), the most coarse mesh showed greater variation in the mushy-zone constant with the 30° and 60° inclinations reporting an A_{mush} value of 5×10^7 as more accurate, and angles of 45° and 90° reporting an A_{mush} value of 1×10^7 as more accurate. These differences were resolved with the increase of mesh size to 96,000 nodes, where a mushy-zone constant value of 5×10^7 returned low percent errors for all but the 45° inclination, similar to the 47°C models at this mesh size.

The melt front development images for the 24,000 node models showed poor interface replication with a linear appearance and a seemingly greater modeled magnitude and number of vortices within the enclosure at the lesser angles. These meshes also displayed a greater volume of PCM along the bottom of the enclosure and closer to the boundary condition for much more of the melt, as compared to the experimental images. Increasing the fineness of the mesh showed some improvements, with the reduction of sharp corners on the modeled interface; but poor replication of the vortices within the enclosure was still present, especially at the greater temperatures and lesser angles.

To further analyze the effects of mesh size and inclination angle on the mushy-zone constant the models at different values of A_{mush} were completed for the 96,000 node meshes at both temperatures, and a finer mesh study was conducted at 384,000 nodes. The 96,000 node mesh at 47°C and 45° inclination showed a significant decrease in the average percent difference with the reduction in A_{mush} from 5×10^7 to 1×10^7, but this difference was observed to increase with the greater reduction to 1×10^6. In comparison, the greater temperature showed a continued decrease in average percent difference with the greater reduction to 1×10^6. At this size of mesh the mushy-zone constant can be concluded as dependent on angle, specifically at the 45° inclination, as well as dependent on temperature. However, the reduction in the mushy-zone constant to achieve better melt front versus time average percent differences comes at the cost of the interface accuracy. The great reduction of A_{mush} causes an observed difference in the melt front development images that more closely resembles those collected from the 24,000 node models. This left some concern with approaches to validation, as reducing the error in one of the standard methods increased the error in the other.

A preliminary study into even greater mesh sizes at 384,000 nodes and a wall temperature of 57°C shows improvement to both the average percentage differences of the melt fraction versus time and the melt front interface shapes when compared to the experiments. One exception is observed with the 90° orientation, in which the average percent difference increases when compared to the more coarse meshes. It is believed that increasing the mushy-zone constant value would help remedy this situation and lead to more accurate results. The melt front development images have better agreement with the

experiments, and the mesh refinement reduced the issues that had been previously observed at the lesser angles.

Results Discussion into Mesh Sizing

Although the 384,000 node mesh was determined to be the most accurate at replicating the experiments, all meshes were discussed as other published papers have used lower mesh sizes to complete their results as displayed in Table 10. The papers of this table that include image comparisons show similar issues as discussed with the more coarse meshes, and lead to conclusions in which the mushy-zone constant may be impacted differently with changes to system parameters such as inclination angle when compared to more refined meshes.

Table 10: Reported mesh sizes in reviewed literature

Study	Mesh Size (cells)
Fadl 2019 [12]	6,000
Zeng 2017 [38]	7,000
Fadl 2019 [12]	13,500
Oliveski 2021 [39]	28,457
Kabbara 2016 [17]	152,400

Changes to mesh size also reportedly had direct impacts onto the effects of the mushy-zone constant value with regards to inclination and isothermal wall temperature, with different unpredictable impacts with mesh refinement. If possible, validation to not only one system configuration (i.e. boundary condition, inclination angle, etc.) but many

would ensure accurate recreation of the liquid percentage over time as well as the interface shapes.

Chapter V

Conclusion

The completed experimental and material property data provide a foundation for future numerical investigations into PureTemp 37. In conjunction with the numerical data, the importance of careful and accurate collection of experimental data and material properties is illustrated with the significant impacts into numerical results with minor changes to the system. The completed numerical studies show the importance of proper mesh refinement, and how a determined mesh independence through melt fraction versus time data does not necessarily mean independence with regards to experimental replication of the interface shape. The models at the three different mesh sizes returned differences with respect to the effects of the mushy-zone constant at different inclinations and wall temperatures, leading to the conclusion that even after mesh independence was confirmed greater refinement to meshes would be necessary to decrease the average percent differences between the experimental and numerical results. This refinement would also be necessary to achieve more accurate replications of the interface shapes when modeling the studied PCM at different inclinations. In conclusion the mushy-zone constant does appear to be somewhat dependent on both inclination angle and temperature depending on the fineness of the modeled mesh.

A continuation to this study could include further investigations into the most refined mesh, with studies both at the lower wall temperature and variations into the mushy-zone constant at the higher temperature and larger angles. The aim of this would be to further define the sensitivity of the mushy-zone constant at this mesh size, and to

determine its impacts on not only the accuracy with respect to melt fraction versus time data but also the melt front development of the solid-liquid interface.

References

[1] M. Tvaronavičienė, J. Baublys, J. Raudeliūnienė and D. & Jatautaitė, "Global energy consumption peculiarities and energy sources: Role of renewables," *Energy Transformation Towards Sustainibility,* pp. 1-49, 2020.

[2] G. Alva, Y. Lin and G. Fang, "An overview of thermal energy storage systems," *Energy,* vol. 144, pp. 341-378, 2018.

[3] N. C. C. Office, "Latent and Sensible Heat," [Online]. Available: https://legacy.climate.ncsu.edu/edu/Heat.

[4] L. Socaciu, A. PLEŞA, P. UNGUREŞAN and O. & Giurgiu, "Review on phase change materials for building applications," *Leonardo Electronic Journal of Practices and Technologies,* vol. 25, pp. 179-194, 2014.

[5] N. Soares, A. R. Gaspar, P. Santos and J. J. Costa, "Experimental evaluation of the heat transfer through small PCM-based thermal energy storage units for building applications," *Energy and Building,* vol. 116, pp. 18-34, 2016.

[6] H. A. Nasef, S. A. Nada and H. Hassan, "Integrative passive and active cooling system using PCM and nanofluid for thermal regulation of concentrated photovoltaic solar cells," *Energy Conservation and Management,* vol. 199, 2019.

[7] M. H. Mahfuz, M. R. Anisur, M. A. Kibria, R. Saidur and I. H. S. C. Metselaar, "Performance investigation of thermal energy storage system with Phase Change Material (PCM) for solar water heating application," *International Communications in Heat and Mass Transfer,* vol. 57, pp. 132-139, 2014.

[8] M. Emam, S. Ookawara and M. Ahmed, "Thermal management of electronic devices and concentrator photovoltaic systems using phase change material heat sinks: Experimental investigations," *Renewable Energy,* vol. 141, pp. 322-339, 2019.

[9] S. Gharbi, S. Harmand and S. B. Jabrallah, "Experimental comparison between different configurations of PCM based heat sinks for cooling electronic components," *Applied Thermal Engineering,* vol. 87, pp. 454-462, 2015.

[10] A. C. Kheirabadi and D. Groulx, "The effect of the mushy-zone constant on simulated phase change heat transfer," in *International Symposium on Advances in Computational Heat Transfer,* New Brunswick, 2015.

[11] H. Shmueli, G. Ziskind and R. Letan, "Melting in a vertical cylindrical tube: Numerical investigation and comparison with experiments," *International Journal of Heat and Mass Transfer,* vol. 53, no. 19-20, pp. 4082-4091, 2010.

[12] M. Fadl and P. C. Eames, "Numerical investigation of the influence of mushy zone parameter Amush on heat transfer characteristics in vertically and horizontally oriented thermal energy storage systems," *Applied Thermal Engineering,* vol. 151, pp. 90-99, 2019.

[13] V. R. Voller and C. Prakash, "A fixed grid numerical modelling methodology for convection-diffusion mushy region phase-change problems," *International Journal of Heat and Mass Transfer,* vol. 30, no. 8, pp. 1709-1719, 1987.

[14] M. Fadl and P. Eames, "A numerical investigation into the heat transfer and melting process of lauric acid in a rectangular enclosure with three values of wall heat flux," *Energy Procedia,* vol. 158, pp. 4502-4509, 2019.

[15] B. Yang, A. Raza, F. Bai, T. Zhang and Z. Want, "Microstructural evolution within mushy zone during paraffin's melting and solidification," *International Journal of Heat and Mass Transfer,* vol. 141, pp. 769-778, 2019.

[16] B. R. Tamuli, S. Nath and D. Bhania, "Phase Change in an Enclosure Under Different Combinations of Boundary Wall Condition: A Numerical Study," *Recent Advances in Mechanical Engineering,* pp. 95-104, 2021.

[17] M. Kabbara, A. C. Kheirabadi and D. Groulx, "Numerical modeling of natural convection driven melting for an inclined/finned rectangular enclosure," in *ASME Summer Heat Transfer Conference*, Washington DC, 2016.

[18] E. M. Sparrow and J. A. Broadbent, "Inward melting in a vertical tube which allows free expansion of the phase-change medium," *ASME Journal of Heat and Mass Transfer,* vol. 104, pp. 309-315, 1982.

[19] E. M. Sparrow, S. V. Pantakar and S. Ramadhyani, "Analysis of melting in the presence of natural convection in the melt regions," *Journal of Heat Transfer,* vol. 99, pp. 520-526, 1977.

[20] C. Gau, R. Viskanta and C. J. Ho, "Flow visualization during solid-liquid phase change heat transfer II. Melting in a rectangular cavity," *International Communications in Heat and Mass Transfer,* vol. 10, no. 3, pp. 183-190, 1983.

[21] G. Ziskind, "Modeling of heat transfer in phase change materials for thermal energy storage systems," in *Advances In Thermal Energy Storage Systems*, Woodhead Publishing, 2021, pp. 359-379.

[22] R. Karami and B. Kamkari, "Investigation of the effect of inclination angle on the melting enhancement of phase change material in finned latent heat thermal storage units," *Applied Thermal Engineering,* vol. 146, pp. 45-60, 2019.

[23] A. D. Brent, V. R. Voller and K. T. J. Reid, "Enthalpy-porosity technique for modeling convection-diffusion phase change: application to the melting of a pure metal," *Numerical Heat Transfer,* vol. 13, no. 3, pp. 297-318, 1988.

[24] C. Gau and R. Viskanta, "Melting and solidification of a pure metal on a vertical wall," *Journal of Heat Transfer,* vol. 108, no. 1, pp. 174-181, 1986.

[25] A. Abdi, V. Martin and J. N. Chiu, "Numerical investigation of melting in a cavity with vertically oriented fins," *Applied Energy,* vol. 235, pp. 1027-1040, 2019.

[26] H. Shokouhmand and B. Kamkari, "Experimental investigation on melting heat transfer characteristics of lauric acid in a rectangular thermal storage unit," *Experimental Thermal and Fluid Science,* vol. 50, pp. 201-212, 2013.

[27] B. Kamkari, H. Shokouhmand and F. Bruno, "Experimental investigation of the effect of inclination angle on convection-driven melting of phase change material in a rectangular enclosure," *International Journal of Heat and mass Transfer,* vol. 72, pp. 186-200, 2014.

[28] B. Kamkari and H. Shokouhmand, "Experimental investigation of phase change material melting in rectangular enclosures with horizontal partial fins," *International Journal of Heat and Mass Transfer,* vol. 78, pp. 839-851, 2014.

[29] B. Kamkari and D. Groulx, "Experimental investigation of melting behaviour of phase change material in finned rectangular enclosures under different inclination angles," *Experimental Thermal and Fluid Science,* vol. 97, pp. 94-108, 2018.

[30] M. Avci and M. Y. Yazici, "An experimental study on effect of inclination angle on the performance of a PCM-based flat-type heat sink," *Applied Thermal Engineering,* vol. 131, pp. 806-814, 2018.

[31] D. Jiang, Z. Liao, P. Li, G. Yu and C. Xu, "The evolution of the mushy zone during the melting process of a binary nitrate salt," *International Journal of Heat and Mass Transfer,* vol. 142, 2019.

[32] V. Shatikian, G. Ziskind and R. Letan, "Numerical investigation of a PCM-based heat sink with internal fins," *International journal of heat and mass transfer,* vol. 48, no. 17, pp. 3689-3706, 2005.

[33] B. Kamkari and H. J. Amlashi, "Numerical simulation and experimental verification of constrained melting of phase change material in inclined rectangular enclosures," *International Communications in Heat and Mass Transfer,* vol. 88, pp. 211-219, 2017.

[34] L. Katsman, *Investigation of phse change in cylindrical geometry with internal fins,* Negev, Beer-Sheva, Israel: Ben-Gurion University, 2006.

[35] A. C. Kheirabadi, M. Kabbara and D. Groulx, "Geometrical impacts on phase change heat transfer modeling," in *First Pacific Rim Thermal Engineering Conference*, Hawaii's Big Island, 2016.

[36] P. H. Biwole, P. Eclache and F. Kuznik, "Phase-change materials to improve solar panel's performance," *Energy and Buildings,* vol. 62, pp. 59-67, 2013.

[37] S. Arena, E. Casti, J. Gasia, L. F. Cabeza and G. Cau, "Numerical simulation of a finned-tube LHTES system: influence of the mushy zone constant on the phase change behaviour," *Energy Procedia,* vol. 126, pp. 517-524, 2017.

[38] L. Zeng, J. L. Y. Lu, W. Li, S. Liu and J. Zhu, "Numerical Study of the influences of geometry orientation on phase change material's melting process," *Advances in mechanical engineering,* 2017.

[39] R. D. C. Oliveski, F. Becker, L. A. O. Rocha, C. Biserni and G. E. S. Eberhardt, "Design of fins structures for phase change material (PCM) melting process in rectangular cavities," *Journal of Energy Storage,* vol. 35, 2021.

[40] N. Sinaga, H. Moria, K. S. Nisar, C. M. Vu, B. Heidarshenas, A. Arsalanloo and M. M. Youshanlouei, "Melting performance enhancement of thermal storage system by utilizing shape and position of double fin," *Case Studies in Thermal Engineering,* vol. 23, 2021.

[41] M. E. Nakhchi and J. A. Esfahani, "Improving the melting performancce of PCM thermal energy storage with novel stepped fins," *Journal of Energy Storage,* vol. 30, 2020.

[42] P. H. Biwole, D. Groulx, F. Souayfane and T. Chiu, "Influence of fin size and distribution on solid-liquid phase change in a rectangular enclosure," *International Journal of Thermal Sciences,* Vols. 433-446, p. 124, 2018.

[43] S. Z. Tang, H. Q. Tian and J. J. L. H. Zhou, "Evaluation and optimization of melting performance in a horizontal thermal energy storage unit with non-uniform fins," *Journal of Energy Storage,* vol. 33, 2021.

[44] O. Betrand, B. Binet, H. Combeau, S. Couturier, Y. Delannoy, D. Gobin and G. Vieira, "Melting driven by natural convection A comparison exercise: first results," *International Journal of Thermal Sciences,* vol. 38, no. 1, pp. 5-26, 1999.

[45] M. Longeon, A. Soupart, J. F. Fourmigue, A. Burch and P. Marty, "Experimental and numerical study of annular PCM storage in the presence of natural convection," *Applied Energy,* vol. 112, pp. 175-184, 2013.

[46] W. B. Ye, "Thermal and hydraulic performance of natural ocnvectio nin a rectangular storage cavity," *Applied Thermal Engineering,* vol. 93, pp. 1114-1123, 2016.

[47] C. J. Ho and R. Viskanta, "Heat transfer during melting from an isothermal vertical wall," *ASME Journal of Heat and Mass Transfer,* vol. 106, pp. 12-19, 1984.

[48] Y. Wang, J. Dai and D. An, "Numerical investigations on melting behavior of phase change material in a rectangular cavity at different inclination angles," *Applied Sciences,* vol. 141, pp. 769-778, 2019.